ABSTRACT

Title of Document: VARIABILITY OF THE GREAT PLAINS LOW-LEVEL JET: LARGE SCALE CIRCULATION CONTEXT AND HYDROCLIMATE IMPACTS

Scott J. Weaver, Doctor of Philosophy, 2007

Directed By: Professor Sumant Nigam, Department of Atmospheric and Oceanic Science

Variability of the Great Plains Low-Level Jet (GPLLJ) is analyzed from the perspective of larger-scale, lower-frequency influences and regional hydroclimate impacts; as opposed to the usual analysis of its frequency, diurnal variability and mesoscale structure.

The circulation-centric core analysis is conducted with monthly and pentad data from the high spatio-temporal resolution, precipitation-assimilating North American Regional Reanalysis, and ERA-40 global reanalysis (as necessary) to identify the recurrent patterns of GPLLJ variability and their large-scale circulation and regional hydroclimate links.

The analysis reveals that GPLLJ variability is, indeed, linked to coherent, large-scale, upper-level height patterns over the Pacific, and NAO variability in the Atlantic. A Rossby Wave Source analysis shows the Pacific height pattern to be potentially linked to tropical diabatic heating anomalies in the west-central basin and in the eastern Pacific sector. EOF analysis of GPLLJ variability shows it to be

comprised of three modes that exert profound influence on Great Plains precipitation variability, and together, account for ~75% of the variance.

Ocean basin centered EOF analysis on summertime SLP anomalies shows similar GPLLJ and precipitation impacts as those found in the Great Plains centric perspective, supporting the claim for remotely generated influences on Great Plains low-level jet and hydroclimate variability.

Pentad analysis of the atmospheric and terrestrial water balances during the 1988 drought and 1993 flood show that, jet variability, while influential over many of the subseasonal anomalous precipitation episodes was not a necessary condition for precipitation anomalies. Great Plains evaporation exhibited a 2-week delay with respect to precipitation suggesting a minor role for precipitation recycling during these events. ENSO and NAO variability are shown to contribute significantly to the large midsummer positive precipitation anomalies during 1993.

EEOF analysis of pentad 900 hPa meridional winds during MJJ show three temporally stable modes of variability, each exhibiting similar spatial characteristics to the monthly EOF spatial patterns. Lead/lag regressions show a one pentad delay in moisture flux convergence generated precipitation anomalies, perhaps, suggesting the importance of moisture transports in generating Great Plains precipitation anomalies.

Climate models are shown to be challenged in depicting the jet and precipitation variability over the Great Plains.

VARIABILITY OF THE GREAT PLAINS LOW-LEVEL JET: LARGE SCALE CIRCULATION CONTEXT AND HYDROCLIMATE IMPACTS

By

Scott J. Weaver

Dissertation submitted to the Faculty of the Graduate School of the
University of Maryland, College Park, in partial fulfillment
of the requirements for the degree of
Doctor of Philosophy
2007

Advisory Committee:
Dr. Sumant Nigam, Chair, Professor
Dr. James Carton, Professor
Dr. Antonio Busalacchi, Professor
Dr. Karen Prestegaard, Associate Professor
Dr. Alfredo Ruiz-Barradas, Assistant Research Scientist

Preface

This work is an examination of the warm season Great Plains hydroclimate variability from the perspective of the primary summertime moisture provider – the Great Plains low-level jet (GPLLJ). The diagnostic analysis undertaken in this thesis originated from the overlapping interests of Sumant Nigam (large-scale climate dynamics) and Scott Weaver (synoptic and mesoscale meteorology). The fusion of these interrelated, however, different paradigms enables an interesting investigation into the lower frequency (monthly – weekly) GPLLJ variability structure and impacts of what many view, as primarily, a diurnally-varying mesoscale circulation feature.

Dedication

For Tricky and friends

Acknowledgements

I consider myself fortunate to have Dr. Sumant Nigam as my advisor. His patience and enthusiasm were instrumental to the fulfillment of my graduate education. His omnipresent positive attitude was a source of strength for me at times when it was desperately needed. I always left his office with a better outlook than when I entered. His insightful scientific vision and attention to detail is unparalleled and a standard to which I will continue to strive for throughout my career.

I am equally grateful to Dr. Alfredo Ruiz-Barradas for his unending technical support. His selfless sharing of data, analysis tools, and strategies was integral to the completion of this research. On numerous occasions Dr. Ruiz-Barradas would sacrifice his own research time to assist myself and other students. This altruistic quality has been a positive example to me throughout my graduate research career.

I would also like to thank Dr. Owen Thompson. Although I never had the pleasure of participating in one of his classes, our many philosophical conversations about atmospheric science or the struggles of graduate school was a beacon of hope for me. Taking me to lunch after my scholarly paper seminar was one of the highlights of my time at UMD.

I would like to thank Dr. James Carton, Dr. Antonio Busalacchi, and Dr. Karen Prestegaard, for serving on the dissertation examining committee and Dr. Phil Arkin for his insightful comments.

Many others were instrumental in their technical support and friendship over the years. I am grateful to Dr. Da-Lin Zhang for introducing me to the topic of low-level jets and for his advisement during my Master's degree work. I am indebted to

Hengmao Wang, Jigme, Chian-Yi Liu, and Hongqing Liu for their technical advice, and Megan Linkin for the many conversations about teleconnection patterns, RU, and New Jersey.

I am lucky to have such a wonderful family and I am grateful for the support of my parents, siblings, and nephews (Donna, Richard, Darlene, Richard, Susan, Richard, Kristen, Jessica, Dave, Dylan, and Nicholas), and especially to Richard G. Seget for the 1995 conversation that started all of this.

I have had the exceptional great fortune to have such a beautiful and charming wife. Carrie's unending support, tolerance, and sacrifice were instrumental to the successful completion of this thesis. I simply could not have done this without her. I continue to learn much from her love.

Table of Contents

List of Acronyms

CDT	Central Daylight Time
ECMWF	European Center for Medium Range Weather Forecasting
ENSO	El Niño Southern Oscillation
EEOF	Extended Empirical Orthogonal Function
EOF	Empirical Orthogonal Function
ERA	European Reanalysis
GCM	General Circulation Model
GEOS	Goddard Earth Observing System
GFDL	Geophysical Fluid Dynamics Laboratory
GPLLJ	Great Plains Low-Level Jet
IMSL	International Mathematical and Scientific Library
LLJ	Low-Level Jet
NAO	North Atlantic Oscillation
NARR	North American Regional Reanalysis
NCAR	National Center for Atmospheric Research
NCEP	National Center for Environmental Prediction
RWS	Rossby Wave Source
SLP	Sea Level Pressure
SST	Sea Surface Temperature
SVD	Singular Value Decomposition
PC	Principal Component
PV	Potential Vorticity

List of Tables

List of Figures

Chapter 1: Introduction

1.1 Motivation

In recent years significant attention has been focused on illuminating the nature and causes of variations in climate. The emerging evidence in support of anthropogenically forced climate change necessitates scientific study of climate variability on all spatial and temporal scales. Nowhere is this more important than in the area of hydroclimate for this aspect of climate is pervasive. Extreme events can cause widespread damage to life and property. Scientific understanding of such hydroclimate fluctuations and extreme events is of paramount importance if society is to adapt to and become proficient at mitigating their effects.

The Great Plains of North America is an area prone to significant hydroclimate variations. This predominantly flat agricultural region extends from the interior Canadian provinces of Alberta, Saskatchewan, and Manitoba south through the west central United States into Texas. During spring and summer, large amounts of heat and moisture are transported north from the Gulf of Mexico into the central United States by the Great Plains low level jet (GPLLJ) – a fast moving river of air in the lower troposphere characterized by vertical and horizontal wind shear.

Fluctuations of the Great Plains low-level jet (GPLLJ) are influential for warm season central U.S. hydroclimate. This link is established through the jet's regulation of regional moisture transports and thermodynamic forcing of precipitation. The connection is most notable during times of extreme hydroclimate episodes such as the great drought of 1988 and flood of 1993.

Many early GPLLJ studies were largely focused on the development of the nocturnal boundary layer in generating the "inertial oscillation" thought to be necessary for low-level jet development (Blackadar 1957; Hoxit 1975). It was reasoned that nocturnal jet evolution was a consequence of the release of the frictional constraint due to diurnally varying boundary layer heating. While this mechanism is operable it does not explain the preferential location of the GPLLJ (and other low-level jets) downstream of a large topographic barrier.

While boundary layer frictional and topographical thermal gradient effects on forcing the GPLLJ were being explored others were taking a larger view and a new paradigm emerged. Wexler (1961) argued that large scale inertial effects and orographic blocking similar to those causing the existence of the Gulf Stream in the western Atlantic Ocean were influential in creating the GPLLJ. He noted earlier authors' failed attempts at reproducing the diurnal structure of the GPLLJ with elaborate mathematical models based on eddy coefficients that varied with the time of day and height above ground. Wexler asserts,

> "It is believed that this deficiency in large measure is due to neglect of the mechanism which in the first place actually causes formation of the low-level jet itself. It is not the radiative and frictional effects which occur locally that create the highly concentrated flow in the western boundary layer, but the bulk properties of the flow caused by the large scale inertial effects. When the southerly flow is present, as in the case when the western end of the Bermuda anticyclone covers the Mississippi valley, then the inertial boundary layer influences enter in an important manner. Without this westward intensification of southerly flow up the Mississippi Valley, there would not be a basic flow on which frictional stresses could operate diurnally and so give the strong diurnal low level jet so characteristic of that region."

Wexler's description implicating the influence of the Atlantic subtropical high on the GPLLJ is demonstrated in figure 1.1 which shows the climatological evolution of

mean sea level pressure during May, June, and July (MJJ) (1949-2001) as diagnosed from the NCEP/NCAR reanalysis. The warm season evolution and strengthening of the large- scale SLP field and the westward flank of the Atlantic subtropical anticyclone covering the central U.S. is indicative of the large-scale inertial effect and anticyclonic low-level flow to which Wexler speaks.

The regional (Great Plains) connection to the Atlantic subtropical anticyclone is depicted in the summer climatological (1979-2005) expression of the low-level flow and precipitation shown in figure 1.2 from the North American Regional Reanalysis. The low-level flow (arrows) connection to both the Pacific and Atlantic subtropical anticyclones is nicely captured as evidenced by the coherent flow structure emanating from the Caribbean Sea and Gulf of Alaska. The 4 ms^{-1} threshold shows the deceleration of the flow associated with the GPLLJ exit region. Not surprisingly the maximum in Great Plains precipitation is found in this area. Notable precipitation is also found along the U.S. Gulf Coast and Mexico and in association with the northern extension of the Intertropical Convergence Zone. The boxes outline areas of interesting Great Plains precipitation (northern box) and low-level jet (southern box) activity. The importance of these two areas will become apparent in subsequent chapters.

Several years prior to Wexler's statement Benton and Estoque (1954) conducted a comprehensive study detailing the North American water vapor transport for the summer of 1949. While the term low-level jet was not in use at the time, vertical profiles of meridional moisture flux across 30°N hints at the existence of the GPLLJ in summer. Furthermore, they note the large contribution by eddy systems to the total

meridional moisture fluxes, suggesting the impact of upstream Pacific based synoptic storm systems.

Rasmusson (1967) confirmed the mean characteristics found by Benton and Estoque. However, by using data over a longer period with higher vertical and temporal resolution and separating the night and daytime components of the integrated water vapor fluxes, the diurnally varying nature and the prospect for interannual variability of the summertime North American water balance and GPLLJ emerged. Rasmusson states:

> "The mean monthly diurnal oscillations of the water vapor transport over North America and the Central American Sea, appear to be produced by a combination of local and large-scale effects. Because of the apparent relationship of these oscillations to the large-scale flow pattern over eastern North America, one would expect changes in detail from year to year."

While these studies were impressive in their scope and foreshadowed the impact of large-scale GPLLJ variability on North American hydroclimate, a comprehensive analysis of the long-term mean state and low frequency variability of the GPLLJ had to await the development of high spatial resolution and long-term consistent data sets. As such the lower frequency ($\omega <$ synoptic), large-scale (> mesoscale) context of the GPLLJ and moisture flux variability remains to be characterized.

Around the same time as the North American atmospheric water balance was being documented, the relationship between the GPLLJ and nocturnal convection over the Great Plains surfaced. Means (1954) asserted that the GPLLJ was capable of transporting such copious amounts of moisture northward that over a 48 hour period the jet could flux enough water to cover the state of Kansas with 4-7 cm of rainfall. Years later, Uccellini and Johnson (1979) found that sensible heat and moisture

transport, increased by a factor of 2 and 3, respectively, during the development of a low-level jet event. Findings such as these coupled with a lack of long term consistent datasets naturally steered GPLLJ research toward more synoptic and diurnally varying observational and modeling analyses; where it would largely reside for the better part of two decades.

The characterization of diurnal and synoptic GPLLJ variability mechanisms was also fraught with potential problems. Due to the coarse temporal resolution twice-daily radiosonde network, the representation of the nocturnally varying GPLLJ was degraded in the larger-scale synoptic observing network, prohibiting adequate capture of some GPLLJ features. As such, the responsibility of elucidating the mechanisms that produce GPLLJ variability and the observed jet-precipitation relationship would necessarily fall on the modeling community.

Success in modeling the GPLLJ has been demonstrated by both mesoscale and general circulation models. The mesoscale modeling efforts of Zhong et. al (1996) was able to capture the features of a single low-level jet event. Based on this success, sensitivity studies were conducted to ascertain the important mechanisms in producing the low-level jet. While land-atmosphere interactions were shown to influence the jet on the diurnal timescale, the importance of a strong synoptic scale pressure gradient was also shown to be critical for jet formation.

The results from one case study of a LLJ event using a high resolution mesoscale model do not necessarily transfer over to the lower spatio-temporal resolution General Circulation Models (GCM). Two investigations of long-term predictability of the GPLLJ were conducted using the European Center for Medium Range Weather

Forecasting (ECMWF) and National Center for Atmospheric Research (NCAR) GCMs (Ghan et. al 1996) and in the Goddard Earth Observing System (GEOS-1) atmospheric GCM (Helfand and Schubert 1996). While success was claimed in capturing the frequency of GPLLJ events over both periods of investigation, the results are tempered by the fact that the simulation benchmark was based on a 2-year climatology of jet frequency proposed by Bonner (1968). Two years is hardly a long enough record to define climatology, especially given the lurking interannual variability. Not surprisingly the Bonner climatology recognized September as the month with largest GPLLJ activity, at odds with the longer period climatological results presented in chapter 2 of this study, which shows July to be the month with the strongest GPLLJ signature.

While the existence of the GPLLJ in simulations is encouraging, the models were not skillful in capturing the spatial distribution of the GPLLJ and the robust relationship to precipitation noted in numerous observational studies. Diagnosing fluctuations of the GPLLJ and precipitation impacts with respect to a long-term stable climatology can advance understanding of mechanisms, and ultimately prediction of GPLLJ variability and related hydroclimate impacts. For example, the prediction capability should be enhanced by an improved description of the relationship of the GPLLJ to recurring modes of climate variability, e.g. El Niño Southern Oscillation (ENSO) and the North Atlantic Oscillation (NAO), if indeed one exists.

Although the pioneering observational and modeling studies relating the GPLLJ to the large scale circulation and ensuing hydroclimate provided significant information with respect to GPLLJ formation mechanisms and precipitation impacts,

there are some notable gaps in our present understanding. For example, the lack of proper placement of the GPLLJ in GCMs noted by Ghan et al. (1996), hints at the possibility of meridional and/or zonal fluctuations of the GPLLJ and varying degrees of associated precipitation impacts. Due to past data constraints the question of how and to what extent large-scale circulation (cf. figures 1.1 and 1.2) variability influences these GPLLJ fluctuations and related precipitation impacts has yet to be fully characterized and is a fundamental one in context of natural variability and global climate change. It is also the question that drives much of this thesis research.

Climate research, in recent decades, has been revolutionized by advances in data assimilation; with the benefits first evident in the global reanalysis generated at the National Centers for Environmental Prediction (NCEP) and the National Center for Atmospheric Research (Kalnay et al. 1996). This reanalysis offers a consistent multiyear 1949-present climate dataset generated with a frozen assimilation system. More recently the European Center for Medium Range Weather Forecasting released their version of a global reanalysis spanning the period 1957-2002. These reanalyses are unprecedented in their depiction of long-term atmospheric climate variability. However, their output is a blend of observations and model generated fields. As such, those fields that are not directly observed, and thus constrained, including divergence and hydroclimate ones (e.g., precipitation, evaporation, surface fluxes) may not be representative of the true climate state.

The limitations imposed by the model dependent fields in the Global Reanalyses may not be too severe for analysis of the large-scale atmospheric fields such as geopotential height, geostrophic winds, and mean sea level pressure, which are

observationally well constrained. However, divergence and hydroclimate fields which are sensitively dependent on the physical parameterization schemes, and thus quite model dependent, are not necessarily realistically represented. To circumvent this problem, NCEP recently generated the North American Regional Reanalysis (NARR). This high resolution precipitation and radiance assimilating dataset spanning 1979-2005 offers a state of the art climate representation for studying all regional aspects of the GPLLJ and attendant hydroclimate impacts. Nowhere is this more important than with regard to the precipitation assimilation, which has been deemed successful (Mesinger at al. 2006).

This work is an in depth diagnosis of the variability and evolution of the GPLLJ, including remote circulation context, land surface relationships, and hydroclimate impacts on pentad (5-day averaged) to monthly timescales using the high quality quasi-observational data provided by the NARR, NCEP/NCAR, and ERA-40 reanalysis datasets. The division of this research is essentially in three parts. The first is a documentation of monthly GPLLJ and large scale circulation variations and precipitation impacts through the identification of preferred modes of both GPLLJ and remote basin SLP variability. Act two is a pentad resolution analysis of the temporal phase lead-lag relationships of pertinent hydroclimate fields during the Great Plains drought of 1988 and flood of 1993. This section addresses the question of land surface vs. remote circulation influences on recent extreme hydroclimate events over the Great Plains. The drought-flood case study motivates the third phase using EEOF analysis to characterize the spatiotemporal evolution of recurrent GPLLJ variability modes at pentad resolution, and the connections to pertinent hydroclimate

fields. The central conclusion is that large scale remotely based circulation variations exert considerable control over the Great Plains jet and hydroclimate variability in the warm season.

1.2 Large Scale Variability

Hydroclimate variations over the Great Plains are typically positively correlated with the intensity and frequency of low-level jets. Much of the event-intensity studies have found interesting relationships between strong LLJs (according to the Bonner criteria, 1968) and precipitation. For instance, in a study of the frequency and intensity of LLJs during the 1993 central U.S. floods it was demonstrated that the occurrence of extreme precipitation events was dependent upon the incidence of strong LLJs. Furthermore, it was shown that these LLJs occurred in relationship to significant large scale atmospheric circulation anomalies (Arritt et al 1997). While interesting, this finding needs to be supported by additional analyses as a case study of a highly anomalous event with a spatially coarse wind profiler network is not sufficient to make the case for a more pervasive relationship between GPLLJ and larger-scale circulation variability.

To address this, an in depth investigation of monthly mean characteristics of the low-level wind field and 1000-700 hPa meridional moisture fluxes is conducted. This represents, as best I know, the first high resolution (i.e., 3-hourly, 32 km, 25 hPa) depiction of the time-mean GPLLJ using a 23 + year climatology. The climatological analysis focuses on the seasonal and diurnal evolution of the low-level meridional wind field and moisture fluxes. The important result here is that while the GPLLJ exhibits significant diurnal variability the jet signature is robust even in the monthly

averaged meridional wind field. Furthermore, the jet shows a coherent warm season evolution and decay with a maximum in July (see figure 2.1). This suggests that lower-frequency (i.e. monthly-seasonal) large-scale circulation anomalies may influence the GPLLJ. This thesis is devoted to characterization of this influence on monthly/pentad timescales.

From the high resolution climatology, a GPLLJ index is constructed to investigate the circulation-precipitation relationships. Regressions of large-scale tropospheric circulation fields against the GPLLJ index indicate that the GPLLJ occurs in context of large-scale hemispheric wide circulation anomalies. The result here is not entirely surprising in light of the previous indication of a continental dipole in geopotential height anomalies during strong GPLLJ episodes (Byerle and Paegle 2003; Chen and Kpaeyeh 1993). This central result opens the door to several interesting hypotheses including remote forcing of low frequency GPLLJ variations via propagated stationary waves. The possibility that competing modes of variability native to each adjoining basin may be operative at the same time, given the hemispheric footprint, is also investigated. While continental scale circulation anomalies have been shown to be important for the GPLLJ, the characterization of planetary scale atmospheric circulation and related diabatic heating anomalies in far-away regions here, leading to an inference for large scale climate variability influencing the regional-scale GPLLJ is novel.

The influence of large-scale remotely generated circulation variability on North American warm season precipitation anomalies have recently been noted in context of summertime teleconnection patterns. Lau and Weng (2002) studied correlations

between East Asian and North American summertime precipitation. Using Singular Value Decomposition (SVD) analysis on the covariance of 500 hPa heights and rainfall anomalies they show a regional scale North American height anomaly embedded within a hemispheric wide upper tropospheric stationary wave train anomaly (i.e., western low-eastern high). Ding and Wang (2005) identified a summertime circumglobal teleconnection pattern in the 200 hPa height field. Their pattern is suggestive of Indian summer monsoon origins with implications for precipitation impacts over North America. Ting and Wang (1997) conducted similar analysis on monthly sea surface temperatures (SST) and found that the leading mode (ENSO-like, tropical origin) was connected to enhanced Great Plains precipitation while the second mode was of North Pacific origin and related to a reduction in Great Plains precipitation.

The impact of remotely forced anomalous stationary waves on Great Plains precipitation does not necessarily generalize to the GPLLJ. Although the jet is a primary influence on Great Plains rainfall it is not a sufficient condition for precipitation. The preference for the GPLLJ to be prevalent to the east of the North American Cordillera suggests that topography is influential; not just for the climatological state but also in context of interannual variability; perhaps, from interactions with the upstream circulation anomalies.

Ting (1994) addresses the question of summertime stationary wave orographic interaction using a GCM and a linear baroclinic model. The linear model is similar to that used by Nigam et al. (1986, 1988) to interpret the GCM generated stationary waves, from a linearized form of the GCM equations. This dynamical diagnosis

allows for apportionment of wave forcing: Heating, orography and transient/eddy fluxes. Ting concluded that global diabatic heating was a key forcing for summertime stationary waves. She also showed the nonlinear terms arising from orographic interaction as being responsible for the equivalent barotropic structure in the midlatitudes. Could the stationary wave-orographic interaction be the reason for the preferred geographic location of the GPLLJ?

Ting and Wang (2006) investigate this possibility using the Geophysical Fluid Dynamics Laboratory (GFDL) and linear and nonlinear stationary wave models. Decomposition of forcing reveals that climatological GPLLJ is generated by nonlinear interaction of the trade winds along the southern flank of the North Atlantic subtropical high with North American topography; which turns the flow northward. Potential vorticity (PV) constraints would enhance anticyclonic shear vorticity and produce the GPLLJ. This recent modeling result echoes Wexler's pronouncement of some 46 years ago. Further analysis suggests that the main impact of transient forcing on the GPLLJ is to extend the northeastward reach of the jet during evolution of synoptic scale storm systems emanating from the Pacific basin. This raises the possibility of superposition of Atlantic and Pacific basin influences on GPLLJ variability.

Byerle and Paegle (2003) also investigated orographic impacts on the GPLLJ using the NCEP/NCAR global reanalysis. They focused on the effect of the upper-level ambient westerly flow, and argued that the GPLLJ is a component of a larger-scale orographically bound summer cyclone whose strength increases with increased cross barrier flow. This conclusion is reached from the positive correlation of the

upper level wind anomalies and those of the GPLLJ. The dynamical explanation is based the Rossby wave phase speed relation:

$$C = (U - \beta/k^2)$$

Where C is the phase speed, U is the mean zonal flow, β and k the meridional gradient of the coriolis force and wave number respectively. When subcritical conditions exist (i.e. $U < \beta/k^2$) as in summer, cyclones are found above mountains and anticyclones above valleys. As the flow (U) increases and approaches resonance (i.e. $U = \beta/k^2$) the orographic cyclone is accelerated and large scale effects on the GPLLJ are realized. The implication is that the Rocky Mountains act as a scale transfer mechanism between the larger scale $\overline{U}$ anomalies and the regional GPLLJ response.

To what extent do separate basin climate anomalies influence the GPLLJ? To address this question a Great Plains centered and a remotely based approach is applied. Using the GPLLJ index and meridional wind principal components (PC), contemporaneous and temporal phase lead/lag correlations and regressions to SST's, large scale circulation features, and to the NAO and ENSO indices are examined. To investigate the circulation influence from the remotely based perspective, Empirical Orthogonal Function (EOF) (monthly) and extended EOF (weekly) analysis on separate basin wide SLP anomalies in the Atlantic and Pacific is performed and hydroclimate links to the Great Plains assessed. The analysis shows that there is a significant impact on the GPLLJ from both the Atlantic and Pacific basins supporting the claims for superposition of remote influences in generating the structure of GPLLJ induced hydroclimate variability over the Great Plains.

1.3 Regional Hydroclimate Impacts

The notable GPLLJ induced hydroclimate and the proximity of the GPLLJ to the surface motivates examination of the symbiotic relationships between regional atmospheric circulation (GPLLJ) and land-surface atmosphere interactions in generating Great Plains hydroclimate variability. A natural question to ask is how does evolution of the regional environment influence the atmospheric and terrestrial water balances over the Great Plains? To address this question a comprehensive case study of the evolution of Great Plains hydroclimate anomalies during the warm seasons of 1988 (drought) and 1993 (flood) is undertaken using the most current 27-year NARR pentad data. The primary debate encompassing these two events is whether local land-atmosphere interactions, large scale remotely forced circulation variability, or a delicately balanced combination of the two is responsible for the severe hydrologic conditions over the Great Plains during the summers of 1988 and 1993.

Many authors argued for the primacy of large scale circulation anomalies in generating the flood of 1993 and drought of 1988. Mo and Paegle (1995) attribute the anomalous persistent trough pattern in 1993 over the U.S to a strengthening and eastward extension of the zonal wind maximum over the eastern Pacific Ocean and augmentation of the upper-level jet over the central U.S. Modeling experiments showed that the trough was maintained by the enhanced westerlies impinging on the Rockies through PV conservation similar to the discussion of Byerle and Paegle (2003). These ideas are corroborated by Bell and Janowiak (1995) who noticed that

the main differences in the two events was that the large persistent upper-level trough (ridge) over the U.S during 1993 (1988) pushed the stromtrack south (north) of its mean position. Both studies note the existence of an enhanced GPLLJ during the summer of 1993.

These large-scale circulation anomalies occurred in the midst of significant tropical heating variations. Trenberth and Guillemot (1996) argue that the La Niña of 1988 and the El Niño of 1993 altered the normal distribution of tropical convection, thereby changing the pattern of latent heating and implying a large-scale switch in the anomalous tropical heating and forcing of quasi-stationary atmospheric waves. The role of tropical SST anomalies in forcing the large scale circulation during the summers of 1988 and 1993 is still the subject of much debate as other observational and modeling experiments demonstrate the primacy of internal atmospheric forcing of the midlatitude circulation anomalies associated with these drought and flood events (Liu et. al 1998, Bell and Janowiak 1995).

The role of the land-atmosphere interactions in generating anomalous precipitation through soil moisture induced evaporation anomalies has also been implicated in extreme Great Plains hydroclimate events. While Bell and Janowiak (1995) focus primarily on the large scale circulation aspect of the 1993 flood, they also observed that soil moisture anomalies began during the summer of 1992 and were exacerbated by above normal precipitation during the fall and winter of 1992-93 and that by March of 1993 much of the continental U.S. east of the Rockies exhibited above average soil moisture.

Several important modeling studies were conducted with an eye toward the role of soil moisture conditions and attendant evaporation in generating the hydrologic conditions during 1988 and 1993. Atlas and his collaborators (1993) conducted sensitivity experiments with varying combinations of both SST and soil moisture anomalies and found that while both had an impact on the drought, the soil moisture anomalies were connected to the largest reduction in precipitation and increase in surface air temperature. In examining the flood of 1993 Paegle et. al (1996) found that the primary influence of surface evaporation was to modify the GPLLJ strength over the southern plains. In their experiments the GPLLJ increased for drier southern plains surface conditions.

The horizontal structure of soil moisture anomalies was found to be important for the development of the GPLLJ (Bosilovich and Sun 1999). They argue that region wide dry or wet soil moisture anomalies had a negative impact on LLJ development. However a regional secondary circulation induced by an east-west soil moisture gradient was found to enhance the GPLLJ over the southern plains. Giorgi et. al (1996) demonstrates that local precipitation recycling is not important for the development of either the flood or the drought case. In fact they opine that the dry initial soil moisture conditions at the onset of the 1988 drought would act to increase buoyancy, sustain convection, and increase precipitation, thus providing a negative feedback mechanism to the drought.

These interesting and sometimes conflicting conclusions based on observational and model experiments paint a clouded picture with regard to the role of soil moisture and evaporative influences on the 1988 drought and 1993 flood. There is little debate

that large scale circulation played an important role, however, the controversy revolves around the degree of impact that the land surface controls had on initiating and/or prolonging extreme hydrologic conditions. To illuminate these important concepts with quasi-observational data, the evolution of the regional land surface and circulation anomalies are examined using the state of the art NARR. The temporal phasing of key hydroclimate fields reveals that the primary influence on the GPLLJ, moisture flux convergence, and precipitation anomalies was from large scale processes and not from the land surface, especially during the 1993 flood; as evidenced by a 2-wek delay in evaporation. However, land surface impacts cannot be entirely ignored, as a recurrent mode of monthly GPLLJ variability may be linked to an east-west anomalous soil moisture gradient. The temporal phasing of the pertinent fields in extreme events motivates the use of extended EOF analysis to determine whether the anomalous hydroclimate structure during the warm seasons of 1988 and 1993 are manifestations of recurrent spatio-temporal patterns.

1.4 Research Questions

The research presented addresses the following questions:

- How is the GPLLJ variability linked to larger scale circulation variations? Observation and modeling analyses of warm season circulation variability show coherent stationary wave patterns in the Pacific North American region. Are some of these patterns of consequence for the GPLLJ?

- What is the structure of regional precipitation anomalies associated with GPLLJ variability?

- What are the recurrent patterns of monthly GPLLJ variability? Does the jet-core expand meridionally or zonally? Which of these patterns is of consequence to Great Plains rainfall variability?

- What is the spatio-temporal structure and evolution of the GPLLJ and regional hydroclimate fields during the drought of 1988 and flood of 1993? Are known climate modes linked to the GPLLJ and these two extreme events?

- What is the spatio-temporal sub-monthly evolution of recurrent modes of GPLLJ variability, large-scale circulation and Great Plains hydroclimate?

- How is the GPLLJ represented in a state of the art GCM? How does the GCM representation compare with the observed climatology and variability?

1.5 Data and Methodology

1.5.1 Datasets

To answer the above questions reanalysis datasets with varying characteristics are employed. The primary dataset used in this study is the North American Regional Reanalysis (NARR). NARR is a 28-year (1979-present), consistent, high-resolution dataset that covers the North American domain (Mesinger et. al 2006). The NARR dataset is similar to the original NCEP/NCAR global reanalysis, however includes several improvements. Most of these lend themselves nicely to the study of long-term mesoscale variability and hydroclimate. The most striking difference between the NARR and the NCEP/NCAR reanalysis is the spatio-temporal resolution upgrade; NARR has a 3-hour analysis cycle and 32 km horizontal resolution. There are 13 vertical isobaric levels below 700 hPa, which is ideal for capturing LLJ characteristics.

Additionally, and more importantly, NARR assimilates direct observations of precipitation over land by nudging precipitation, moisture, temperature (diabatic heating) and cloud-water mixing ratio. NARR also takes advantage of the regional ETA model including many of the upgrades that were made to this model and the

data assimilation scheme. Specific among these is the use of the improved version of the Noah land surface model (Ek et. al 2003). While the most significant improvements to Noah have been realized for the winter season, the authors do note a marked improvement in reducing the warm bias in spring and summer. This is attributed to a modification of the bare soil evaporation and soil thermal conductivity formulations that improve low-level humidity values and ameliorate the damped diurnal temperature cycle apparent in the previous Noah realization.

The ERA-40 is a global reanalysis project with output spanning the period September 1957-August 2002 produced at ECMWF. It is comprised of conventional observations and satellite data streams. Analyses were produced at 6 hourly intervals for the entire time period and archived on a 2.5° longitude x 2.5° latitude horizontal grid. There are 23 vertical isobaric levels from 1000 hPa to 1 hPa with 12 levels below 150 hPa. This dataset is especially useful here for its long record and global coverage enabling the global circulation features related to GPLLJ variability to be diagnosed.

The sea level pressure (SLP) pressure variability analysis in chapter 4 is undertaken using the NCEP/NCAR reanalysis dataset (Kalnay et al 1996). This global reanalysis comprises the longest homogenous data record dating back to 1949. While the 5.0° x 2.5° resolution is the most coarse of all three reanalysis datasets, the long term record presents the best choice for determining stable large scale climate variability patterns, especially when using type 1 (i.e., densely observed) fields such as winds and geopotential heights.

Due to varying degrees of online data availability at the time of the investigations some analyses may use different data record lengths. For instance the monthly NARR data used in chapters 2 and 3 is largely comprised of the years 1979-2002, while the pentad analysis of chapters 5 and 6 benefits from a recently constructed 27-year NARR record produced at the Department of Atmospheric and Oceanic Science, University of Maryland.

1.5.2 Data Analysis Techniques

The strategy and methodology used in these studies is largely rooted in applied statistical techniques. Climatological analysis using monthly and pentad averages of global and regional circulation (i.e., winds and geopotential height etc.) and land surface features (i.e, precipitation and evaporation etc.) define the mean state. Field anomalies, defined as the departures from the long term mean climate state are used for more advanced techniques such as lead/lag linear regression, correlation, and regular and extended Empirical Orthogonal Function (EOF) analysis.

Much of the linear association between important field variables is established through traditional forms of correlation and regression. The correlation and regression coefficients are defined as follows:

$$\text{Correlation} = \frac{\sum_{i=1}^{n} A'B'}{\sqrt{\sum_{i=1}^{n} A'^2}\sqrt{\sum_{i=1}^{n} B'^2}} \qquad \text{Regression} = \frac{\sum_{i=1}^{n} A'B'}{\sqrt{\sum_{i=1}^{n} A'^2}}$$

Where A′ and B′ are the index anomalies or principal component time series and field anomalies of interest respectively. The absence of the standard deviation of B′ in the

denominator of the regression renders the units of that field intact, whereas the correlation is unitless and describes the degree of linear association between the two variables. While correlation and regression techniques identify linear association and possible cause and effect relationships they are not efficient at separating preferred modes of variability. Given the interest here to diagnose recurrent variability patterns, a more comprehensive technique is needed to address the questions driving this research.

EOF analysis is a data reduction technique that allows the most recurring variability patterns in a dataset to emerge. This technique and its many forms are widely used in atmospheric sciences and related disciplines. The first step is to construct the anomaly matrix weighted by the cosine of latitude. The cosine weighting is necessary to take into account the increased density of data points as the longitudes converge towards the poles. The covariance matrix is then formed and reduced to the simple eigenvalue problem by constraining the data to express the maximum amount of variance. This eigenvector representation is robust in that maximum variability may be gleaned by selecting, in order, the eigenvectors associated with the largest eigenvalues of the covariance matrix. For a detailed explanation and derivation please see Kutzbach (1967).

This common EOF procedure is computationally intensive and a powerful method has been developed to circumvent this burden. Singular Value Decomposition (SVD) is a more tractable technique that allows the eigenvalue problem to be derived directly from the anomaly matrix, which has the same dimensions as the original data. This technique and its derivation can be found in appendix A of Nigam and Shen

(1993.) For this thesis research the International Mathematical and Scientific Library (IMSL) of FORTRAN routines were used in the SVD analysis.

The extended empirical orthogonal function (EEOF) analysis is a powerful technique for extracting spatio-temporal recurrence (Weare and Nasstrom 1982); not just spatial or temporal, as in traditional EOFs. The additional focus on temporal recurrence yields spatially *and* temporally coherent patterns, generating insights into antecedent/subsequent phases; and thus modal evolution and mechanisms. The technique's emphasis on evolution obviates the need for data pre-filtering because similar-looking, overlapping patterns that evolve differently can now be easily separated. Also, the pre- and post-mature phase patterns identified from EEOF analysis needn't bear any resemblance to the mature-phase structure; the case (and limitation) in lead/lag regression analysis.

The technique is a straightforward extension of EOF analysis, except for the new anomaly definition: Anomalies at time $t=t_o$ are no longer field snap-shots at that time, i.e., $\psi(x,y,t_o)$, but a snap-shot *sequence* centered at $t=t_o$. For a 5-member sequence, for example, the anomaly at $t=t_o$ is a composite of 5 spatial patterns that are staggered in time: $[\psi(x,y,t_o-2\Delta t), \psi(x,y,t_o-\Delta t), \psi(x,y,t_o), \psi(x,y,t_o+\Delta t), \psi(x,y,t_o+2\Delta t)]$. The interval, Δt, is chosen so that the temporal sequence covers a significant portion of the variability episode. Note, that there is no imposition of any periodicity here, unlike some other methods that target evolution.

1.5.3 Diabatic Heating Diagnosis

Diabatic heating is a key forcing because of its substantial influence on the tropical and extratropical circulations, but it is, unfortunately, not an observable

quantity. It must therefore be diagnosed from other atmospheric observations, and is thus prone to estimation uncertainties. The 3D diabatic heating is diagnosed from ERA-40 as a residual in the thermodynamic equation (e.g., Nigam 1994) using the analyzed vertical velocity (ω):

$$\overline{Q} = \frac{\Delta T}{\Delta t} + \bar{\vec{v}} \cdot \vec{\nabla}\overline{T} + (p/p_o)^{(R/C_p)}\overline{\omega}\frac{\partial\overline{\Theta}}{\partial p} + (p/p_o)^{(R/C_p)}[\vec{\nabla} \cdot \overline{\vec{v}'\Theta'} + \frac{\partial(\overline{\omega'\Theta'})}{\partial p}]$$

Here, the over-bar denotes the monthly average and prime the departure of the 6-hourly analysis from the monthly average. Residual diagnosis however does not provide information about the constituent sensible, latent, and radiative heating components, but partitioned heating components are available, at least from the 6-hour NCEP model forecasts starting from each time-step's reanalyses. (We have not found corresponding fields in the NARR public archives, but that is not to say that they cannot be obtained from NCEP's internal NARR archives.) Diabatic heating is diagnosed with and without mass-balancing, to ascertain the impact of this procedure; we found minimal impact in the ERA-based diagnosis. The credibility of heating estimates can, of course, only be gauged by the extent of their dynamical consistency with the large-scale circulation, i.e., through diagnostic modeling.

1.5.4 Thesis Organization

Chapter 2 examines the monthly variability structure of the GPLLJ and large scale circulation from a Great Plains centric viewpoint. Chapter 3 shows the preferred modes of GPLLJ variability and precipitation links through EOF and PC analysis. Interesting patterns related to anomalous Great Plains hydroclimate emerge. Chapter

4 takes a remote basin centric view of Great Plains summertime circulation and precipitation variability through EOF and EEOF analysis of Atlantic and Pacific basin SLP anomalies and their regional GPLLJ and precipitation footprints. Chapter 5 is a detailed analysis of the regional hydroclimate anomalies during the drought of 1988 and flood of 1993. The temporal phase relationships to various hydroclimate fields are discussed. Chapter 6 is an EEOF analysis of pentad resolution Great Plains hydroclimate. This analysis, motivated by the results from chapter 5 enables the preferred modes of spatio-temporal evolution of the GPLLJ and circulation, evaporation, surface air temperature, soil moisture, and precipitation fields to be discerned. Chapter 7 evaluates the ability of atmospheric GCMs in representing GPLLJ variability. The models can represent the climatology with some fidelity, however are severely challenged in representing the intraseasonal and interannual variability. The concluding discussion and future research direction follow in chapter 8.

1.6 Chapter 1 Figures

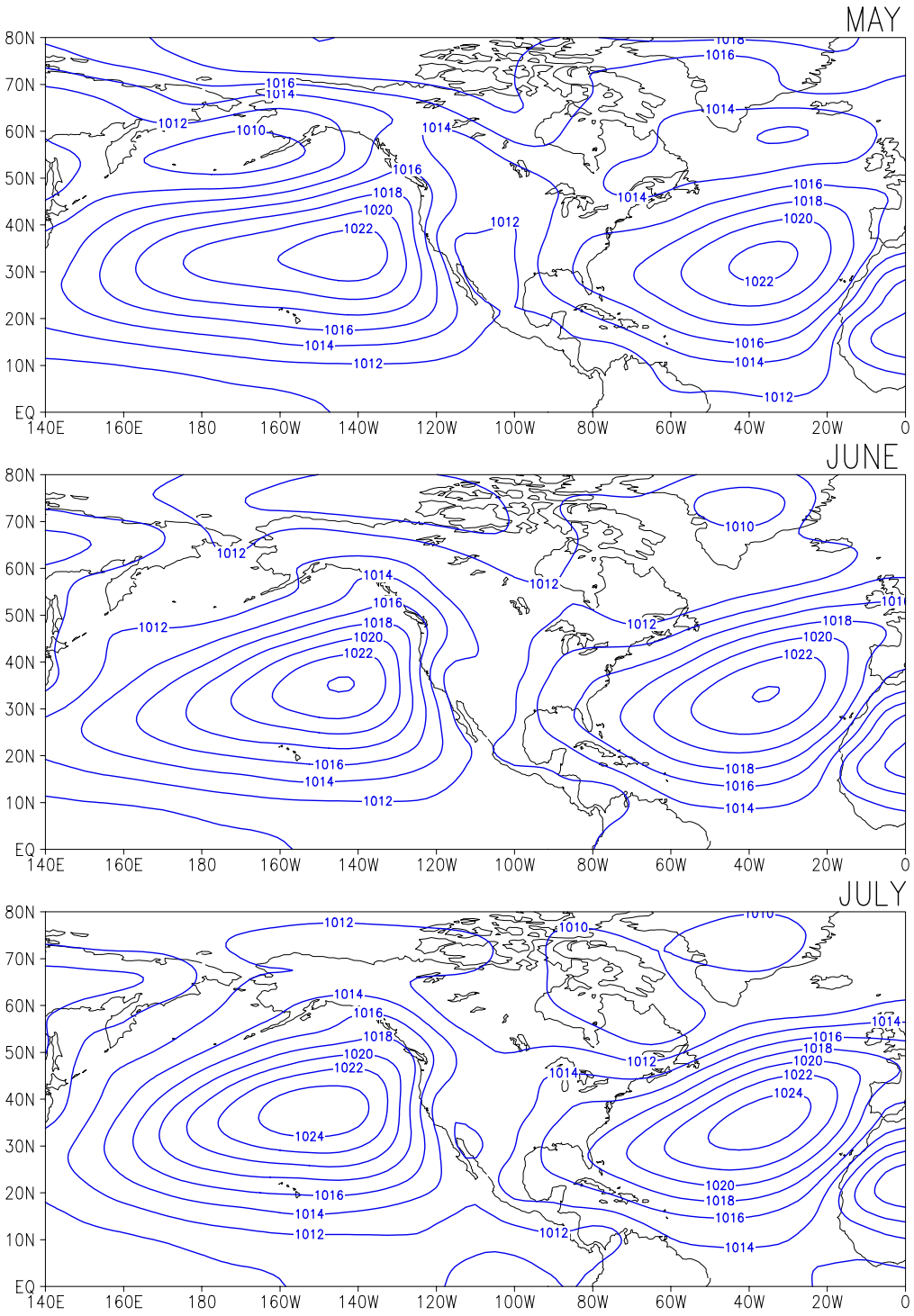

Figure 1.1 Warm season climatological monthly mean Sea Level Pressure (SLP) from the NCEP reanalysis (1949-2001).

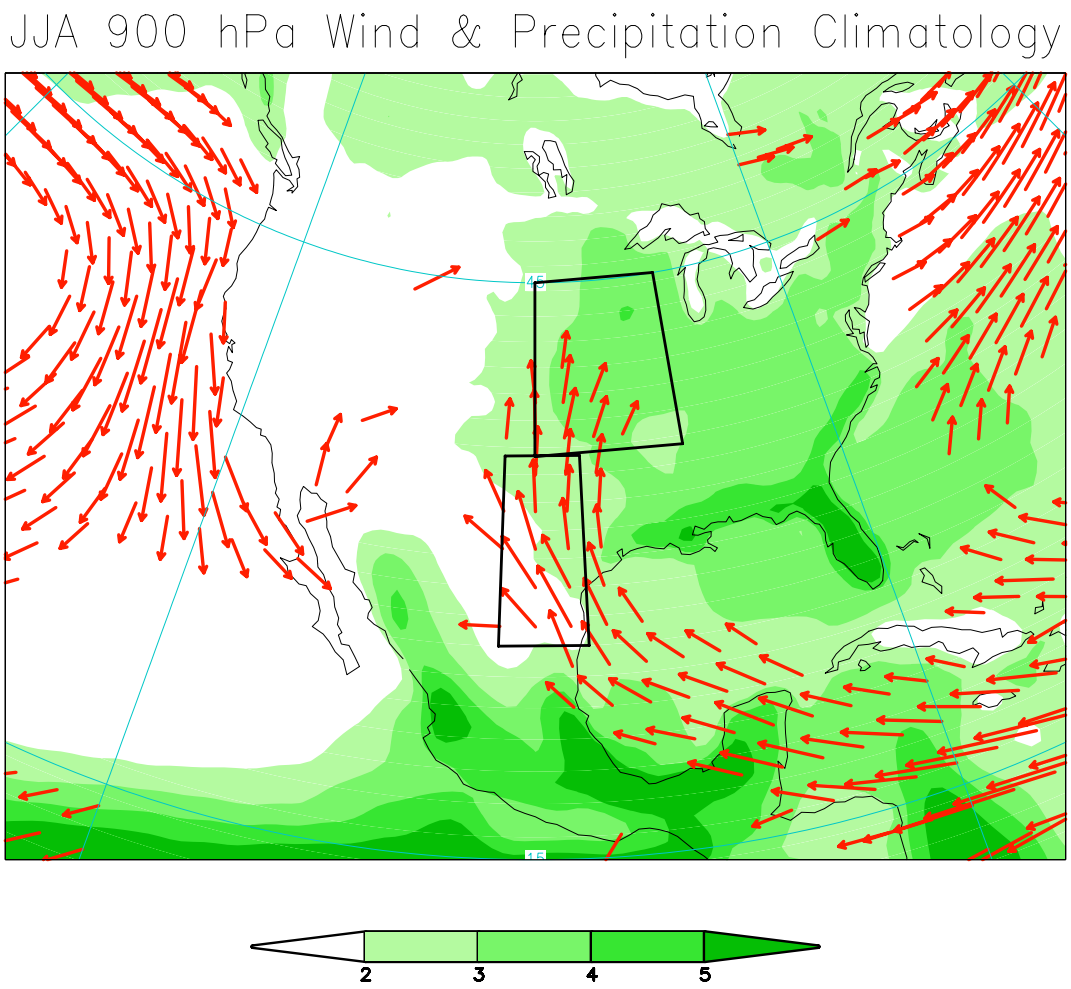

Figure 1.2. Seasonal climatology (JJA) of precipitation (shaded) and the Great Plains low-level jet as reflected in the 900 hPa meridional winds (arrows) in the North American Regional Reanalysis from 1979-2005. The northern and southern boxes outline the areas defined by the Great Plains precipitation and low-level jet indices respectively. Winds > 4 m s^{-1} are displayed and precipitation > 2 mm day^{-1} is shaded.

Chapter 2: Monthly Index Based Variability

2.1 Low Level Flow Climatology

2.1.1 Jet Profile

Longitude-height cross-sections of monthly meridional wind at 25°N and 30°N are shown in Figure 2.1, for May, July and September. Significant vertical wind shear is present above the jet core at both 25°N and 30°N, except in September. The jet maximum increases with the advance of the warm season, peaking in July at both latitudes. The jet core is located between 900-950 hPa at 25°N but somewhat higher (900-850 hPa) at 30°N. The core is tightly packed at 25°N, likely, because of steep topography to the west. Topography is known to impact the jet structure from generation of shallow baroclinicity on its slopes (e.g., Zhang et al. 2006). At 30°N, the core has shifted to the west and exhibits a more gradual eastward-downward slope, reflecting the underlying terrain slope and related thermal attributes. The seasonal demise of the LLJ in August-September is gradual at 30°N, but notably precipitous at 25°N.

2.1.2 Diurnal Cycle

Figure 2.2 displays longitude-height cross sections of the July meridional wind (contoured) and temperature (dashed) fields at the time of minimum (4PM CDT) and maximum (7AM CDT) jet magnitude.[1] The late afternoon to early morning development in jet speed and extent is striking. Previous studies have noted a nighttime doubling of wind speed (e.g., Stensrud 1996), and while NARR does not

[1] A monthly rendition of diurnal variability is generated by averaging each diurnally stamped data across all the month days; for example, from a 31-day average of 7AM July data, and so on.

generate quite a doubling in the monthly-averaged diurnal-cycle at 25°N (from 6 m/s to 9 m/s), it does so at 30ºN (from 4 m/s to 9 m/s). The average over all eight 3-hourly NARR time steps in July was shown earlier (middle panels in figure 2.1), and is evidently closer to the 7 AM monthly mean, especially at 25°N. This suggests that the monthly-mean jet remains strong across many of the 8 time steps, and that diurnal variability of the jet increases with latitude.

The thermal structure shows significant diurnal variations, much as anticipated: Isotherms slope steeply toward the plains in the afternoon but not in the early morning when a warm dome of air is present along the eastern slopes above the 950 hPa level. Although tempting, one must refrain from verifying the thermal-wind balance between $\partial V/\partial z$ and $\partial T/\partial x$ in figure 2.2. The extent to which geostrophic balance, and thus thermal-wind balance, hold at sub-synoptic scales of the GPLLJ and in the planetary boundary layer (PBL) region is unclear; and under investigation. Should the thermal-wind balance be applicable, the eastward down-sloping isotherms in figure 2.2 would imply a northerly thermal wind, and thus a diminished GPLLJ at upper levels; more diminished in case of steeper isotherms, in accord with depicted diurnal variations, especially at 25°N. Note, the isotherms are not only less steep during early morning, but their east-west gradient changes sign below 950 hPa in the vicinity of topography. The location of the jet-core near this level is again, not inconsistent with thermal-wind balance considerations.

2.1.3 Meridional Water Vapor Flux

The primary impact of the GPLLJ on hydroclimate is through northward column moisture transport from the Gulf of Mexico, and its subsequent convergence in the jet

exit region. A benefit to viewing the climatological jet in terms of column fluxes is two fold: The variable vertical range of the jet-core is accounted for by the vertical integral, and the jet's influence on hydroclimate of the Great Plains is readily apparent.

Figure 2.3 displays the column integrated NARR meridional moisture flux in spring and summer months. Enhanced fluxes are present in several regions: Modest inflow from the Gulf of Mexico begins in spring and increases through early summer, reaching a peak of 200 kg $m^{-1}s^{-1}$ over northeastern Mexico in July, when its reach into the southern and central Great Plains is greatest. Moisture fluxes associated with monsoonal flow over southwestern United States in late summer, especially, the Gulf of California low-level jet,[2] are captured nicely as are the northward fluxes associated with the westward flank of the Bermuda high, which skirts the eastern seaboard in boreal summer months.

This meridional moisture flux view of the GPLLJ is consistent with its meridional wind based depiction (cf. figure 2.1), in that the jet-core is located at ~25°N with a northwestward tilt in both descriptions. If meridional fluxes over northeastern Mexico and south-central U.S. are primarily due to the GPLLJ, then these fluxes must exhibit diurnal variability akin to the jet. Figure 2.4 shows the diurnal cycle of the monthly and vertically integrated meridional moisture flux in NARR for May, July, and September; as diagnosed from harmonic analysis. The arrow-length indicates flux-magnitude while the direction denotes the time of day when the flux is a maximum. For example, an arrow pointing due north indicates a flux-maximum at 6 AM CDT.

[2] It is interesting that the northward moisture flux associated with the Gulf of California low-level jet is maximum full 1-2 months after the GPLLJ related flux attains its peak.

The diurnal amplitude of the northward moisture flux is evidently strongest in July over both land and water. Over the Gulf of Mexico (and California) and over the southern tier states, the northward flux is strongest at midnight, but fluxes over central United States and the eastern seaboard are maximum in the wee hours of the morning (~6AM CDT). The reason for clockwise veering of the arrows with increasing latitude over the southern Great Plains is noted with interest. The diurnal cycle of meridional moisture flux has its origin in the diurnal variability of low-level meridional winds; diurnal variability of specific humidity was ascertained to be negligible.

2.2 Low Level Jet Index

2.2.1 Index Definition

To facilitate analysis of GPLLJ variability, an index is constructed from areal averaging of the meridional wind in a 5ºx10º longitude-latitude box (102°W-97°W; 25°N-35°N). The box is chosen to encompass the core sectors of the meridional wind and moisture flux climatologies, including many local maxima.[3] The wind vertical level in index definition is chosen after inspection of the vertical profile of the box-averaged meridional wind.

Figure 2.5 shows the April-August NARR profiles and the July ERA-40 profile, all of which exhibit the classic low-level jet structure. The coarser vertical resolution (75 hPa) ERA-40 data places the wind maximum at 850 hPa and is a bit challenged in

[3] The sensitivity to longitudinal averaging was assessed by computing correlations of indices generated using slightly shifted boxes; correlations are ~0.95. Note, the coarser resolution Bonner (1968) GPLLJ climatology indicates 95-100W as the sector of maximum meridional winds, i.e., very close to the longitude range identified here.

depicting vertical shear, especially in comparison with the 25 hPa resolution NARR data. The NARR southerly flow is strongest at 900 hPa in all months, which helps with the choice of level in index definition. The southerly jet is especially strong in May, June, and July, and thus only these months (MJJ) will be considered in the following interannual variability analysis. The GPLLJ index is finally defined as the box-averaged 900 hPa meridional wind. A similarly defined precipitation index is used to facilitate connections to Great Plains precipitation. The area averaged precipitation in the 90°W-100°W and 35°N-45°N box is used here as in RBN (2005).

2.2.2 Index Variations

Figure 2.6 plots the GPLLJ index *anomalies* from ERA-40 and NARR datasets. The top two panels show the ERA-40 index anomalies; the display period is broken into two panels to facilitate comparison with the NARR index anomalies (bottom panel) in the overlapping data period (1979-2001)[4]. The GPLLJ index has substantial intraseasonal variability, switching sign in 28 of the 40 ERA-40 summers. During the common period, the ERA-40 index exhibits 16 sign changes as opposed to 14 in NARR. Monthly indices in NARR and ERA-40 are strong and reasonably consistent. The monthly standard deviation is 0.98 in ERA-40 and 1.20 in NARR, and the common period correlation is a robust 0.97, indicating remarkably similar representation of GPLLJ variability in modern global and regional reanalyses. The May-July (July only) GPLLJ and Great Plains precipitation indices are correlated at 0.55 (0.71).

[4] The ERA-40 index was computed using the 925 hPa winds, i.e., winds at the closest archive level to 900 hPa.

An interesting feature of the GPLLJ index is its characterization of the 1988 drought and 1993 floods. The index is most negative in the overlapping period in June 1988; note, a negative index denotes a weakened GPLLJ and reduced northward moisture flux. On the other hand, the index is large and positive in 1993 June and July; indicating a stronger jet and related moisture transports.[5]

Interannual variability of the index is highlighted by the superposed bold lines in figure 2.6, which were generated by a 1-2-1 smoothing of the seasonal (MJJ) index anomalies. Focusing on lower frequencies, the GPLLJ exhibited a maximum in early 1960s followed by a weakening trend until the 1980's. The jet was weakest in 1988 and has been gradually strengthening since then.

2.3 GPLLJ's Circulation and Hydroclimate Links

Indices are a widely used simple statistic for characterizing regional variability, and links with other variables and regions. The GPLLJ index is used in developing a comprehensive view of regional climate variability related to jet variations, through computation of index regressions during the MJJ months; a period in which jet variability is fairly uniformly distributed: Standard deviation of the May, June and July GPLLJ index is 1.32 m/s, 1.09 m/s and 1.08 m/s. Precipitation variability is also uniformly distributed in these months: The Great Plains precipitation index standard deviations are 1.1 mm/day, 1.09 mm/day and 1.08 mm/day, respectively.

Although the circulation and precipitation standard deviations are fairly uniformly distributed in MJJ months, the circulation-precipitation links are generally manifest in June and July, e.g., the notable GPLLJ anomalies in May of 1962 and

[5] It is interesting to note that the extremely high index value in 1996 was not coincident with an anomalously wet summer (cf. figure 3a in RBN 2005).

1996 (cf. figure 2.6) are not associated with significant hydroclimate episodes. In contrast, jet anomalies in June 1988 and July 1993 are both linked with notable precipitation anomalies. With July exhibiting maximum GPLLJ amplitude and significant interannual variability, and given that July has historically represented summer conditions, an expansive view of LLJ variability is developed from the July index regressions. The July regressions however need not be characteristic of other summer months for various reasons, including the dependence of climate teleconnections on the seasonally evolving background flow.

2.3.1 Precipitation Links

Index regressions on the 900hPa NARR meridional winds are shown in figure 2.7a. Southerly anomalies are present over the central U.S., with maximum values along the northeastern edge of the index box, indicating a slight eastward (westward) shift of the strengthened (weakened) GPLLJ. Jet intensification is also accompanied by northerly anomalies off the west and east coasts of Canada; indicating that jet modulation occurs in context of continental-scale circulation anomalies. The index regressions on NARR and ERA-40 precipitation are shown in figures 2.7*b* and *d*, respectively. The precipitation regressions differ considerably in magnitude; not surprisingly, since NARR assimilates observed precipitation while ERA-40 generates its own from a forecast. The jet strengthening is associated, not surprisingly, with positive precipitation anomalies (~1.5 mm/day) in the jet-exit region, where climatological precipitation is ~3 mm/day; the precipitation anomaly is thus quite significant. The downstream location of the precipitation anomaly is consistent with previous studies showing low-level convergence and ascending motions in the jet exit

region. Oppositely signed but smaller anomalies are present over the southeastern states and the Gulf of Mexico.

Due to the short 24-year record of NARR it is possible that the extremely anomalous GPLLJ and related precipitation in 1993 may be inducing a misrepresented precipitation regression. To test the sensitivity to the events of 1993 the GPLLJ index was scaled by 0.5 in July 1993 and the regressions were recomputed. A modest 0.2 mm/day reduction in the maximum was noted still leaving a large anomaly intact.

2.3.2 Circulation Links

The GPLLJ index regressions on 200 hPa geopotential height and SLP are shown in Figs. 2.7c,e; the regressions are on ERA-40 data.[6] The height regressions show a coherent wave pattern over the North Pacific-North American region and over the midlatitude Atlantic. The pattern suggests that GPLLJ can be influenced by the hemispheric-scale summertime teleconnection patterns, assuming robust lower tropospheric extensions of these upper-level anomalies; the case, given the structure of sea-level pressure regressions. Regressions obtained from the June index (not shown) contain similar patterns except for the sign of the height and SLP anomalies in the western Pacific and Atlantic basins. Aspects of the remote influence are thus somewhat sensitive to the choice of the month, but not the three-cell height pattern of consequence for the GPLLJ: The one with centers over eastern north Pacific, western North America, and southeastern U.S., which is present in all summer month regressions.

[6] The ERA-40 fields are used here in order to identify the hemispheric scale linkages; something not feasible with regional NARR data.

It is noteworthy that this height pattern bears strong resemblance to the summertime stationary wave pattern forced by western Pacific diabatic heating (along with secondary interaction with North American orography) in a linear baroclinic model and a GCM (Ting 1994). Specifically noted was an orographically forced wave train (an alternating high-low-high pattern) emanating from the Rockies, with downstream extensions over the southeastern U.S and the North Atlantic. An enhancement of this very feature is seen in the panel *c* regressions. The observed 200 hPa height anomalies in the North Pacific-North American region during the notably wet Midwest summer of 1993 (cf. figure 2.3 in Liu et al. 1998) are almost identical to those shown in figure 2.7c, except for the amplitude differences.

The sea-level pressure associated with GPLLJ variability (panel *e*) shows a coherent pattern in the North Pacific-North American region similar to the overlying 200 hPa height pattern (panel *c*). This equivalent barotropic structure of the anomalies – a characteristic feature of the far-field (i.e., far from the wave source) stationary wave response (e.g., Held 1983) – in the North Pacific-North American region argues for the significance of remote forcing of GPLLJ variability. The GPLLJ related anomalies in the Atlantic also exhibit equivalent barotropic structure, not withstanding the weak 200 hPa high over northeastern Canada.[7]

2.3.3 NAO Links

Sea-level pressure anomalies in the Atlantic also exhibit coherent structure, but one reminiscent of the North Atlantic Oscillation (NAO) in winter. Given that the NAO is a robust mode of winter variability, most studies have focused on

[7] The positive height anomalies are not fleshed out in this region, perhaps, because the 200 hPa level is above the tropopause here.

characterizing NAO structure and impacts during this season; including index development to mark winter NAO variability. The variability is however not confined to the winter season: Sea-level pressure variability with meridional-dipole structure in the extratropical Atlantic basin, closely mimicking the NAO winter structure, is manifest in other seasons, too, including summer; as here. NAO variability in summer was also recently noted in context of Great Plains hydroclimate variability (RBN 2005).

Monitoring NAO variability in seasons other than winter is however not straightforward. The canonical NAO index (e.g., Hurrell 1995) cannot be indiscriminately used as it is based on the structure of winter sea-level pressure variability. Although a summer NAO index can be developed employing the strategy used for the winter index, a 700 hPa geopotential-based NAO index is used for comparative analysis here. The index was developed at NOAA's Climate Prediction Center from EOF analysis of height variability in summer (http://www.cpc.ncep.noaa.gov/data/teledoc), and as such, appropriate for use here; in addition to being readily available.

The link between GPLLJ and NAO variability, suggested by SLP regressions in figure 2.7e, is reexamined, this time from the NAO perspective. The NAO's influence on GPLLJ and regional hydroclimate is directly assessed in figure 2.8, from regressions of the July NAO index. The sea-level pressure footprint is shown first (top panel), and is evidently very similar to the GPLLJ index regressions in the Atlantic (figure 2.7e); pattern correlation in the American-Atlantic sector (20-70N, 250-360W) is −0.8, supporting the claim of linkage between GPLLJ and NAO

variability. The linkage is probed further via NAO index regressions on NARR meridional wind and precipitation fields. The regressions exhibit cohesive structure that is strikingly similar to that found in GPLLJ index regressions (figures 2.7 a-b); except for the sign. It is interesting that while the NAO influence on the GPLLJ is modest (~0.5 m/s, i.e., about half the amplitude of that in figure 2.7a), its influence on Great Plains rainfall (~1.2 mm/day) is substantial and comparable to that in figure 2.7b.

Despite considerable correspondence between the GPLLJ and NAO index regressions, the two July indices are temporally correlated at –0.46, i.e., rather modestly. The reason for this is not entirely clear but the possibility that the GPLLJ index reflects a superposition of variability modes (as it must) not all of which are hydroclimate sensitive is currently being investigated. Notwithstanding this concern, this section's analysis buttresses our claim of significant links between NAO summer variability and Great Plains hydroclimate. Dynamically, the link is fostered by modulations of the most prominent feature of the Atlantic's summertime sea-level pressure distribution, the Bermuda High (see RBN 2005).

2.3.4 Diabatic Heating Links

Although coherent wave patterns in the Pacific and Atlantic sectors in figures 2.7-2.8 make the case for remote forcing of GPLLJ variability, the nature/location of forcing that generate these wave patterns (and GPLLJ variability) remains to be elucidated. The forcing is examined in figure 2.9 from GPLLJ index regressions on July's diabatic heating. Vertically averaged diabatic heating is shaded in figure 2.9a while the Rossby wave source is contoured. Significant heating anomalies are present

in the western-central (and eastern) tropical Pacific as well as over Central America and the Gulf of Mexico. The heating anomalies, including diminished heating over Nordeste, resemble heating distribution in the post-El Niño summer. Characteristic ENSO heating distributions are, unfortunately, available mostly for winter (Nigam et al. 2000). Characteristic ENSO precipitation, from which tropical diabatic heating anomalies can be inferred, is however available for all 4 season in a web-supplement of Joseph and Nigam (http://www.atmos.umd.edu/~nigam/renu/main_frame.htm; 2006). Inspection of the DJF Niño3 regressions on the following JJA precipitation reveals some similarity with the figure 2.9a heating distribution.

Although tropical heating is the progenitor of significant climate anomalies across the globe, the underlying circulation teleconnections are dynamically instigated not directly from regions of deep tropical outflow but from adjacent subtropical ones determined by the Rossby wave source (RWS, Sardeshmukh and Hoskins 1988). The Rossby wave source, as the name implies, is the source or forcing term for Rossby waves in the barotropic vorticity equation.

The RWS contains terms involving divergent flow: RWS= $-\nabla\bullet(v'_\chi\ \zeta_c)\ -\nabla\bullet(v_{\chi c}\ \zeta')$, where v_χ is the divergent component of the wind, ζ is the absolute vorticity ($\eta+f$), and primes and subscript 'c' denote anomaly and climatology, respectively. The first term on the RHS is generally dominant and can be expressed as the sum of a tropical ($-v'_\chi\bullet\nabla\zeta_c$) and extratropical ($-\zeta_c\nabla\bullet v'_\chi$) RWS component (e.g., Qin and Robinson 1992). Given the meridional reach of tropical divergent outflows (v'_χ), the RWS can be large thousands of kilometers northward of an equatorial diabatic heating anomaly,

especially, in the western Pacific sector, where meridional vorticity gradients ($\nabla\zeta_c$) are large in the extratropics due to the presence of the Asian-Pacific jet.

The 200 hPa absolute vorticity and divergent winds are shown in figure 2.9b. The equatorial divergent outflow centers in the western and eastern Pacific basin, coincident with positive diabatic heating anomalies, stand out. The wave sources arising from these outflows are prominent features in the northern subtropics of the top panel: the negative RWS in the western-central Pacific and Central American longitudes. Note, the RWS distribution in the middle and high latitudes is part of the quasi-geostrophic response itself, and as such, not insightful about the wave emanation (or source) regions.

What does the RWS analysis tell us about remote forcing of the GPLLJ height regressions? Inspection of the RWS distribution suggests that both of the negative sources noted above are influential in instigating the July height regression pattern (figure 2.7c). While the height regression structure, itself, is not suggestive of these links, this is not surprising since geopotential is not a variable of choice in tropical-extratropical teleconnections analysis; since height gradients are very weak in the Tropics on account of the smallness of the Coriolis parameter there. As such, streamfunction is often used in lieu of the geopotential, or one can simply compute height correlations (and not regressions). The height correlations (figure 2.9c) are much more strongly suggestive of tropical links, especially, in the longitudinal sectors of the above noted RWS sources.

The Great Plains Low-Level Jet thus appears susceptible to remote influences, including those originating in the western-central subtropical Pacific; in addition to

the more local ones originating to the south. Although specific attribution is beyond the scope of this diagnostic study, Ting's (1994) analysis of the influence of Pacific SST anomalies, and Ding and Wang's (2005) and Lau and Weng's (2002) recent analyses linking Great Plains precipitation with teleconnection patterns emanating from tropical Pacific and Asian regions are insightful in this regard.

2.3.5 SST Links

The July GPLLJ index correlations on SST are shown in figure 2.10. The contemporaneous ones are displayed in the bottom panel, while the somewhat stronger antecedent ones are in upper panels. Both Pacific and Atlantic basins exhibit large regions of 0.3-0.4 correlations. The SST evolution, not surprisingly, is quite similar to that associated with July's Great Plains precipitation index (cf. figure 10 in RBN 2005). Notable evolution features include the meridional broadening of equatorial SST anomalies over time. SST evolution in the Atlantic is however less coherent as evident from the complete sign reversal in the extratropical basin between May and July.

Although Pacific SST anomalies cannot be characterized with certainty, several features of the contemporaneous pattern, including tropical focus, resemble the post-mature ENSO phase, i.e., the SST anomaly pattern in the summer following El Niño's winter peak-phase (cf. Guan et al. 2007). Some contribution from other modes of Pacific SST variability, including decadal ones, cannot be ruled out though, given the short record. The longitudinal distribution of the heating anomalies in the tropical Pacific (figure 2.9a) is in accord with the underlying July SST distribution; recalling the warm-west and cool-east Pacific SST climatology, which introduces a westward

bias in the position of diabatic heating (and rainfall) anomalies vis-à-vis SST anomalies; given the SST-threshold for occurrence of deep convection (e.g., Graham and Barnett 1987).

2.3.6 Subseasonal vs. Interannual Regression Contributions

The GPLLJ index exhibits both subseasonal and interannual variability. The sign-change of the index in most summers suggests that subseasonal variability will make a significant contribution to index regressions. This subseasonal contribution was ascertained from regressions of a modified GPLLJ index; the modification involved subtracting the seasonal (May-July) anomaly from each month of that season. Regressions of the modified index are very similar to those displayed in figure 2.7, and thus not shown. The similarity reflects the dominance of subseasonal influence in index regressions, especially, in regional fields, e.g., the subseasonal contribution to GPLLJ and Great Plains precipitation variability (figure 2.7a-b) is ~80%. The contribution to upper-level height and sea-level pressure regressions in the Pacific longitudes is not as overwhelming, though. While the subseasonal-interannual apportioning of the response is helpful, it does not, necessarily, convey the relative importance of forcing at these timescales, e.g., ENSO SSTs can elicit a subseasonal response from monthly evolution of the background flow (e.g., Opsteegh and Van den Dool 1980).

2.4 Chapter 2 Figures

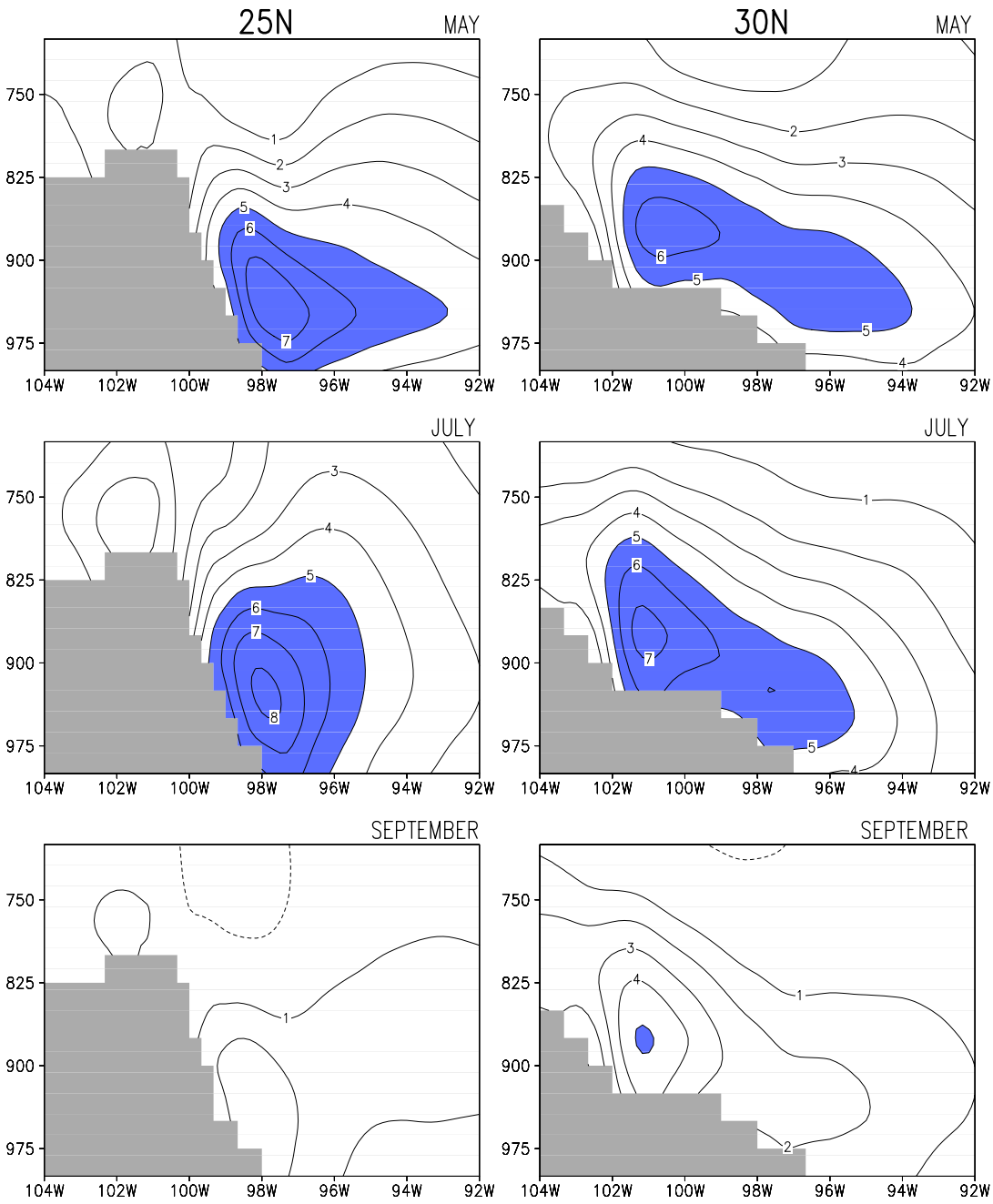

Figure 2.1. Seasonal evolution of the Great Plains Low-Level Jet. Meridional wind at 25° N (left column) and 30° N (right column) in the North American Regional Reanalysis (NARR) at approximately .3° x .3° horizontal and 25 hPa vertical resolution. Contours > 5 m s^{-1} are shaded. Topography is blocked out.

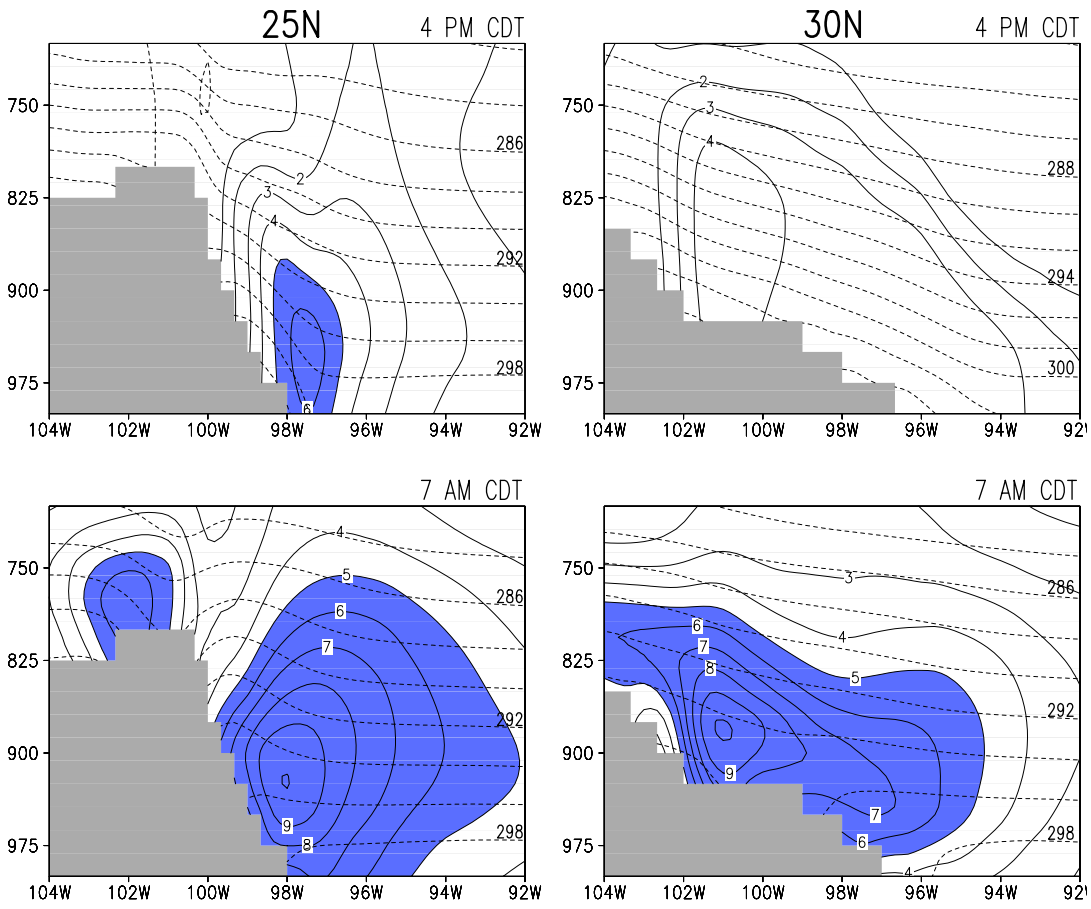

Figure 2.2. Diurnal variability of the Great Plains low-level jet in July. Meridional wind (solid) and temperature (dashed) at 25° N (left column) and 30° N (right column) for 4PM LT and 7AM LT in NARR. Contour intervals are 1 m s^{-1} and 2K. Contours > 5 m s^{-1} are shaded. Horizontal and vertical resolution is the same as fig. 2.1.

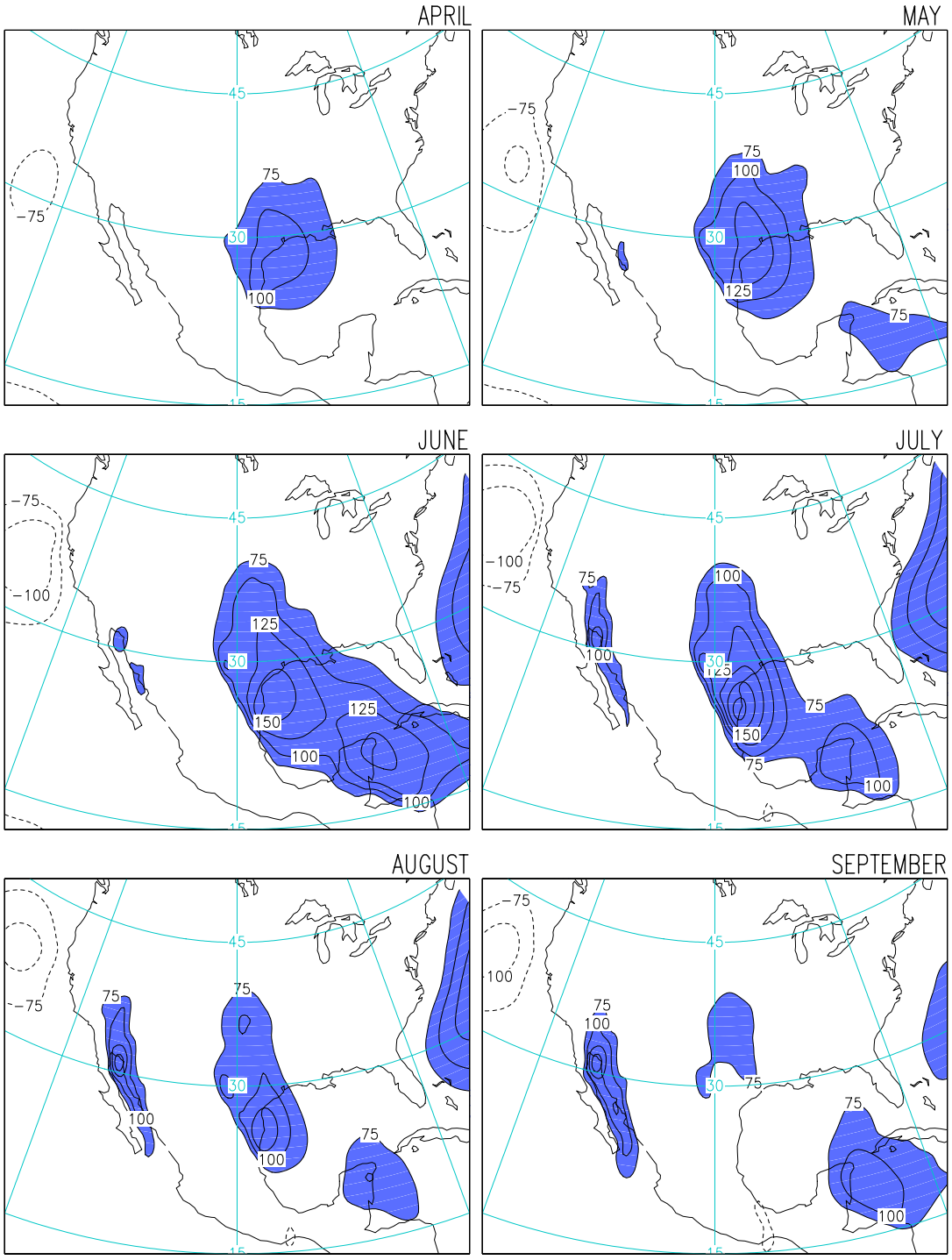

Figure 2.3. Seasonal evolution of the column integrated meridional water vapor flux in NARR. Contour interval is 25 kg m $^{-1}$ s $^{-1}$ and values in excess of 75 kg m $^{-1}$ s $^{-1}$ are shaded.

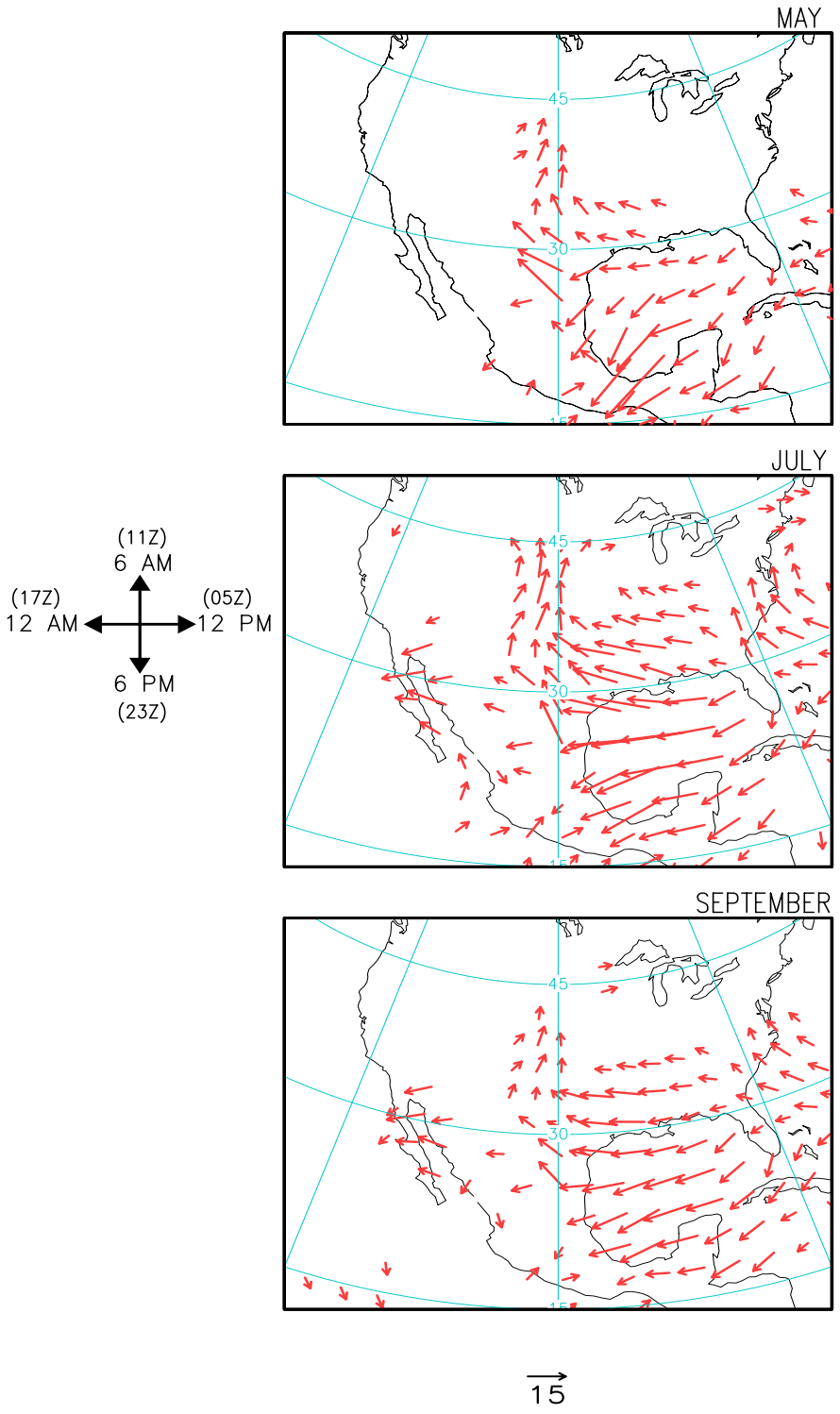

Figure 2.4. Seasonal evolution of the diurnal amplitude and phase of the column integrated meridional water vapor flux in NARR. Units are kg m^{-1} s^{-1}. Direction of the arrow determines local time of maximum amplitude. Arrow length denotes magnitude.

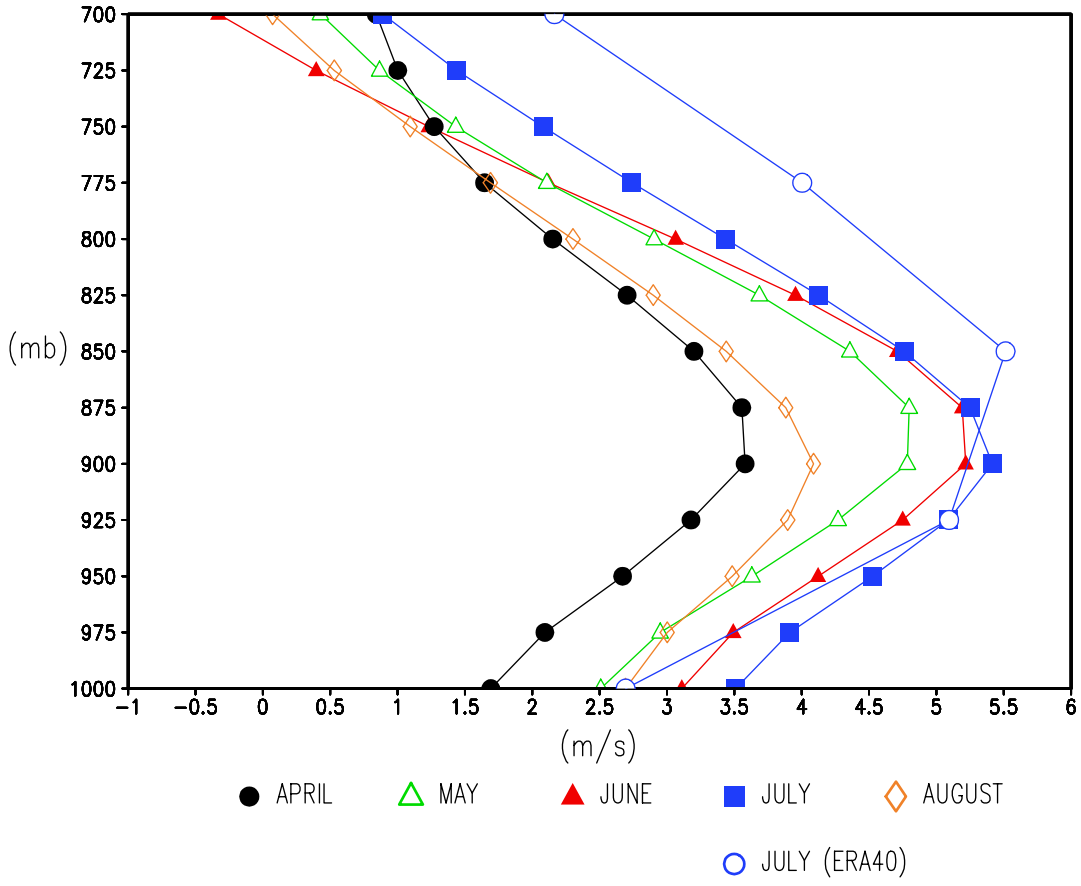

Figure 2.5. Vertical profile of the GPLLJ as reflected in the area averaged (102-97°W, 25-35°N) meridional wind for the warm season months of April-August in NARR. For July, the ERA-40 reanalysis is included for comparison. The vertical resolution is 25 hPa in NARR and 75 hPa in ERA-40. Units are m s^{-1}.

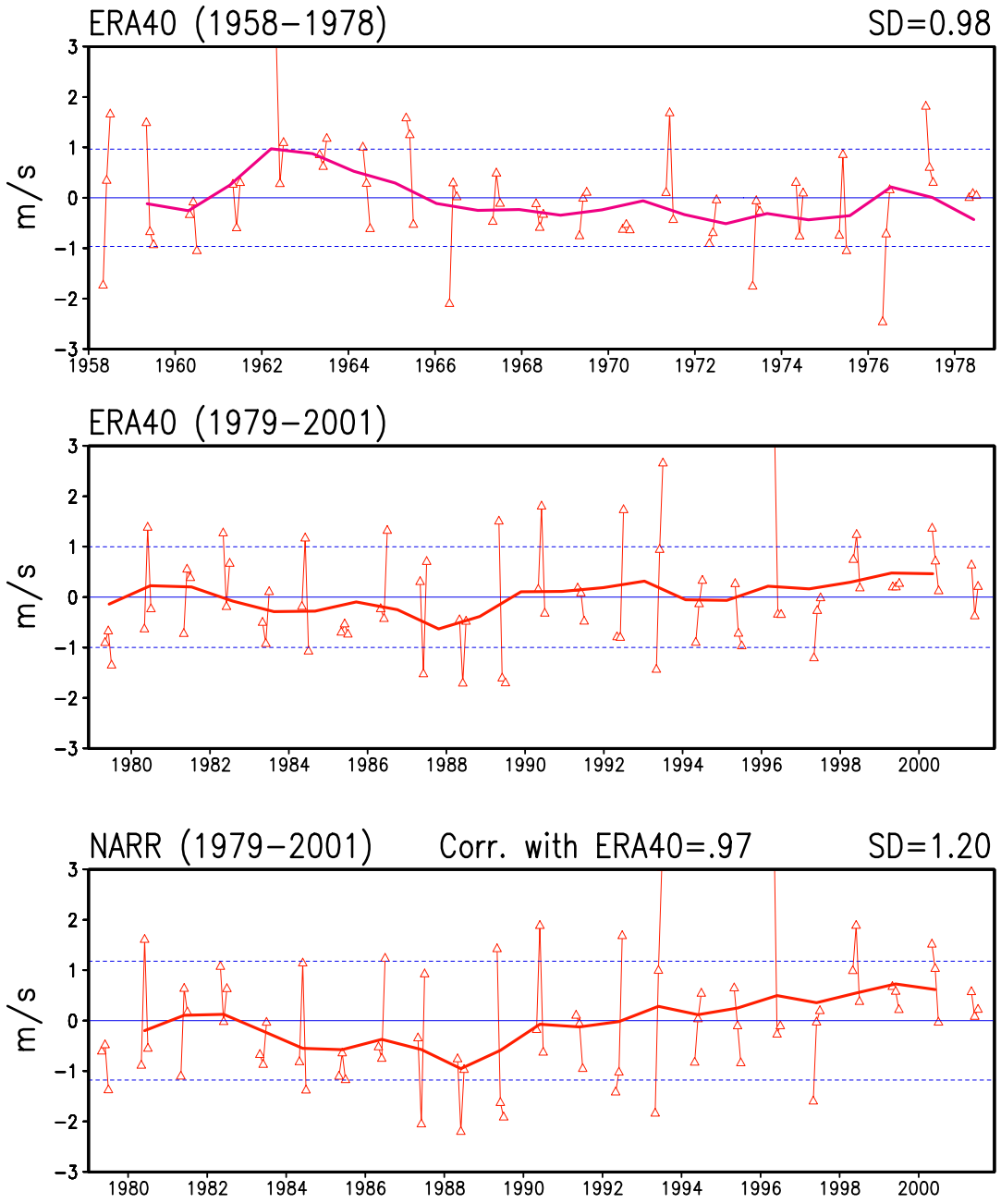

Figure 2.6. GPLLJ index anomalies during the warm season (May-July) in (top 2 panels) ERA-40 and in (bottom panel) NARR. Monthly values are shown using a triangle while the smoothed index obtained from a 1-2-1 averaging of the seasonal mean anomalies is displayed using solid lines. Horizontal dashed lines mark the plus minus 1 standard deviation range in each panel.

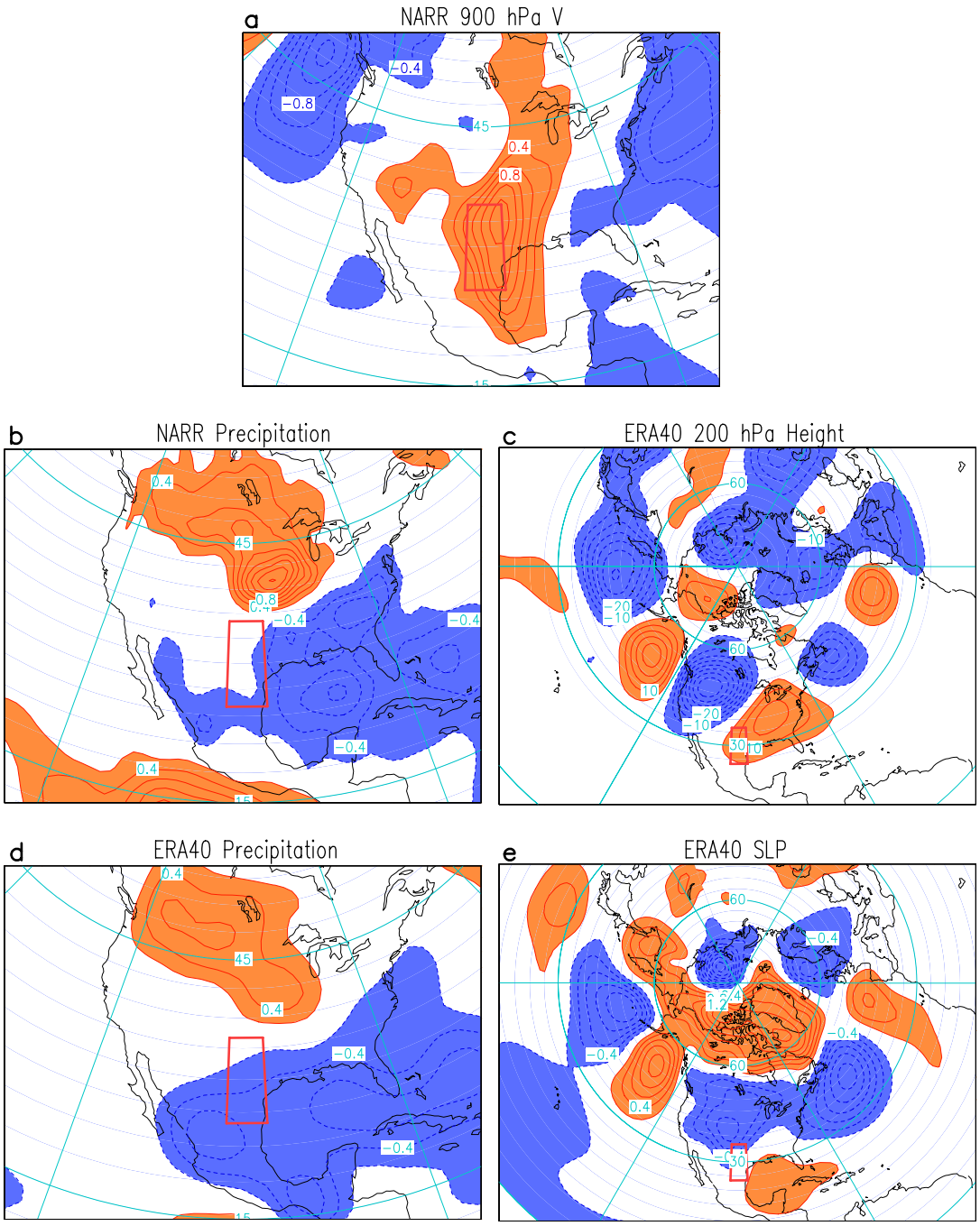

Figure 2.7. July regressions of the GPLLJ index (1979-2001) on: NARR 900 hPa wind (a) and precipitation (b), ERA-40 200 hPa geopotential height (c) and precipitation (d), and sea level pressure (e). Contour interval for: wind is 0.2 m s^{-1}, height is 5 m. Precipitation and SLP contours are 0.2 mm day^{-1} and 0.2 hPa respectively. In all panels the positive (negative) values are shaded orange (blue). The rectangular box outlines the area defined by the GPLLJ index.

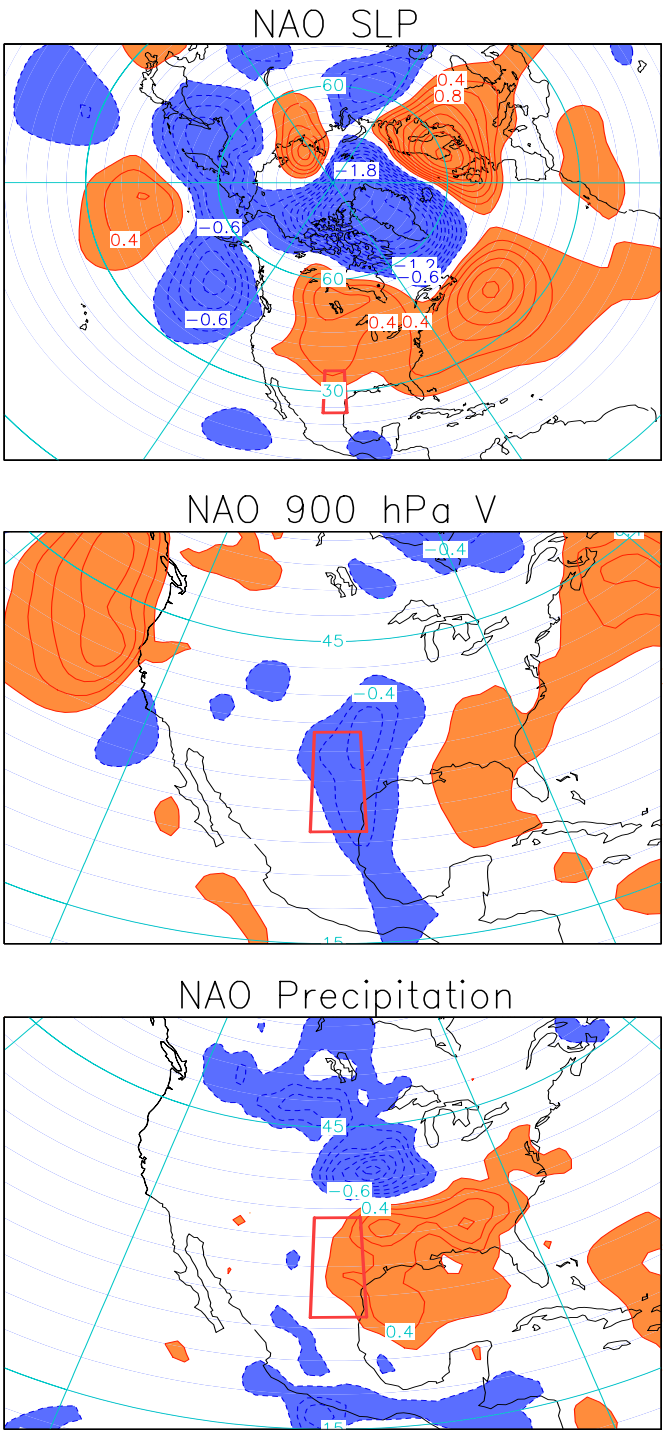

Figure 2.8. July regressions of the NAO index on SLP (top panel) in ERA40, 900 hPa meridional winds (middle panel) and precipitation (bottom panel) in NARR. In all panels the positive (negative) values are shaded orange (blue). The contour interval in the top panel is 0.2 hPa while in the middle and lower panels it is 0.2 ms^{-1} and 0.2 mm day^{-1} respectively. The rectangular box outlines the area defined by the GPLLJ index.

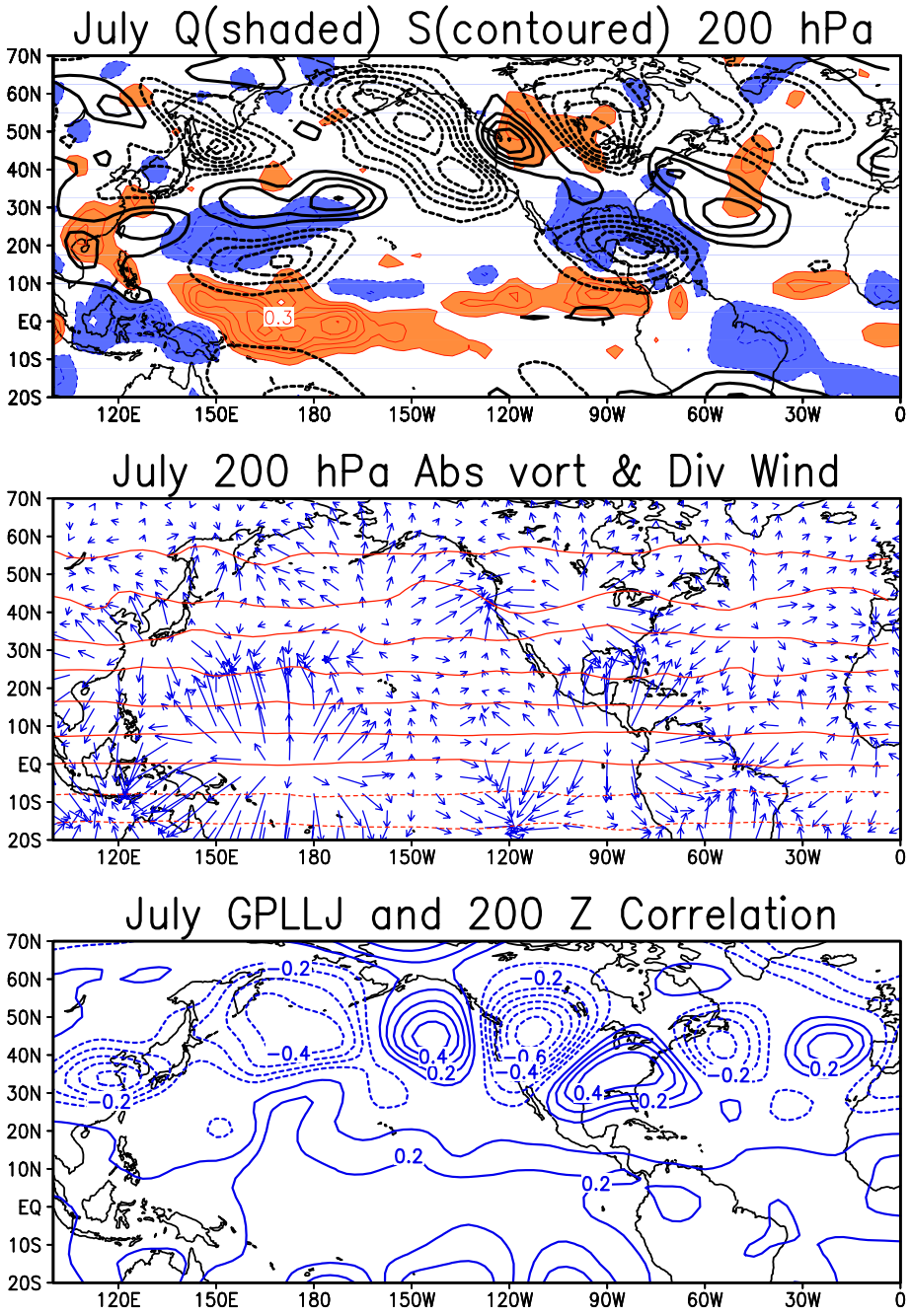

Figure 2.9. July regressions of the GPLLJ index on 1000-200 hPa average diabatic heating and the Rossby wave source (top panel), 200 hPa divergent winds and absolute vorticity (middle panel), and July correlations of the GPLLJ index on 200 hPa height (bottom panel). Diabatic heating contours are 0.1 k day $^{-1}$ and orange (blue) shading denotes positive (negative) values. The Rossby wave source is contoured for positive (solid) and negative (dashed) values. Divergent winds are displayed using arrows. Absolute vorticity is contoured at $10^{-5}s^{-1}$.

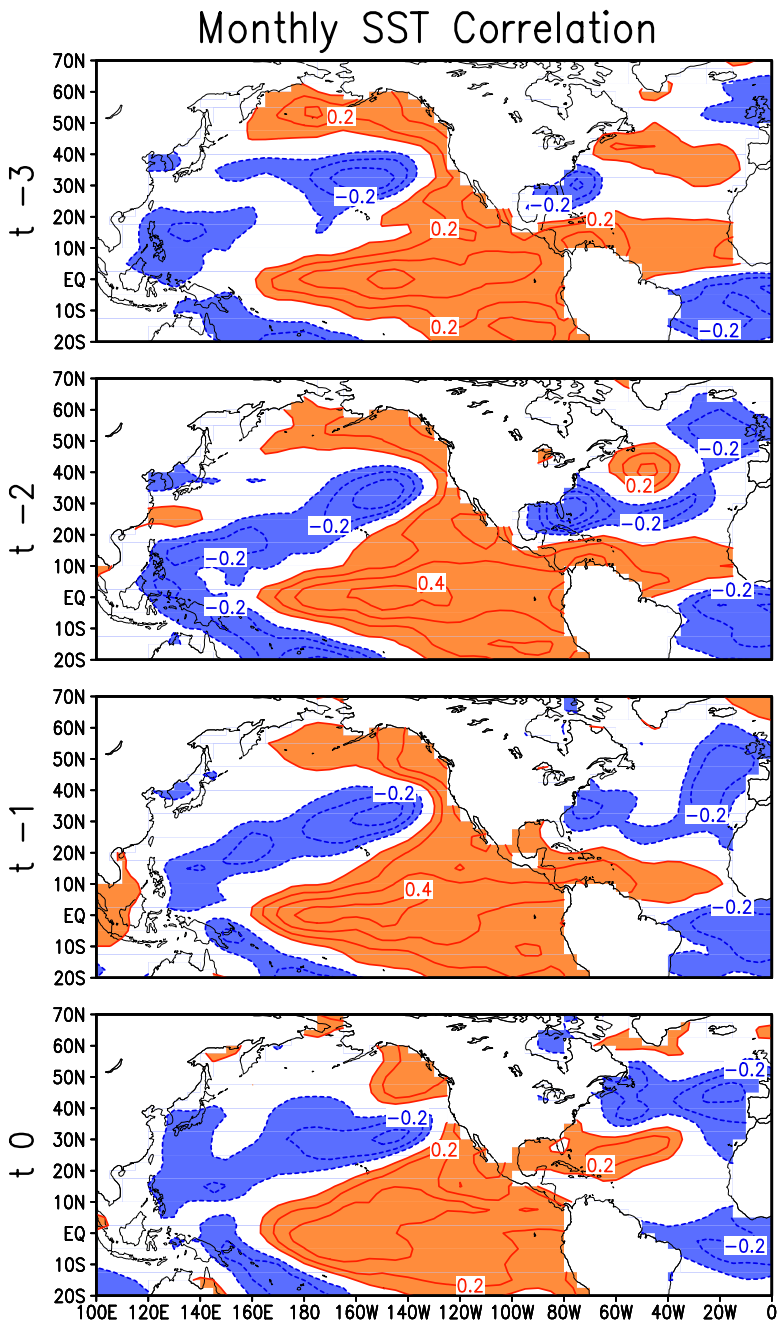

Figure 2.10. Correlations of the July GPLLJ index on SST at monthly lags. Orange (Blue) shading denotes areas of positive (negative) correlation.

Chapter 3: Recurrent Patterns of GPLLJ Variability

An index is a widely used simple statistic to track regional variability. While its simplicity is attractive, it is not without some costs, especially, when the region of interest is the locus of several variability patterns. In such situations, the index represents a superposition of variability patterns, and as such, index regressions cannot be counted upon to provide insights into the operative mechanisms. Given our interest in the latter, an EOF analysis is conducted to identify the recurrent patterns of GPLLJ variability.

3.1 EOF Analysis: Three Modes of Variability

The EOF analysis was conducted on monthly 900 hPa NARR meridional wind anomalies in the 105-85W and 20-50N domain, for the May, June and July months. The domain was chosen to fully encompass the jet core and its precipitation impacts. The left column of figure 3.1 displays the first three EOFs (contoured) atop the climatological MJJ 900 hPa meridional wind (i.e., the climatological GPLLJ, which is shaded when >5 ms^{-1}); the corresponding principal components (PCs) are in the right column. The three leading EOFs explain 37.8%, 23.3% and 12.2% of the regional meridional wind variance, respectively.

The leading mode of variability (mode 1) is characterized by substantial strengthening and spatial expansion of the jet core. Although there is a northward shift of the core, the meridional expansion of the jet keeps it tied to the moisture source, the Gulf of Mexico. The enhanced core-region jet-speed should result in stronger low-level convergence in the jet-exit region, and thus precipitation (as shown

later in figure 3.3a). An inspection of PC1 shows substantial intraseasonal variability, with the PC switching sign in 19 of the 24 analyzed summers. PC1 is most negative in June 1988 and strongly positive in June-July 1993, coincident with severe drought and floods over central United States in those summers. This PC should we well correlated with the GPLLJ index on account of significant v_{900} amplitude in the GPLLJ index box; and it is, at 0.86.

Mode 2 represents a significantly northward shifted GPLLJ; much more than in mode 1. The negative values over northern Gulf of Mexico along with anomaly-core location at 40-45N, effectively isolate the perturbed GPLLJ from the Gulf moisture source. The PC2 distribution shows this mode to be in positive phase during the 1988 summer. There is more intraseasonal variability manifest in PC2 as evidenced by sign changes in 21 of the 24 analyzed summers. Given the weak meridional wind amplitudes in the marked index box, PC2 is weakly correlated with the GPLLJ index (−0.15).

In contrast with modes 1 and 2, mode 3 shows an in-place strengthening of the climatological GPLLJ, along with reduced meridional flow over central/northern Great Plains, i.e., a meridional dipole anomaly. In the positive phase, northward moisture flux is enhanced over the western Gulf from increased jet speed but diminished over the central-eastern sectors of the Gulf, which is under the influence of climatology-opposing meridional wind anomalies in this phase. Strengthening (weakening) of the climatological LLJ is associated with floods (droughts) in the central U.S. due to enhanced (suppressed) moisture flux convergence; as seen later from the modal precipitation links (figure 3.3). The PC3 distribution indicates that

mode 3 was not notably anomalous during the 1988 and 1993 summers, indicating a modest role for this mode of GPLLJ variability in the recent prominent hydroclimate episodes.[8] PC3 is modestly correlated with the GPLLJ index (0.46).

3.2 Stability of EOF Analysis

The stability of the identified GPLLJ variability patterns was assessed from EOF analysis of variability in the much longer (40+ years) ERA-40 data set (1958-2001). The coarser resolution of ERA-40 data vis-à-vis NARR data was a concern but not an overwhelming one given the opportunity to assess pattern stability. Figure 3.2 shows the second-leading EOF from the ERA-40 based analysis, which should be compared with the second-left panel in figure 3.1; this EOF was chosen for intercomparison because of its interesting height regressions. Intercomparison indicates remarkable structural robustness of this variability pattern; the case for the other patterns, as well. To be sure, there are amplitude differences – ERA-40's are weaker – but some are, undoubtedly, due to coarser ERA-40 data.

Also shown in figure 3.2 are the July height regressions of PC2: NARR PC2 regressions on ERA-40 heights (1979-2001) are in the upper panel while the ERA-40 PC2 regressions on ERA-40 heights (1958-2001) are in the bottom panel. The structural similarity of the large-scale patterns is notable, given the differences in regression period and, potentially, in the PCs themselves. The similarity attests to the robustness of regressions, not just in the analyzed variable (v_{900}), but also in related circulation and hydroclimate. The upper-level anticyclone over the north central U.S.

[8] All 3 PCs are positive in July 1993.

is noteworthy given its prominence in U.S. droughts (Bell and Janowiak 1995; Mo et al. 1997).

It is interesting to compare the PC2 height regressions with the GPLLJ index ones (figure 7c). The index regressions depict a zonally-oriented, coherent wave pattern with limited connectivity to the tropics/subtropics, while the PC ones have an arching structure with greater connectivity; one that is, to an extent, manifest even in the height field. The US features in the two regressions are also in spatial quadrature. These differences suggest that while the GPLLJ index can be a useful fulcrum for many analyses, it is not suitable for probing mechanisms generating GPLLJ variability.

3.3 PC Regressions

3.3.1 Precipitation

Figure 3.3 shows NARR PC regressions on NARR's July precipitation. The PC1 regressions in Northern Plains are large (~1.5 mm/day) and their structure very similar to the GPLLJ index regressions (fig. 3.7b); not surprising, given the 0.86 correlation between PC1 and the index. The precipitation pattern linked with PC2 (middle panel) is more focused over the Gulf coast states and eastern seaboard where anomalies are ~0.8 mm/day; and Mexico. Unlike PC1, PC2 regressions have a meridional dipole structure between the GPLLJ entrance and exit regions. PC2's correlation with the GPLLJ index is modest (–0.15) as noted before, but the mode is important for Gulf States' precipitation variability. The bottom panel displays the PC3 regressions, which show diminished precipitation over south central U.S., Mexico, and the Gulf of Mexico, along with modest positive amplitudes over the

Great Plains. It is interesting that despite similar meridional wind structure along Mexico's Gulf coast in modes 1 and 3, their local precipitation footprints are so different. Clearly, meridional wind divergence ($\partial v/\partial y$) alone cannot account for mode 3's negative precipitation anomalies. Of the three modes, only 2 and 3 evidently influence Mexican rainfall.

3.3.2 SST

The July PC regressions on SST are shown in figure 3.4. SST regressions have coherent structure but modest amplitudes (0.2-0.4K); not surprising, given strong subseasonal variability of the PCs (and the GPLLJ index). PC1's SST regressions are focused in the equatorial central Pacific, and while the short record precludes definitive characterization, the anomalies resemble the SST pattern seen in summer following the El Niño peak phase; as also noted in context of figure 2.10d, which shows correlations. The underlying GPLLJ index regressions (not shown) resemble the PC1 ones, as expected from the 0.86 correlation between the index and this PC.

In contrast, PC2's SST regressions can be unambiguously associated with El Niño growth, i.e., with SST anomalies typically seen in the summer prior to El Niño's peak phase. Anomalies are also present in the midlatitude basin in both cases, but their significance is questionable in view of small index correlations there (cf. fig. 2.10d). The PC3 regressions, on the other hand, are associated with NAO variability. Banded SST anomalies in the extratropical Atantic basin and the structure of related sea-level pressure anomalies (not shown) attest to this linkage.

3.4 Chapter 3 Figures

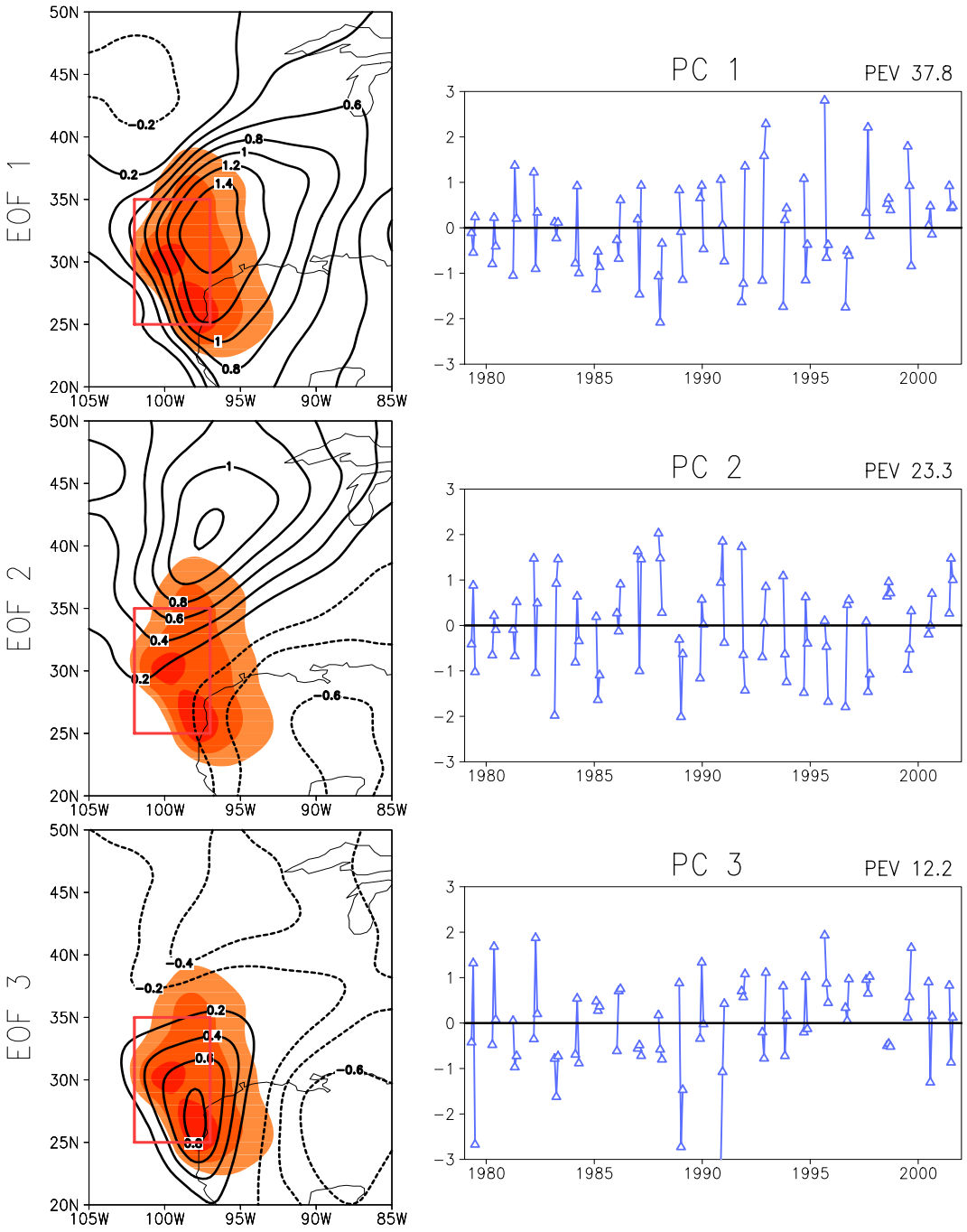

Figure 3.1. Recurring patterns of MJJ GPLLJ variability. MJJ 900 hPa wind climatology (shaded) and the first three EOF modes (contours) for MJJ in the left column. Meridional wind climatology values in excess of 4 m s^{-1} are shaded at 1 m s^{-1} intervals. The contour interval for the EOF spatial patterns is 0.2 m s^{-1}. MJJ principal component time series associated with each mode is displayed in the right column with percentages of explained variance.

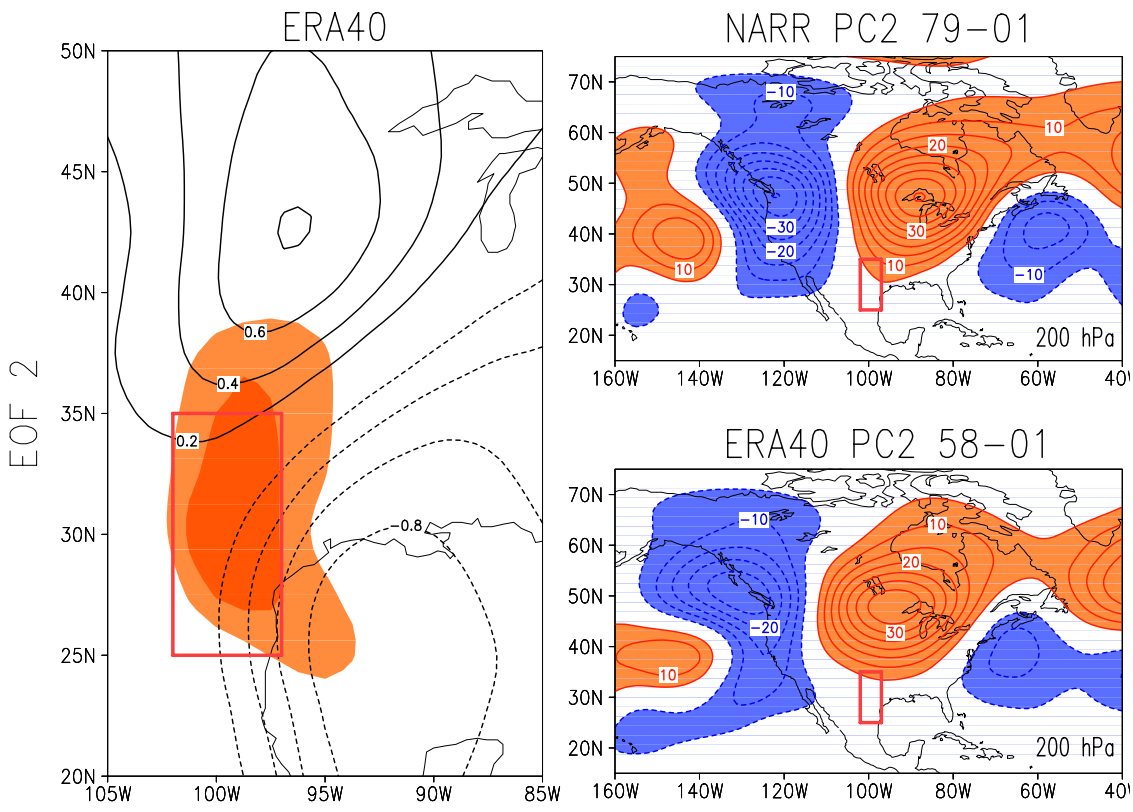

Figure 3.2. Sensitivity of GPLLJ EOF modes to different time periods of NARR (23 years) and ERA40 (44 years). EOF 2 (left panel; contoured) from principal component analysis and MJJ climatology (shaded; same as in fig. 11) of ERA-40 900 hPa meridional winds, and PC2 regression on July 200 hPa height in both NARR (upper right) and ERA40 (lower right). The EOF contour interval is 0.2 m s^{-1} and the 200 hPa height regressions are contoured at 5 m. The NARR regression is over the 1979-2001 time period while the ERA40 one is over 1958-2001. The rectangular box outlines the area defined by the GPLLJ index.

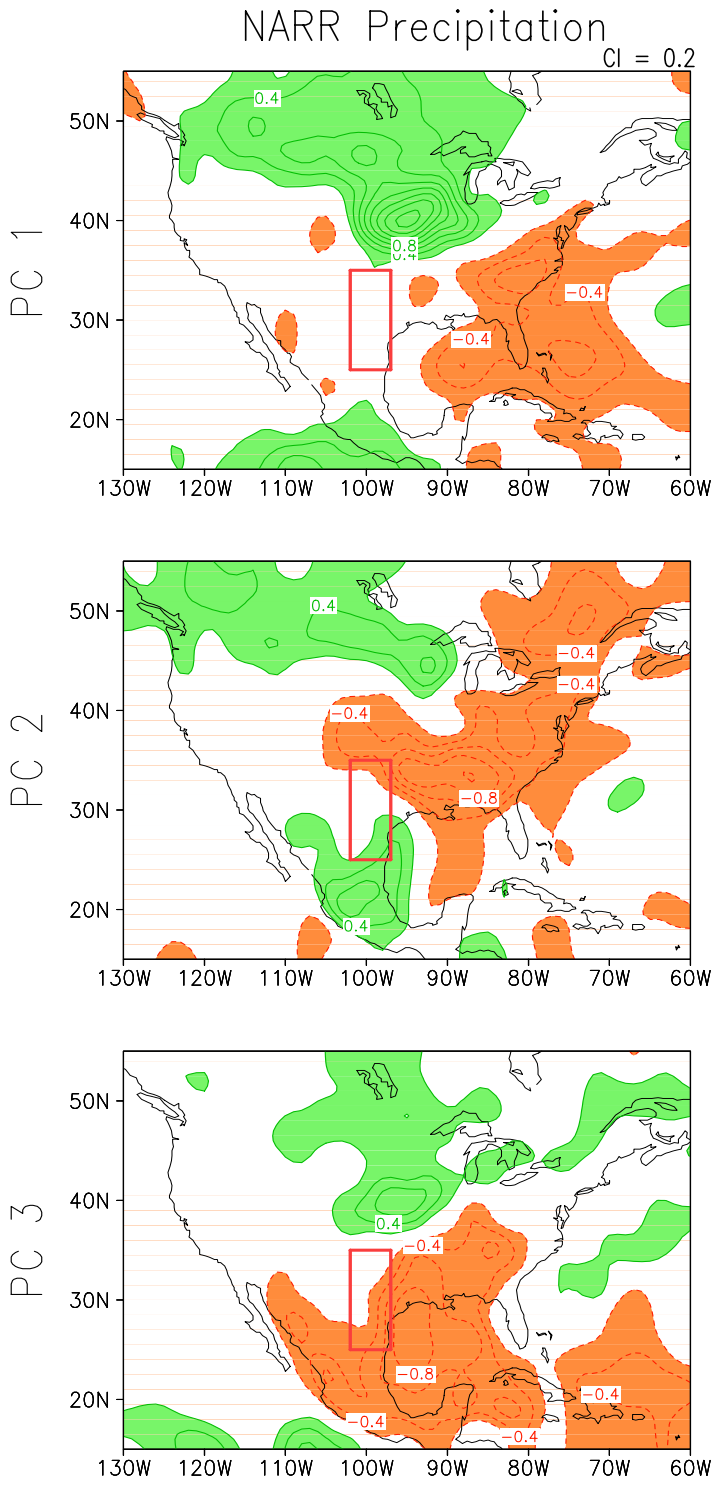

Figure 3.3. GPLLJ principal component regressions on NARR precipitation during July. The contour interval is 0.2 mm day $^{-1}$. Green (orange) shading indicates positive (negative) values. The rectangular box outlines the area defined by the GPLLJ index.

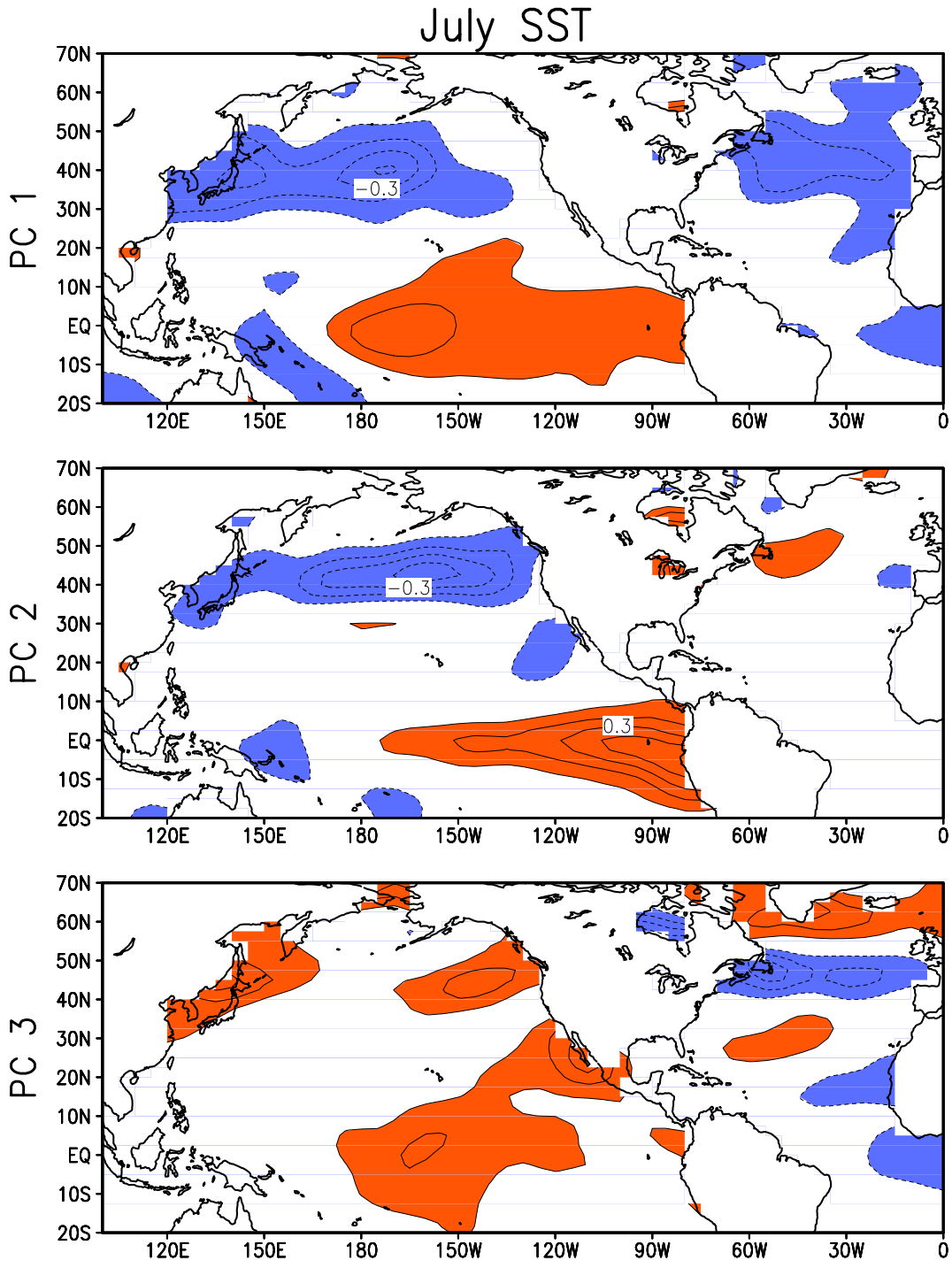

Figure 3.4. July principal component regressions on SST for PC1 (top), PC2 (middle), and PC3 (bottom). Orange (blue) shading denotes positive (negative) SST values contoured at 1 K.

Chapter 4: Remote Basin Variability

The primary concern of the preceding chapters has been to characterize the large-scale atmospheric variability structure and continental precipitation impacts from the perspective of the GPLLJ. The Great Plains centric viewpoint has shown the presence of large-scale circulation and SST footprints over the adjoining basins and connections to the July NAO. The extraction of GPLLJ variability modes, while interesting and useful, still shows connections to circulation anomalies occurring in both oceanic basins. Furthermore, GPLLJ index links to diabatic heating, SST anomalies, and known variability modes emanating from both the Atlantic and Pacific, motivates the need to characterize the contributions from the basin centric perspective, and at the very least, as corroboration to the results of chapters 2 and 3.

The strategy adopted in this chapter follows from RBN (2005) whereby preferred modes of combined SST-circulation variability were identified and used to examine connections to Great Plains hydroclimate: The summertime GPLLJ index and precipitation. Given the expansive extent of the subtropical sea level pressure anticyclones in the Atlantic and Pacific (cf. figure 1) and their potential for influencing Great Plains circulation and hydroclimate variability (Wexler 1967; Rodwell and Hoskins 2001; Ting and Wang 2006), the variable of use here will be SLP. While much of the preceding analysis has been for the MJJ period, in this chapter the target period is forward shifted by one month to JJA for a more direct comparison with other studies, including RBN (2005) and to be in line with the canonical summer definition. Furthermore, the NCEP/NCAR reanalysis (1949-2001)

is used in this chapter for it has the longest data record. This will provide the most stability possible with regard to the derived EOF patterns.

4.1 The Pacific Mode

Study of SLP variability and Great Plains hydroclimate links will begin by showing the Pacific mode of variability that is most closely associated with anomalous hydroclimate over the Central United States. The first 9 Pacific SLP EOF modes were generated and each PC was regressed on various hydroclimate fields. As the target here is the GPLLJ and precipitation impacts, only modes that exhibit interesting Great Plains hydroclimate footprints are examined. These need not be the modes that explain the most variance. Canonical covariance-based EOF analysis is applied to area weighted monthly mean JJA SLP anomalies over the Pacific sector (20-85N 120E-120W). The Rotation of the EOFs is not necessary due to the small domain[9].

The mode most associated with Great Plains hydroclimate is Pacific SLP EOF 4, which explains 9% of the total variance. The SLP loading vectors and PC regression on 200 hPa is shown in figure 4.1. The SLP field exhibits a tripole standing wave pattern emanating from the western North pacific into the Gulf of Alaska. The 200 hPa height regression shown in the middle panel depicts the upper level reflection of the SLP pattern, i.e., an equivalent barotropic structure; a signature of a propagated stationary waver response. This pattern shows a positively tilted negative height anomaly stretching from the California coast northeastward toward the Hudson Bay. Interestingly this pattern is similar to the 200 hPa regressions against the July GPLLJ

[9] RPCA or Rotated Principal Component Analysis is often used to ensure that modal structure is not sensitive to the analysis domain.

index (cf. fig. 2.7) with a spatial correlation of 0.76 over the 160°E-80°W and 20-70°N.

The similarity is readily apparent if the height regressions are compared with the July height correlations which are shown in figure 2.9c using the same projection. The 4 cells over the Pacific beginning with the weak high to the west of Hawaii have each a counterpart; but not the cell positioned over the Gulf Coast states in figure 2.9c. This is consistent with the Rossby wave source analysis discussed in the earlier chapter in that the wave sources are present over the western tropical/subtropical Pacific and the Central American sector; with the former generating the 4 cell pattern over the Atlantic beginning with the cell over the Gulf Coast and Eastern seaboard.

The Pacific SLP PC4 time series is shown in the bottom panel. There is strong intraseasonal variability associated with this pattern, which suggests fluctuations on the sub monthly timescale, although lower frequency variability is also evident. Another interesting aspect is the low PC value during 1988 and the extremely large July value in 1993 – given the extreme hydrologic drought (1988) and flood (1993) over the Great Plains. The presence of this mode is clearly not a sufficient condition, for large PC values occur in some other months as well, not all of which are notably anomalous with respect to hydroclimate.

Figure 4.2 shows the Pacific SLP PC4 time series regressed against NARR precipitation, 900 hPa meridional winds, and 1000-700 hPa integrated moisture flux convergence. The precipitation regression (top panel) shows a dipole structure with positive precipitation anomalies in the northern half of the central U.S. and negative over the southern Great Plains. The structure here is similar to that of figure 3.3 (top

panel) although the magnitude is diminished. The 900 hPa meridional wind anomalies associated with the Pacific pattern suggest a meridional stretching of the GPLLJ similar to that depicted in GPLLJ mode 1 (cf. figure 3.1 - top panel). The spatial correlation between the GPLLJ index and Pacific SLP PC4 regression patterns over the Great Plains is 0.83 for 900 hPa meridional winds and 0.77 for precipitation. The moisture flux convergence shows a dipole structure with divergence in the Gulf of Mexico and northeast Mexico and convergence in the northern Great Plains. This pattern is not surprising given the strong contribution of the GPLLJ to the dynamic convergence (divergence) in the exit (entrance) region of the jet. The structure and magnitude of the MFC can account for much of the precipitation anomaly.

4.2 The Atlantic Mode

The connections of the July NAO index to Great Plains hydroclimate discovered in chapter 2 call for an Atlantic basin SLP analysis, similar to one conducted for the Pacific. The domain for the Atlantic analysis is 80W to the Prime Meridian and 20-85N.

The Atlantic mode most influential on Great Plains hydorclimate variability is shown in figure 4.3; it is the leading mode in the analysis. This mode is consistent with the pattern identified as the North Atlantic Oscillation (NAO, cf. figure 2.8) and explains 37% of the total variance. The top panel represents the SLP expression of the NAO in summer. This mode is characterized by a dipole in SLP between the North and central Atlantic basin. The anomalous SLP pattern can evidently modulate the northern half of the climatological Bermuda high (cf. figure 1.1).

The Atlantic influence on upper tropospheric circulation is shown by PC regressions on 200 hPa heights (middle panel). The westward extension of the NAO anomalies into central North America is seen, and in months when this phase is present, the Bermuda High shrinks, meridionally, especially from the north; leading to a southward shift of its core. The enhanced LLJ and moisture flux activity associated with this phase produces enhanced precipitation over the Great Plains. If this were in the opposite phase, the anticyclonic anomaly over the central Atlantic would flux moisture westward along the southern flank, which upon interaction with Rocky orography would turn into northward and southward streams, with the latter opposing the climatological GPLLJ. A similar impact on low-level moisture fluxes was noted by RBN (2005).

The bottom panel shows the PC time series associated with the Atlantic PC1. The time series exhibits substantial intraseasonal variability and changes sign in 30 of the 51 summers. The high PC value during July 1993 suggests that Atlantic variability, i.e., summertime NAO, exerts considerable influence on Great Plains hydroclimate anomalies. This link is further investigated in chapter 5.

Regressions of the Atlantic Mode 1 (i.e. NAO – not shown) are similar to those in figure 2.8 with the exception of amplitude differences and a weaker northeastward extension of the 900 hPa meridional wind anomalies. Inspection of the June regressions of the NAO index (not shown) shows weakened precipitation and meridional wind amplitude, and a somewhat retracted meridional wind structure in comparison with the July footprints (figure 2.8); suggesting some seasonality of NAO influence. The spatial correlation between the GPLLJ index and Atlantic SLP PC1

regression patterns over the Great Plains is 0.87 for 900 hPa meridional winds and 0.59 for precipitation.

4.3 Regional and Remote PC Correlation

The connection between basin SLP and GPLLJ variability is assessed from correlations of the respective PCs in the JJA and July only periods of 1979-2000. The correlations are noted in table 4.1. The JJA SLP correlations with the GPLLJ index and GPLLJ PCs indicate that jet fluctuations are similarly impacted by both SLP modes when viewed over the entire summer. However, when focusing on July, which has been shown to be particularly hydroclimate sensitive (cf. figure 3.3), the connections become a bit more clear. The GPLLJ index and especially PC 1 is tightly correlated to the Pacific mode while the Atlantic (NAO) connection to GPLLJ mode 3, noted in chapter 2, is present with the –0.44 correlation. The SLP variability modal connections to GPLLJ PC2 are not robust with regard to the Pacific mode, however shows a 0.31 correlation to the Atlantic (NAO) mode.

JJA	**GPLLJ INDEX**	**GPLLJ PC1**	**GPLLJ PC2**	**GPLLJ PC3**
ATL PC1	-0.36	-0.28	0.19	-0.26
PAC PC4	0.45	0.37	0.13	0.25
JULY				
ATL PC1	-0.42	-0.34	0.31	-0.44
PAC PC4	0.62	0.67	-0.14	0.22

Table 4.1. Correlation of the JJA and July only GPLLJ index and GPLLJ PC's 1-3 with the corresponding PC's from EOF analysis of JJA monthly SLP in the NCEP/NCAR reanalysis.

4.4 Pacific and Atlantic Modal Evolution

The previous analysis has dealt with the contemporaneous mature patterns of monthly SLP variability in summer. However the PC time series show substantial intraseasonal variability. Furthermore, studying the progressive structure of these anomalies is necessary if any predictive value is to come to pass. An important tool for extracting the evolution of spatial and temporal variability modes is extended EOF (EEOF) analysis. This technique maximizes spatio-temporal variance and elucidates the evolution and decay characteristics of recurrent modes of variability. Weekly SLP (same spatial domain as sections 4.1 and 4.2) anomalies generated from daily NCEP/NCAR reanalysis are used; the data spans a slightly shorter period of 1958-1998. Summer is defined as 14 weeks, with the first week centered on the Wednesday closest to June 1. 14 weeks is chosen to define summer, so that the lagged data sets required for EEOF analysis all remain within summer months and to avoid significant loss of endpoint data. The impact that the combination of summertime NAO and Pacific SLP mode 4 has on Great Plains precipitation necessitates that we present those two modes here.

Figure 4.4 displays the EEOF associated with the fourth mode of variability in the Pacific from lag -2 to +2 weeks. This timescale is chosen based on the decay scale for teleconnection patterns (Nigam 2003). At lag –2 weeks the pattern begins as a meridional dipole in the central north Pacific SLP with positive anomalies centered over the Bering Strait and negative anomalies to the south near 35° N. Substantial changes occur from week to week in the evolution of this pattern as can be seen from the lag –1 panel. The dipole structure has shifted zonally in that the positive

(negative) anomaly centers have shifted south (north). The mature phase (lag 0) is characterized by strengthening of the anomalies and a 10° westward shift of the anomaly centers. A positive anomaly around 140°E 25°N has also appeared, completing the presence of a wave train structure arching from the subtropical pacific to the Gulf of Alaska. The decay of the pattern shows weakening of the midlatitude features at lag +1 and a northwestward shift of the positive anomalies near Alaska. The lag +2 panel shows no cohesiveness with the mature phase.

Figure 4.5 shows the first EEOF mode in the Atlantic. This is the evolution of the NAO in summer. The main evolutionary feature leading the NAO is the eastward movement and strengthening of the anomaly center over the British Isles and the remarkable westward extension of the pattern into North America. The decay occurs with more rapidity as the pattern weakens by two weeks after maturity with a small weaker center over the central North Atlantic Ocean. A notable attribute of the summertime NAO is the temporal stability of the evolving pattern when compared with the Pacific mode.

The Great Plains hydroclimate implications of these two large scale circulation variability modes is intriguing, especially in the context of recent drought and flood episodes. In 1988 the NAO during spring was positive inducing a broad longitudinal ridge extending over North America. This would suppress precipitation by pushing the upper level jet stream further north and inducing climatologically opposing low level flow anomalies (see RBN 2005) thus preconditioning the central U.S. to hydrologic drought. The summer of that year saw a budding La Niña with attendant convective shifts that may have perpetuated the ridge over the Central U.S.

(Trenberth and Guillemot 1996). Thus an anomalously dry spring was followed by a dry summer.

Conversely in the summer of 1993 there was a persistent ENSO event, with antecedent and contemporaneous precipitation influences over the Great Plains. Antecedent spring precipitation anomalies have been shown to enhance the likelihood of same sign summer hydrologic anomalies (Bell and Janowiak 1995). Additionally the NAO was in the negative phase during the spring and summer of 1993 thus providing no buffer via negative feedback against the positive anomalous precipitation. The next chapter is entirely devoted to the analysis of these anomalous hydroclimate episodes using state of the art high spatial and temporal resolution datasets.

4.5 Chapter 4 Figures

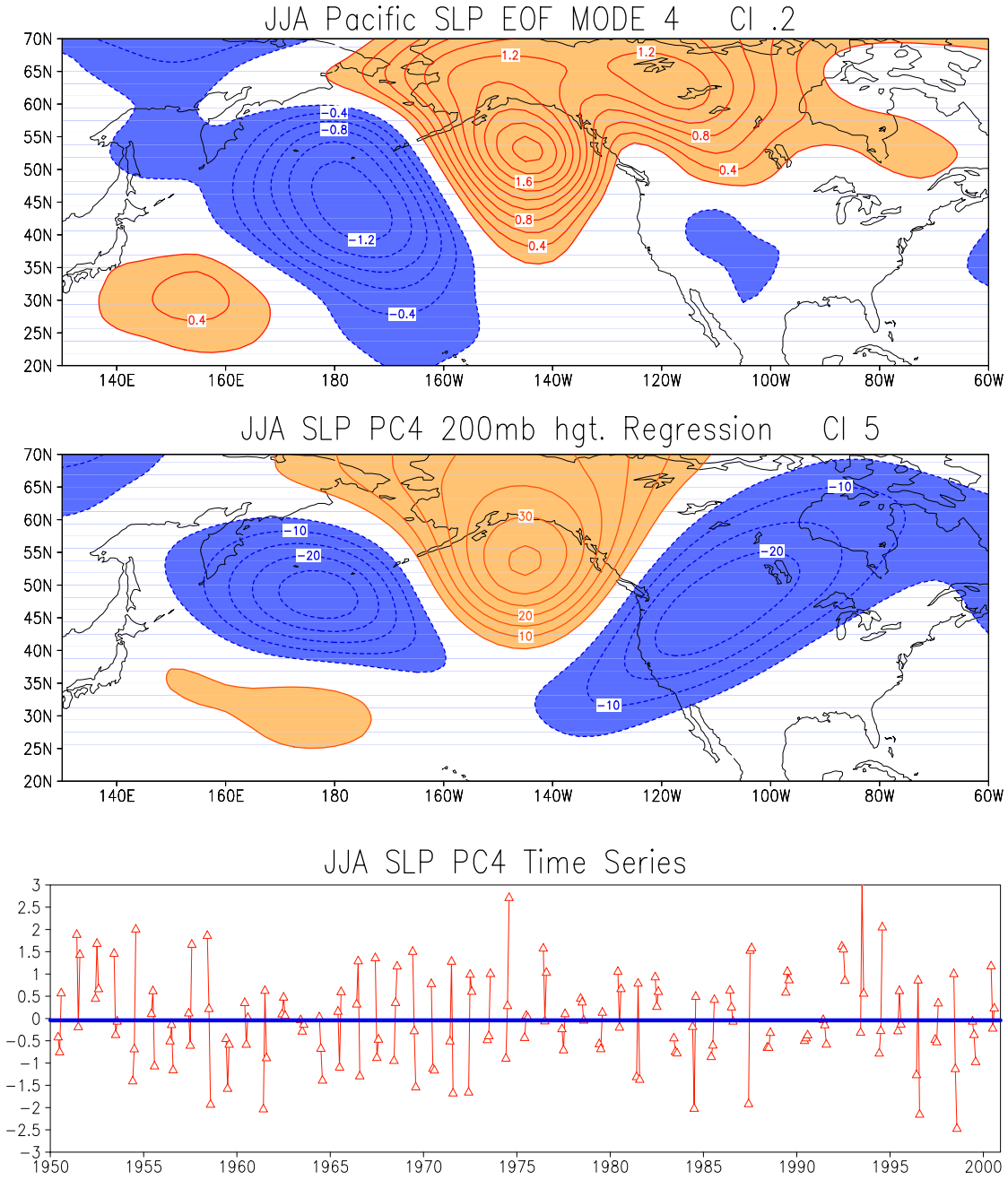

Figure 4.1. JJA Pacific SLP EOF mode 4 (top panel) in hPa, the associated PC regression on 200 mb heights (middle panel) in m, and the PC time series (bottom panel). Positive (negative) values are shaded in orange (blue). The contour interval is 0.2 hPa and 5 m in the top and middle panels respectively. The zero contour is suppressed in all panels.

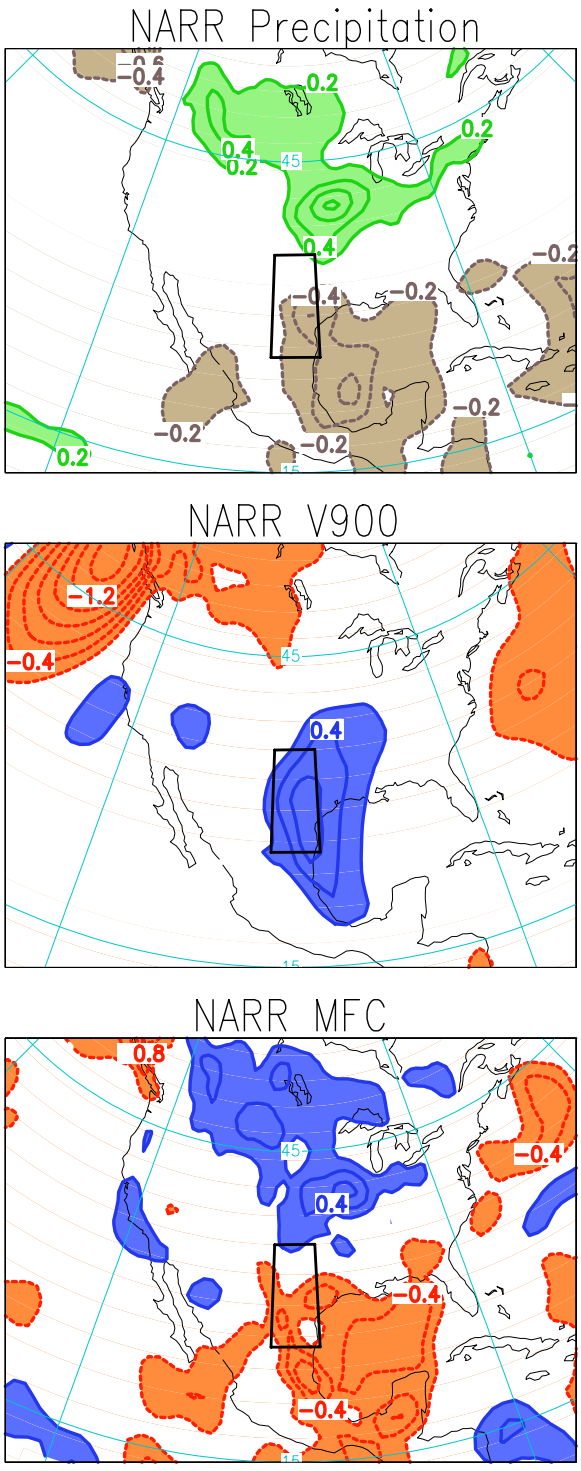

Figure 4.2. JJA Pacific PC4 regressions on NARR precipitation (mm day^{-1}), 900 hPa meridional winds(m s^{-1}), and column integrated moisture flux convergence (mm day^{-1}). For all panels the contour interval is 0.2. Positive (negative) values are shaded in green (brown) in the top panel, and blue (orange) in the middle and bottom panels.

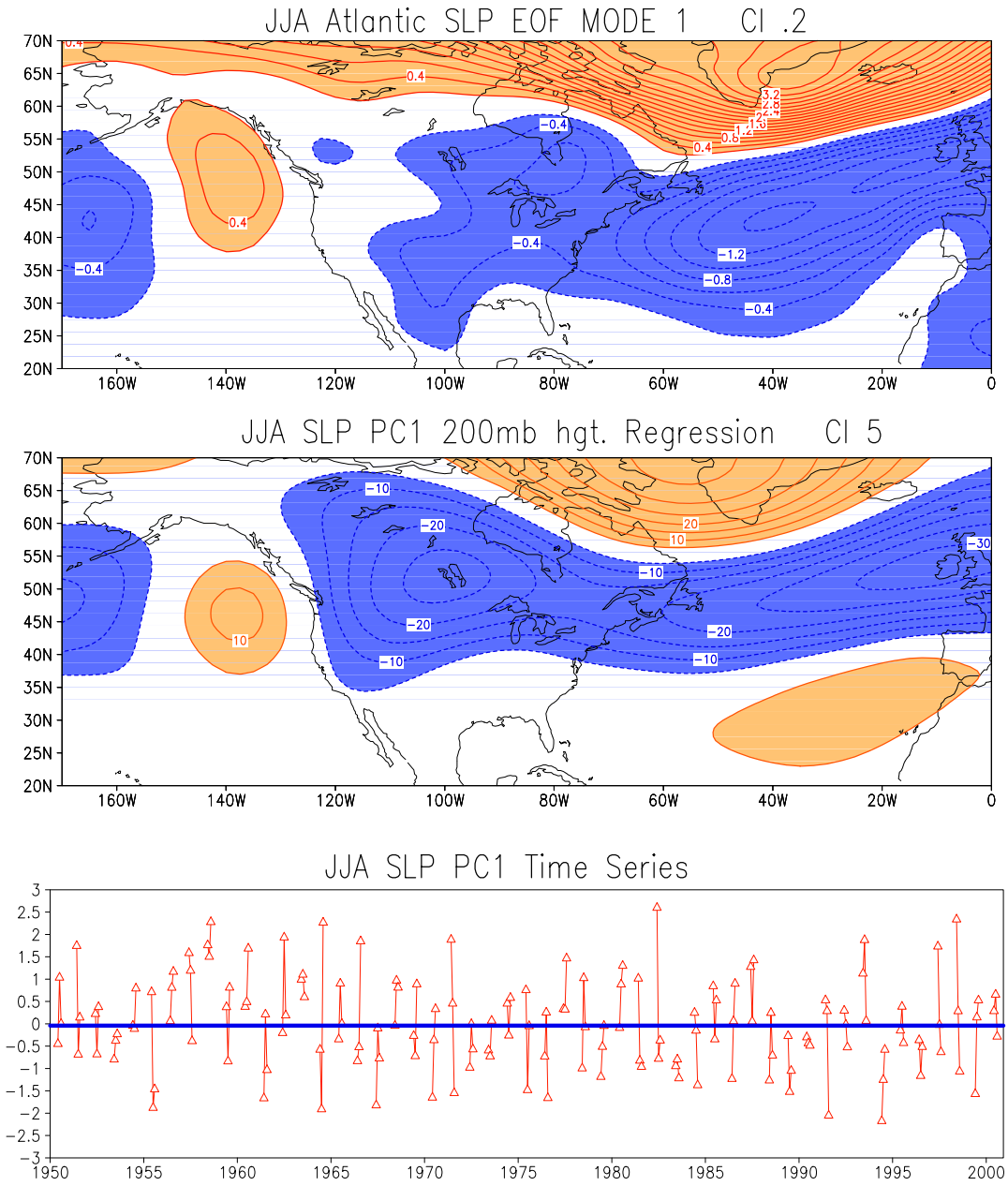

Figure 4.3. JJA Atlantic SLP EOF mode 1 (top panel) in hPa, the associated PC regression on 200 mb heights (middle panel) in m, and the PC time series (bottom panel). Positive (negative) values are shaded in orange (blue). The contour interval is 0.2 hPa and 5 m in the top and middle panels respectively. The zero contour is suppressed in all panels.

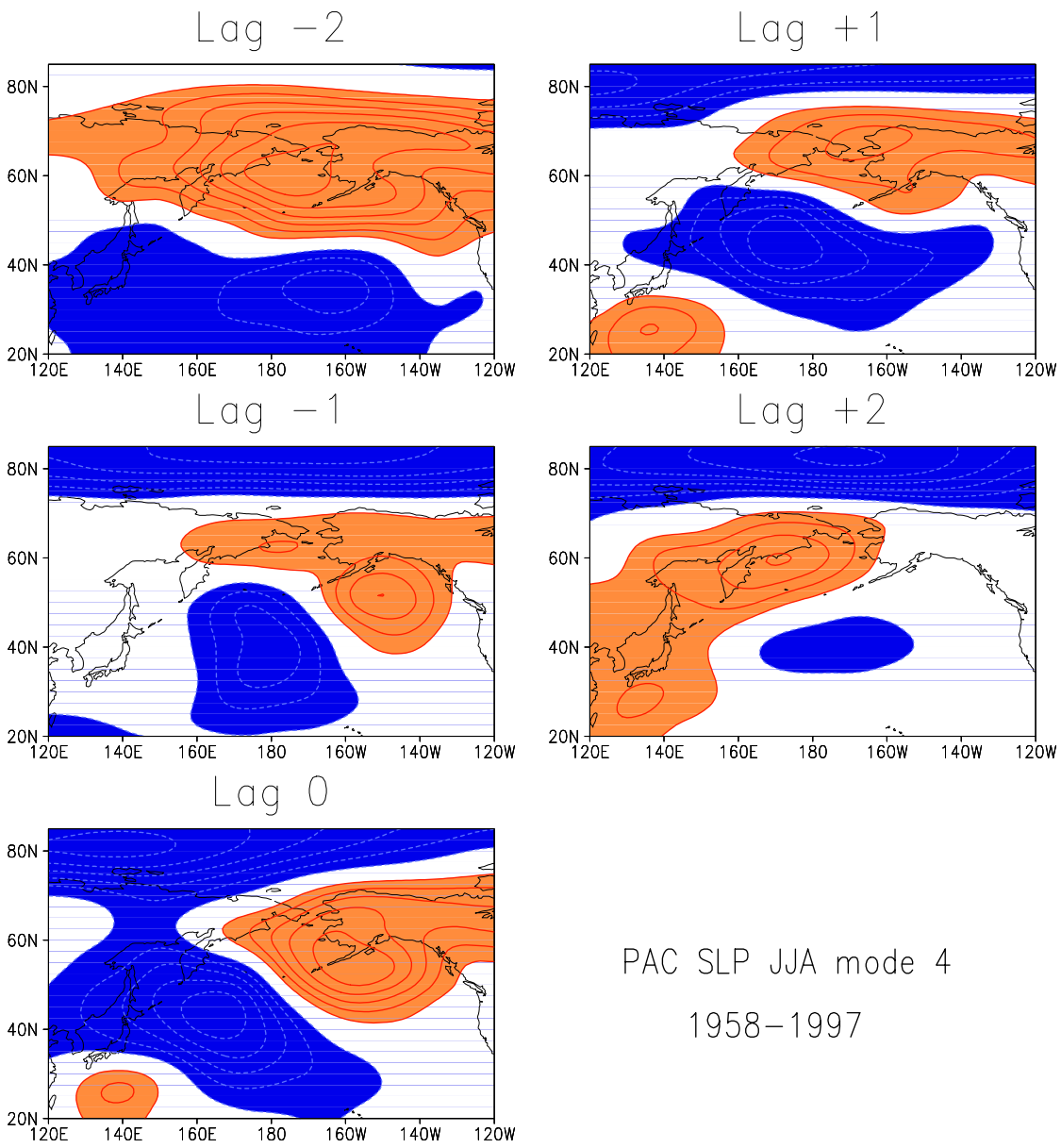

Figure 4.4. Weekly evolution of Pacific SLP mode 4 during JJA. Positive (negative) values are shaded in orange (blue) and the contour interval is 0.3 hPa. The zero contour is suppressed in all panels.

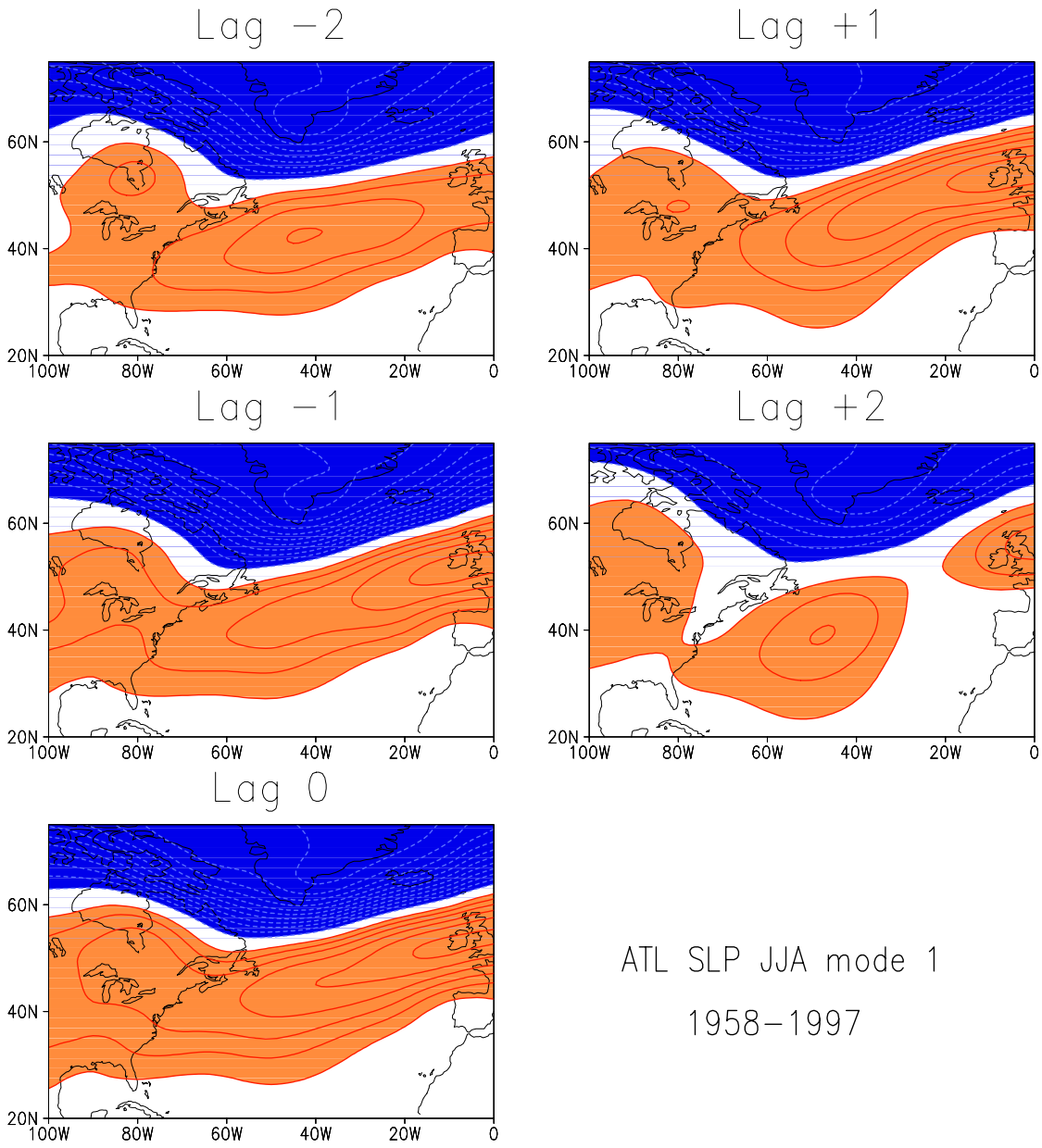

Figure 4.5. Weekly evolution of Atlantic SLP mode 1 during JJA. Positive (negative) values are shaded in orange (blue) and the contour interval is 0.3 hPa. The zero contour is suppressed in all panels.

Chapter 5: The Extreme Events of 1988 and 1993

5.1 Rationale

The subseasonal variability of the GPLLJ and large scale circulation and sea level pressure fields, manifest in within-season sign changes of the monthly PCs/indices in the preceding analysis, is investigated at higher temporal resolution in this chapter, in context of notable recent hydroclimate episodes over the Central United States. Although the GPLLJ still emerges as an important feature in these events, the present analysis is not directly or indirectly based on the jet index.

The 1988 drought and 1993 flood in the central United States were among the most extreme climatic events in recent decades. The socioeconomic impact of these episodes was massive with a price tag in the tens of billions of dollars and significant loss to life and property. Agricultural interests were particularly impacted as much of the United States farming production occurs in the Great Plains. From a scientific perspective these anomalies are equally impressive as they represent extreme departures from the warm season climatology. A high spatio-temporal resolution description of the regional hydroclimate anomalies during the warm seasons of 1988 and 1993 is needed to gain insight into the genesis of extreme hydroclimate events over the Great Plains. The use of pentad resolution data from a state-of-the-art reanalysis system will advance understanding by targeting the submonthly evolution of the circulation and land-atmosphere anomalies during the warm seasons of 1988 and 1993.

Studies explaining the origin of these climatic extremes abound in the literature. Observational inquiries suggest that the 1993 flood events were characterized by a

persistent trough in the lee of the Rocky Mountains maintained by upstream eddy activity, providing favorable conditions over the Great Plains for enhanced rainfall (Bell and Janowiak 1995; Mo et. al 1995,1997; Trenberth and Guillemot 1996). The situation during the late spring of 1988, on the other hand, was characterized by large upper-level anticyclonic height anomalies over North America whose main effect was to shift the summer storm track well north of its climatological position into central Canada (Namias 1991; Trenberth and Branstator 1992, Trenberth et al. 1988).

That these anomalies occurred during significant El Niño (1993) and La Niña (1988) events also suggests a role for tropical forcing of the anomalous midlatitude circulation via equatorial Pacific heating anomalies (Trenberth and Branstator 1992; Trenberth and Guillemot 1996). While intriguing, the origin of the forcing for the atmospheric circulation anomalies is still a topic of much debate. Modeling experiments have been inconclusive with some demonstrating an important role for tropical SST forcing (Bates and Hoerling 2001; Sud et. al 2003), internal atmospheric forcing mechanisms (Liu et. al 1998), and soil moisture effects (Atlas et al 1993; Bosilovich and Sun 1999).

Although there is no consensus on the causes of the large-scale circulation anomalies associated with each of these events, the influence of these large-scale anomalies is widely reckoned to be manifest through local orographic interaction, meridional shifts of the North American stormtrack, and modulation of local land-atmosphere interactions. Interestingly, the focus on causes of the large-scale circulation anomalies has diverted research attention from development of a high

resolution, evolutionary description of atmospheric and land surface states during these notable variability episodes. This thesis chapter attempts to fill this void.

The data used in this analysis are pentad averages (5-day mean) during the NARR period 1979-2005. NARR pentads were created by averaging the 3-hourly data, and in leap years the pentad beginning on February 25 is a six day average so as to keep the number of pentads (73) per year consistent throughout the 27-year record. All anomalies are with respect to their pentad climatology; a notable attribute.

5.2 Pentad Resolution Hydroclimate

To appreciate the geographic orientation and magnitude of the hydroclimate anomalies of 1988 and 1993, figure 5.1 presents the warm season (MJJ) climatology of precipitation (shaded) and the GPLLJ (contoured) as diagnosed from 900 hPa meridional winds in NARR. The boxes used to define the precipitation index from RBN (2005) (northern plains) and the GPLLJ index (southern plains) are outlined for reference. These areas have been previously identified as regions of interesting precipitation and GPLLJ variability in chapters 2-4, and are also representative of the main focus areas during 1988 and 1993[10]. Warm season continental precipitation is pronounced over the eastern half of North America with regional maxima along the U.S. and Mexican Gulf Coasts and in the central Plains. The GPLLJ is active in a narrow corridor extending from the northwestern Gulf of Mexico northward toward the continental interior.

Figure 5.2 shows the 1979-2005 climatological evolution of the meridionally averaged GPLLJ (25-35°N), precipitation (35-45°N), and evaporation (35-45°N)

[10] While the extreme precipitation anomalies during 1988 and 1993 are geographically expansive a large portion of the extrema occurred over the lat-lon boxes in figure 1.

from April to September in NARR; all at pentad resolution. Interesting spatial and temporal relationships emerge in the pentad climatology. The GPLLJ exhibits pulses of activity throughout the warm season each lasting approximately 2-3 weeks. The largest precipitation values are found to the right of the GPLLJ core, indicating the influence of the nocturnally veering LLJ on the location of maximum precipitation (Zhang et al. 2006). Although the July GPLLJ pulse is as long-lived and longitudinally expansive as the preceding ones (as tracked by the 6 m/s, for example), the largest climatological precipitation is found during May and June. Notable characteristics of the evaporation are the time lag with respect to precipitation and the midsummer maximum. Note, evaporation is larger than precipitation over a broad longitudinal range and for a good portion of summer; a well known feature of U.S. hydroclimatology (e.g., Nigam and Ruiz-Barradas 2006).

5.3 Hydroclimate Anomalies of 1988 and 1993

5.3.1 Atmospheric Water Balance

Improved hydroclimate representation in NARR and the presence of competing large-scale circulation and local land surface influences in generating extreme hydroclimate anomalies warrants a description of the evolution and temporal phasing of the key hydroclimate fields. Figures 5.3 and 5.4 show the meridionally averaged (as in figure 5.2) pentad evolution of precipitation (shaded), 900 hPa meridional winds (blue contours), and moisture flux convergence (red contours) during the warm seasons of 1993 and 1988 respectively. For 1988 the months of April, May, and June (AMJ) are used, while in 1993 May, June, and July are examined for discussion. These months were chosen as they are most representative of the extreme events.

Note that the third term in the atmospheric water balance, evaporation, is shown in subsequent figures (5.5 and 5.6) in context of the terrestrial water-balance to which it also contributes.

Significant anomalous precipitation during 1993 was largely concentrated during mid-late June and early July with the GPLLJ (blue) slightly leading both the precipitation and moisture flux convergence (red) anomalies. As noted in the pentad climatology the coincident precipitation anomaly is right shifted with respect to the anomalous GPLLJ. The moisture flux convergence with a maximum of 8 mm/day can account for the magnitude of precipitation anomalies during the late June to early July maximum of 1993. The 10 mm/day precipitation anomaly and the > 1 mm/day evaporation anomaly (cf. figure 5.5) indicate that the columnar atmospheric water budget over the Great Plains in NARR is well balanced ($P \approx E + MFC$), with moisture transports dominating local evaporation.

The summer hydroclimate evolution in 1993 portrayed in figure 5.3 has other notable features as well: a significant amplitude pentad-duration GPLLJ episode in early June (and also one in the second week of May) associated with modest downstream convergence and precipitation (< 2 mm/day); indicative of, perhaps, a GPLLJ – EOF3 mode of variability. In contrast, the notable pentad duration precipitation anomalies in the first week of May (and mid June) are not associated with any significant jet variability. It is likely that in such cases, the low-level convergence accompanying precipitation anomalies is generated from processes other than kinematic convergence ($-\partial v/\partial y$) in the jet exit region.

The evolution of circulation and precipitation during 1988 (figure 5.4) is similar in many ways to that in 1993 but for the opposite sign. A striking difference between the two years is the longitudinal range of precipitation impacts. The main area of precipitation anomalies in 1993 covers approximately 15° of longitude, while those in 1988 extend up to the east coast (not shown), almost doubling the size of the 1993 precipitation footprint. This may indicate a greater role of the GPLLJ in the 1993 anomalies than in the 1988 ones. Here too, one sees instances of precipitation variability generated both with and without the involvement of the GPLLJ. For example, the rainfall deficit in mid-April follows substantial weakening of the GPLLJ and generation of downstream divergence; a classic jet influenced hydroclimate episode. The major dry episode beginning in late May is however not as clear cut since sizeable rainfall deficits are apparent without significant antecedent jet attenuations; especially in the eastern half of the domain.

5.3.2 Terrestrial Water Balance

Observational and modeling studies of the 1988 and 1993 hydroclimate events suggest a contributing role for soil moisture anomalies (Atlas et. al 1996; Bell and Janowiak 1995; Sud et al 2003). Figures 5.5 and 5.6 show the pentad evolution of precipitation (shaded), 0-2 meter soil moisture (blue contours), and evaporation (red contours) anomalies during 1993 and 1988, respectively. All quantities are meridionally averaged over 35-45°N, so that the terrestrial water balance can be assessed[11]. Note, that while some soil moisture anomalies exist prior to the onset of both events their significance is marginal, *as is their water budget contributions*; for

[11] Ideally, soil moisture variations should be represented as recharge, i.e., $\partial(SM)/\partial t$, where SM is soil moisture; since the terrestrial water balance is $\partial(SM)/\partial t = P-E-R$, where R is runoff.

the strongest anomalous evaporation temporally lags precipitation by 1-2 weeks in both 1988 and 1993 episodes; and especially in view of the sizeable coincident anomalous moisture flux convergences due to GPLLJ variability in figures 5.3 and 5.4. That however still leaves open the possibility of soil moisture influencing the local thermodynamic environment, i.e, column stability; an influence that will be defined in future work.

The nature of the terrestrial water balance associated with these extreme hydroclimate events can be surmised even in the absence of an explicit recharge term (i.e., $\partial SM/\partial t$) assuming that half of the recharge coincident with a precipitation episode (e.g., the 1993 mid-June event, with rain rate in the 4-6 mm/day range) is released as delayed evaporation ($\approx$ 1 mm/day in the case of this event), the water-balance during the rain event must imply a rather large run-off; since P $\sim$ 4-6 mm/day, coincident evaporation is $\leq$ 0.5 mm/day, recharge is $\sim$ 2 mm/day; yielding runoff to be 2.0 – 2.5 mm/day. That is a runoff comparable to recharge during the 1993 wet episode. Interestingly, the water balance is simpler during a prolonged dry spell such as the one in June 1988. The soil moisture is apparently soon exhausted, especially, during the latter part of the episode, when soil moisture isolines are almost vertical; the case in the 100-95W sector. Here precipitation deficits are balanced by simultaneous (and not delayed) evaporation deficits, with runoff and recharge being minimal; not surprisingly.

The notably marginal contribution of evaporation to the atmospheric column water evident in figures 5.3 – 5.6, which depicts the column budget to be P $\approx$ MFC, and the temporal lagging of evaporation with respect to precipitation (i.e., delayed,

and not coincident, recycling) at pentad resolution fully supports findings of Ruiz-Barradas and Nigam (2005, 2006) on the dominant role of transported moisture in Great Plains precipitation variability: the same authors also show that most current climate models are quite unrealistic in this regard as coincident evaporation is the dominant moisture source in the models.

A weak local recycling relationship is however not necessarily indicative of a negligible role for land surface influences. Recent modeling evidence suggests that an east-west southern Plains soil moisture gradient is responsible for influencing fluctuations of the GPLLJ and the attendant increase in northern Plains precipitation during 1993. The wet (dry) eastern (western) southern Plains region may produce a local enhancement of the east (high) to west (low) low-level pressure gradient, and thus the GPLLJ (Bosilovich and Sun 1999). An evaporation-LLJ relationship has also been advanced based on boundary layer forcing of the nocturnal jet and its modulation by the diurnally varying radiative responses of dry soil (Zhang et al. 2006; Zhong et al 1996)[12]. However the modeling analysis of Giorgi et al. found that evaporation and soil moisture forcing was a minor contributor to the drought of 1988 and had it been dominant would have provided a negative feedback to the drought via enhanced dynamical forcing of the low-level circulation (i.e., the GPLLJ).

The third monthly EOF GPLLJ mode representing 12% of the variance and exhibiting only a local strengthening of the jet magnitude (cf. figure 3.1) is linked to an anomalous and contemporaneous east-west soil moisture gradient over the southern Great Plains (regression pattern not shown). This principal component was

[12] While the diurnal evolution of the GPLLJ and land surface anomalies is not treated here, if their impacts are significant they should be manifest in the pentad anomaly structure, especially due to the temporal stability of soil moisture anomalies.

active during July 1993, however due to its modest Great Plains precipitation footprint could not have contributed significantly to the July precipitation episode. This mode was shown linked to the NAO, making attribution of soil moisture forcing of the GPLLJ implicit, if any. Monthly regressions however cannot discern the submonthly evolution of the GPLLJ, precipitation, and soil moisture anomalies, and as such, causality. These issues are probed in chapter 6.

5.3.3 Structure of the Anomalous GPLLJ

Given that GPLLJ variability and related moisture transports and moisture flux convergence are major contributors to the precipitation anomalies over the Great Plains in 1988 and 1993, and given considerable influence of the large-scale circulation on the GPLLJ on super-synoptic to seasonal timescales (Byerle and Paegle 2003; Higgins et al. 1997; Weaver and Nigam 2007), it is of great interest to examine the 3-dimensional structure conduit from the Gulf of Mexico.

Figure 5.7 shows the longitude-height cross section of the latitudinally averaged meridional winds in July 1993 and June 1988; the monthly averaged winds (contoured) are shown atop that months wind cliamtology (shaded). In 1993, the core of the GPLLJ is strengthened (by more than 50%) and vertically stretched. While in 1988 it is shifted westward and barely meets the 3 m/s contour threshold (i.e., a 50% reduction). The latitudinal reach of the jet in the bottom panels is depicted using latitude-height cross sections of zonally averaged (102-95°W) meridional winds. The nose of the jet is meridionally extended in 1993 while in 1988 there is a significant northward displacement of the entire jet core from its climatological June position; effectively isolating the jet from its primary moisture source - the Gulf of Mexico.

Clearly it is not the lack of the GPLLJ in 1988 that suppressed the moisture fluxes as suggested by the (25-35N) domain analyses, but its extreme meridional displacement, with attendant disconnection from the Gulf, that characterizes the summer of 1988. The 1988 (meridionally displaced) and 1993 (meridionally stretched) GPLLJ patterns are reminiscent of monthly GPLLJ modes 1 and 2 which showed significant connections to large scale circulation variability emanating from the ocean basins. The connection of these modes to land surface fields was ascertained to be negligible.

5.4 Remote Circulation Influence

5.4.1 Precipitation

The large scale circulation's influence on the evolution and intensity of regional hydroclimate extremes raises the prospects of predictability and begs the question: Do the known climate variability modes contribute to the Great Plains precipitation anomalies? To investigate this possibility, the ENSO and NAO climate variability modes were chosen due to their SST, diabatic heating, and circulation links noted in previous chapters, and in RBN (2005).

As a case study, we analyze contributions in July 1993 – the recent extremely wet period. Both the Niño 3.4 and NAO indices were constructed at pentad resolution for the period 1979-1997. To extract the ENSO signal optimally the Niño 3.4 index in the antecedent spring months was used in regression analysis; the May based analysis provided the best ENSO footprint in July. NAO's precipitation influence, on the other hand, was obtained from contemporaneous regressions given NAO's intraseasonal character; a SLP or 700 hPa gepotential height based index yielded similar precipitation footprints.

Precipitation regression patterns in NARR were generated using each index separately over the period (1979-1997) to discern the characteristic precipitation pattern produced by each mode. The pentads comprising July (P36-42) for the NAO and May (P24-30) for Niño 3.4 were used to extract the precipitation footprint. The product of the pentad index value during 1993 and the characteristic regression pattern was then used to assess the contribution of each mode to the total July 1993 precipitation anomaly.

Figure 5.8 (top left) shows the evolution of the total precipitation anomaly in the 37-45°N latitude belt during July 1993[13]. Positive precipitation anomalies persisted throughout the month, however the first 10 days exhibited the largest signal. Figure 5.8 (bottom left) shows the resulting anomaly after removing the combined NAO and ENSO precipitation from the total anomaly. While the characteristics of the spatial pattern are largely intact the early July precipitation anomaly was reduced in some areas by 2-4 mm/day, i.e., by about a third. However, the mid-month precipitation anomalies were reduced by >4 mm/day in some areas.

To enhance visualization of the contribution of each variability mode the right panels show the ENSO (top) and NAO (bottom) contributions to the total July precipitation anomaly respectively. The ENSO exhibits significant spatial and temporal stability when compared to the NAO, with the longitudinal gradient nearly constant and exhibiting minor temporal evolution. The NAO influence is more variable in contrast, and is robustly manifest after the big early July precipitation event. Rodwell and Hoskins (2001) show that subtropical anticyclones over the

[13] 37-45°N was used to focus on the strong positive anomalies.

Atlantic and Pacific basins are modulated by "monsoon" heatings to the west with a characteristic poleward flowing low-level jet. Perhaps anomalous precipitation induced heating over the Great Plains in July provides a downstream influence on the NAO in summer resulting in a positive feedback in sustaining the positive but weaker anomalies. Alternatively, the diabatic heating forced divergent outflow over the GP in conjunction with that over west coast of central America as in figure 2.9 forces the weak anomalous upper level convergence over the Gulf of Mexico creating the local surface high and essentially increasing the already existing climatological large scale pressure gradient which in turn strengthens the jet and enhances the moisture fluxes into the Great Plains. While engaging in discussion of probable mechanisms is enticing, high confidence in attribution is prohibited by the analysis strategy here and predicated on more robust analysis (i.e. diagnostic modeling).

5.4.2 Circulation

The significant contributions by the NAO and ENSO to the July 1993 precipitation anomaly calls for the characterization of each mode's contribution to the large scale antecedent circulation. As such, the same analysis strategy as in the precipitation diagnosis is adopted here. Again, for ENSO, the May index is used while for the NAO the contemporaneous (June in this case) value of the index is employed as the regression predictor.

The top panel in figure 5.9 shows the total 200 hPa height anomaly for June 1993 as diagnosed from NCEP/NCAR reanalysis. A nearly hemispheric wide negative height anomaly is present north of 30ºN and is strongest over the central midlatitude Pacific. Geostrophic considerations suggest that enhanced upper level zonal flow was

present over the central North Pacific during June 1993. Mo and Paegle (1995) suggest that this upper level flow pattern was instrumental to the flood generating large-scale circulation anomalies.

The two middle panels show the ENSO and NAO contributions to the June 1993 200 hPa anomaly. Immediately apparent is the robust ENSO connection and the lack of an NAO link. The interesting feature is the large regional ENSO contribution to the negative height anomaly that stretches from the Hudson Bay to Pacific coast. This anomaly is conducive to cyclogenesis in the lee of the Rockies and attendent precipitation over the Great Plains. Also notable in the ENSO contribution is the North Atlantic negative height anomaly found in the NAO region. Could this be a precursor to the coming strong NAO anomaly observed during July 1993? Compo et. al (2001) note substantial differences in high frequency vs. low frequency midlatitude circulation responses to ENSO forcing during winter, especially in the North Atlantic. It is possible that such characteristics may be influential here in summer, although, while interesting and enticing, attribution of an ENSO NAO connection cannot be stated here with certainty.

The difference field (bottom panel) still shows a significant signal over the Atlantic and Pacific basins, however the anomalous trough over the western U.S. is almost completely removed and in some areas is replaced by a modest ridge. The situation in July of 1993 (not shown) was characterized by a strong NAO signal with a weakening ENSO impact; further suggesting that ENSO contributed positively to the setup for the strong precipitation event while the NAO impact was realized in a

contemporaneous sense. The NAO ENSO connection in summer will be further probed in future observational and modeling scenarios.

5.5 Chapter 5 Figures

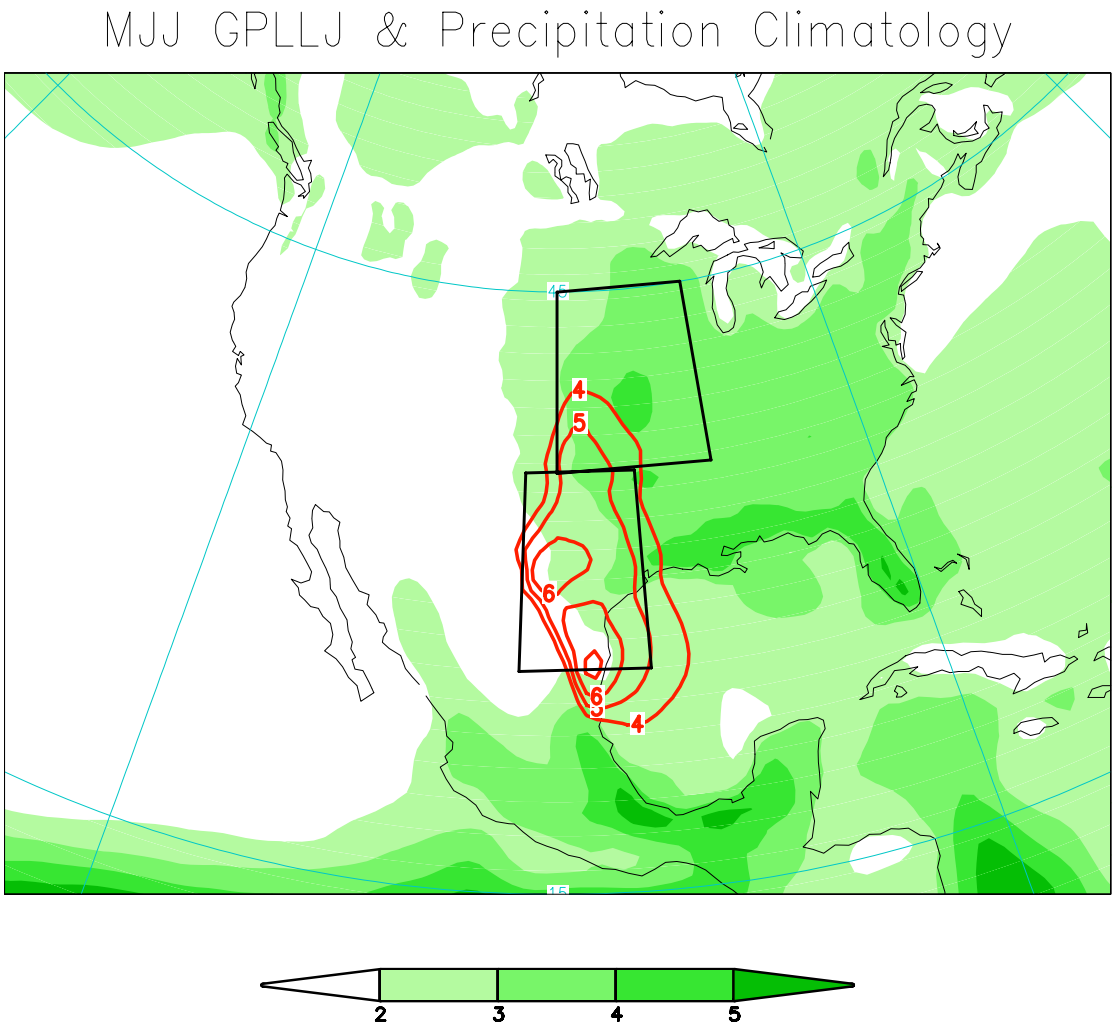

Figure 5.1. Seasonal climatology (MJJ) of precipitation (shaded) and the Great Plains low-level jet as reflected in the 900 hPa meridional winds (contoured) in the North American Regional Reanalysis from 1979-2005. The northern and southern boxes outline the areas defined by the Great Plains precipitation and low-level jet indices respectively. Winds > 4 m s^{-1} are contoured at 1 m s^{-1} intervals and precipitation > 2 mm day^{-1} is shaded .

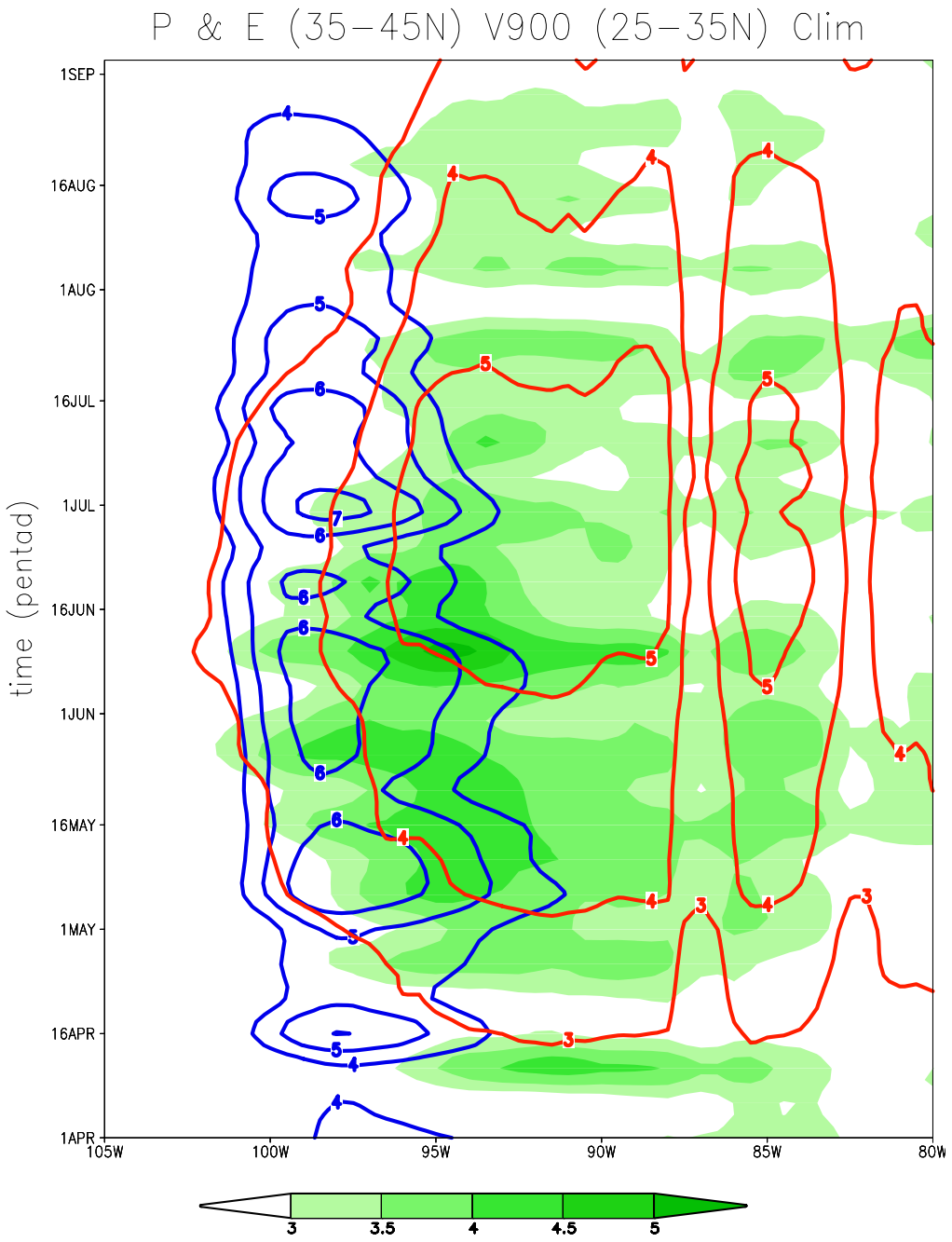

Figure 5.2. Warm season climatological (1979-2005) pentad evolution of: precipitation (shaded), 900 hPa meridional wind (blue contours), and evaporation (red contours) in NARR. Precipitation and evaporation are meridionally averaged over 35-45°N and units are mm day^{-1} while the GPLLJ is meridionally averaged over 25-35°N and units are m s^{-1}.

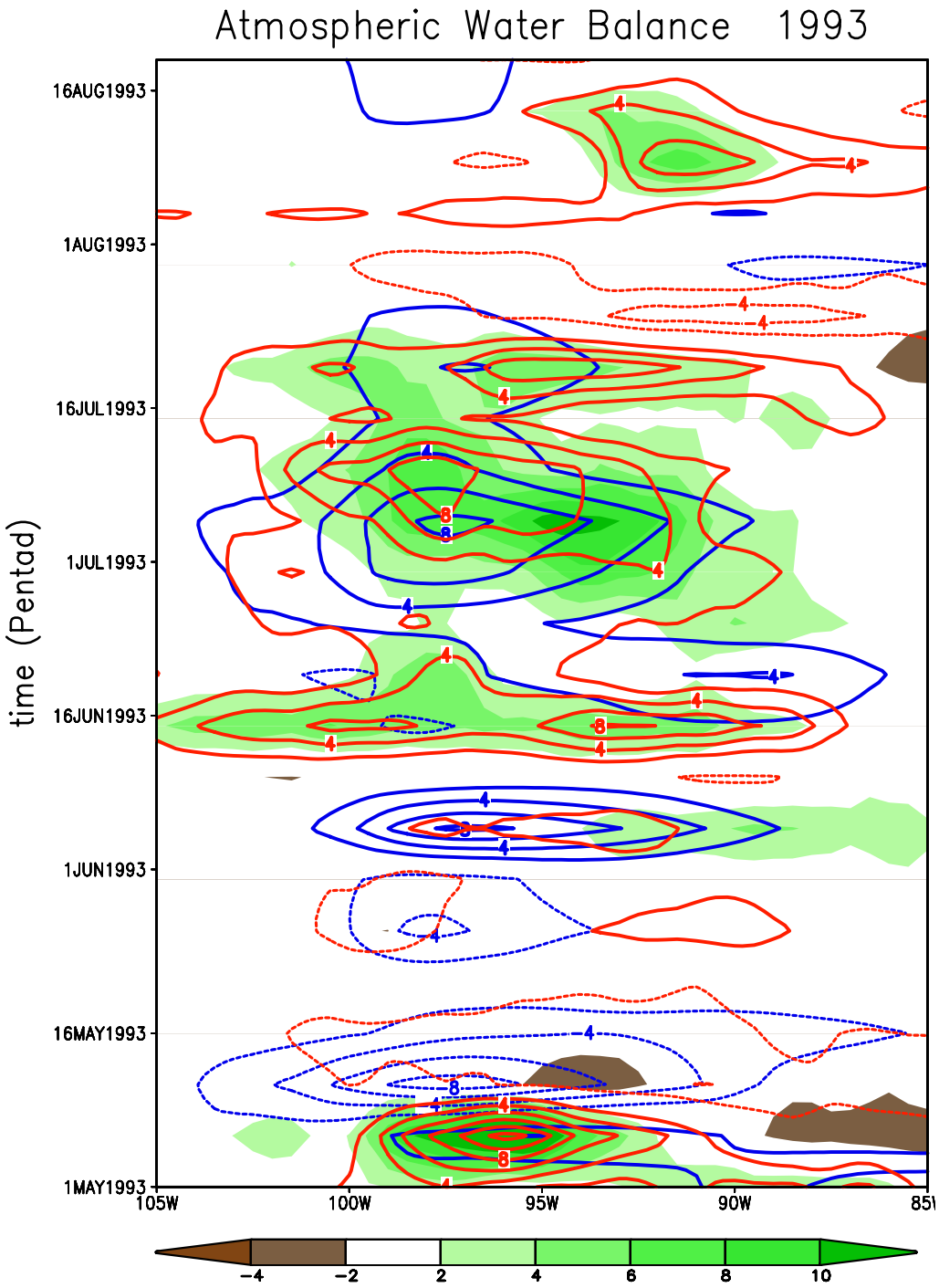

Figure 5.3. Pentad evolution of MJJ precipitation (shaded), the GPLLJ (blue contours), and moisture flux convergence (red contours) anomalies during 1993 in NARR. Precipitation and moisture flux convergence are meridionally averaged over 35-45°N and units are mm day^{-1} while the GPLLJ is meridionally averaged over 25-35°N and units are m s^{-1}.

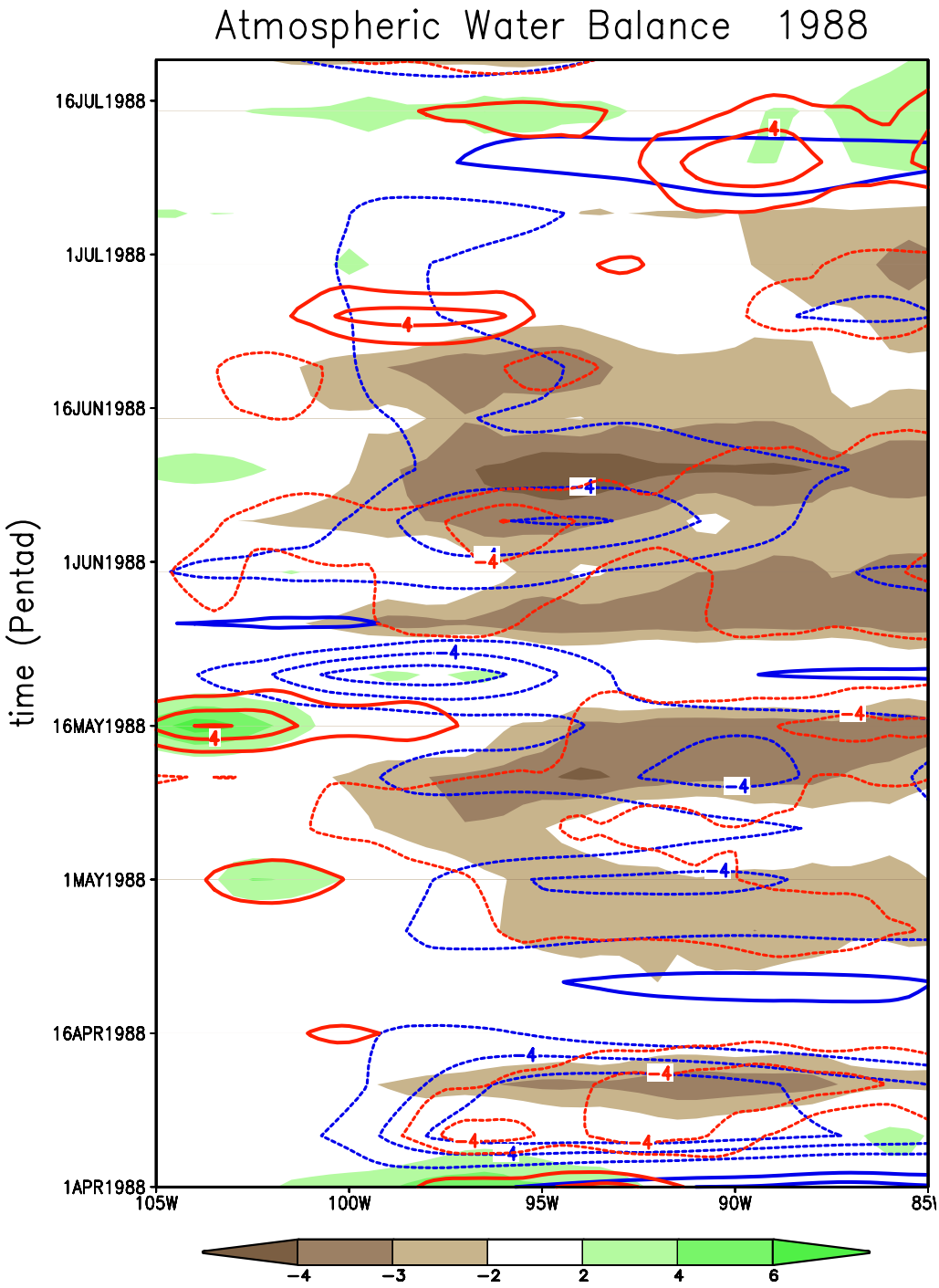

Figure 5.4. Pentad evolution of MJJ precipitation (shaded), the GPLLJ (blue contours), and moisture flux convergence (red contours) anomalies during 1988 in NARR. Precipitation and moisture flux convergence are meridionally averaged over 35-45°N and units are mm day^{-1} while the GPLLJ is meridionally averaged over 25-35°N and units are m s^{-1}.

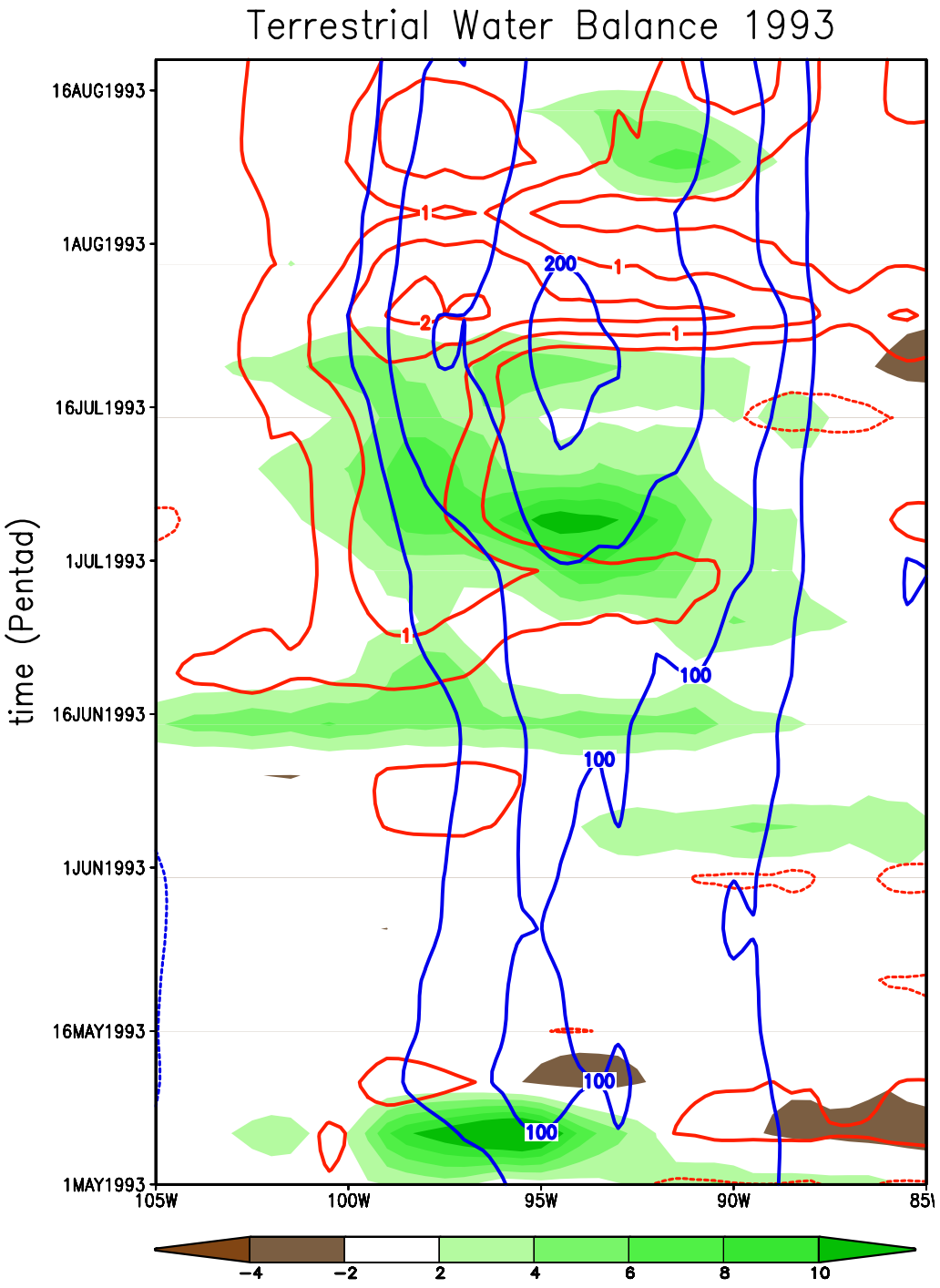

Figure 5.5. Pentad evolution of MJJ 35-45°N meridionally averaged: precipitation (shaded), evaporation (red contours), and soil moisture (blue contours) anomalies during 1993 in NARR. Precipitation and evaporation are in mm day^{-1} while soil moisture is in mm.

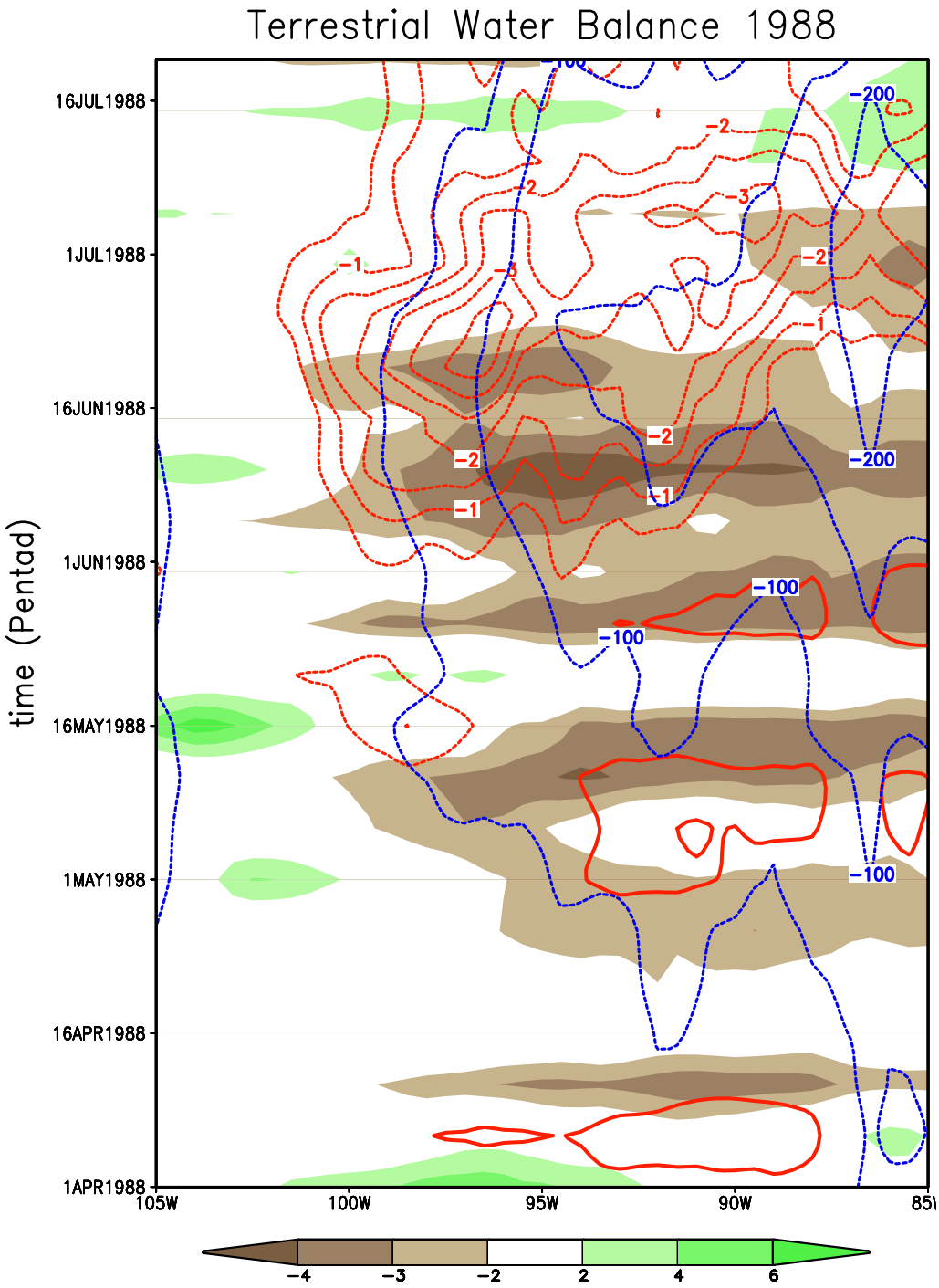

Figure 5.6. Pentad evolution of MJJ 35-45°N meridionally averaged: precipitation (shaded), evaporation (red contours), and soil moisture (blue contours) anomalies during 1988 in NARR. Precipitation and evaporation are in mm day^{-1} while soil moisture is in mm.

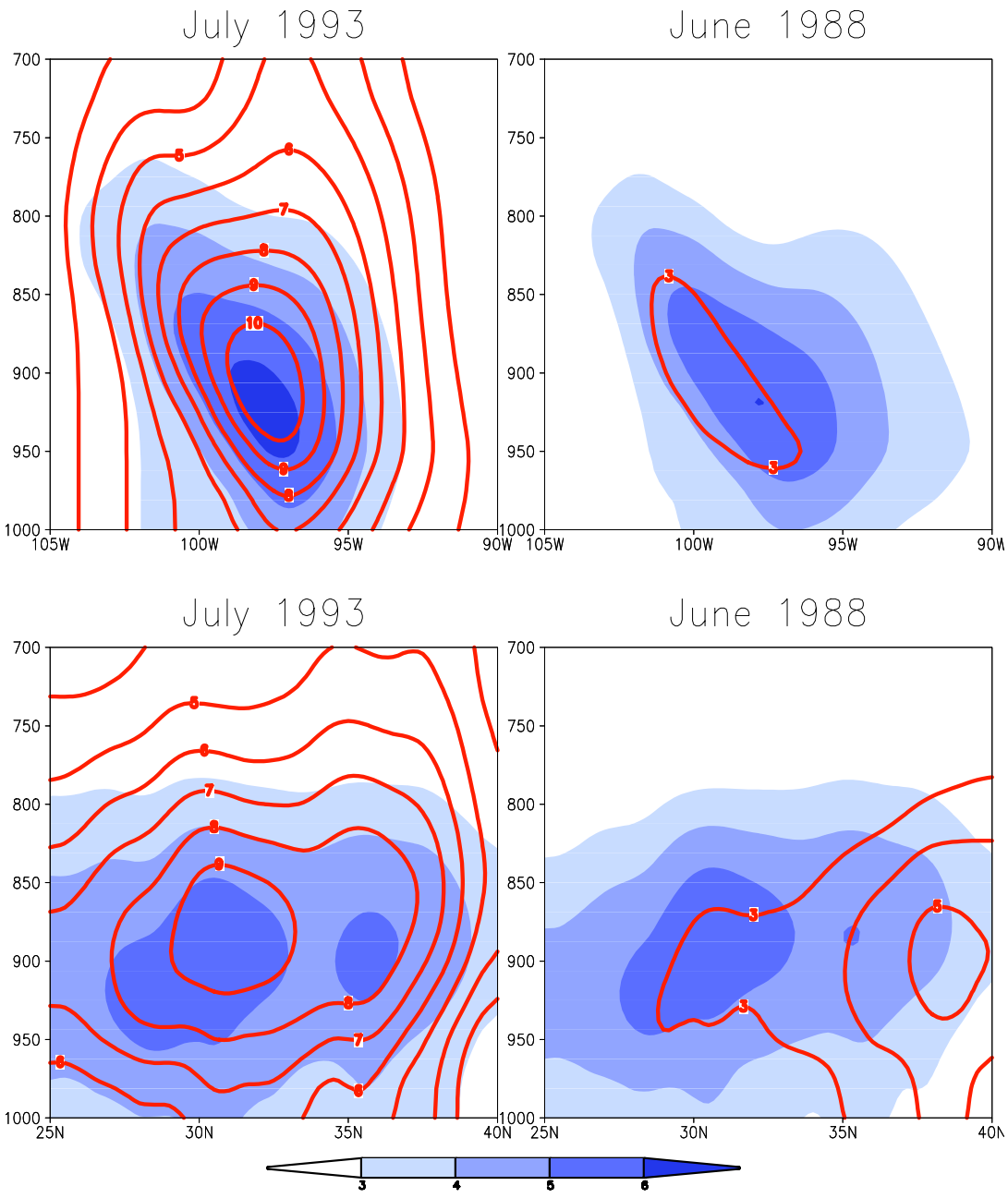

Figure 5.7. (top left) Longitude – height cross section of the 25-35°N meridionally averaged meridional wind for July climatology (shaded) and July 1993 anomalies (contoured). (top right) Same as above except for June climatology (shaded) and June 1988 anomalies (contoured). (bottom left) Latitude – height cross section of the 102-97°W zonally averaged meridional wind for July climatology (shaded) and July 1993 anomalies (contoured). (bottom right) Same as in bottom right except for June climatology (shaded) and June 1988 anomalies (contoured). Units are in m s^{-1}.

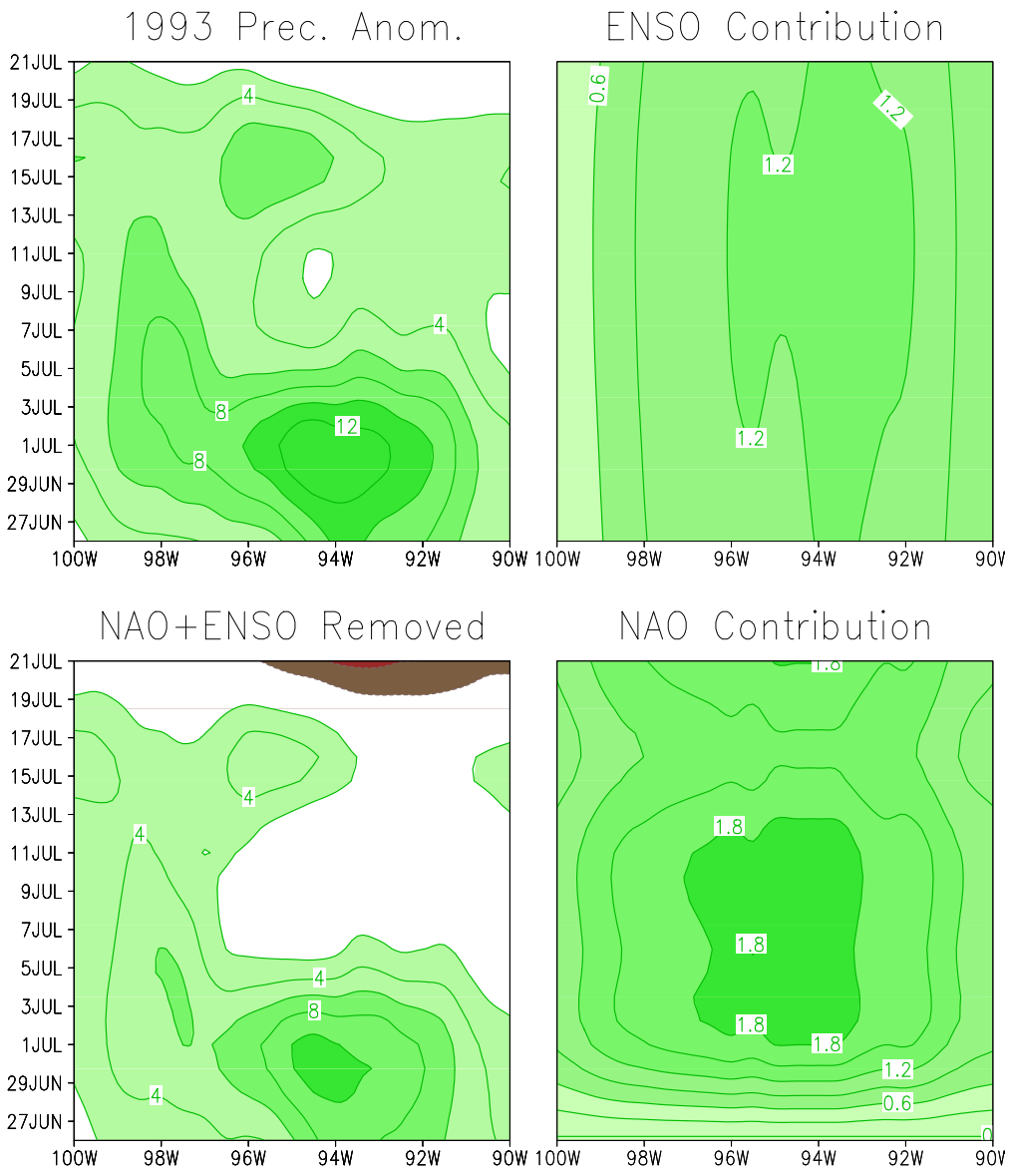

Figure 5.8. Contribution by the NAO and ENSO to the July 1993 precipitation anomaly in NARR pentad data. Total anomaly (top left), Total anomaly minus the combination of the NAO and ENSO precipitation footprint (bottom Left), ENSO and NAO contributions contributing to the total anomaly (top right and bottom right respectively). Contour interval for left panels is 2 mm day^{-1} and for the right is 0.3 mm day^{-1}.

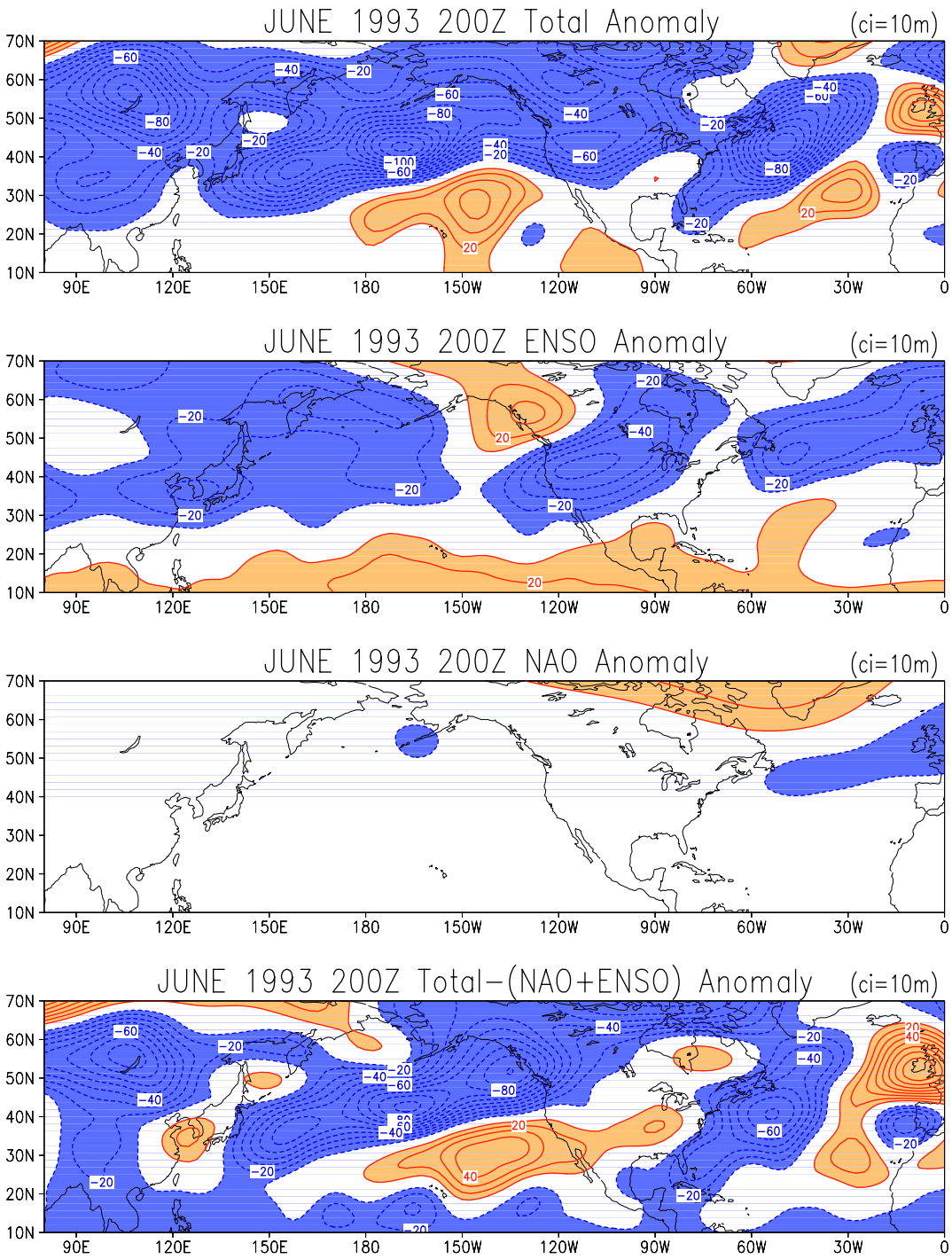

Figure 5.9. Contribution of the NAO and ENSO to the 200 hPa height anomalies during June 1993. Negative (positive) anomalies are shaded in blue (orange) and contoured at 10 meter intervals. The total anomaly is in the top panel while the ENSO, NAO, and total minus NAO+ENSO are in the second, third, and fourth panels respectively.

Chapter 6: Evolution of Great Plains Hydroclimate

The interesting case study presented in chapter 5 calls for an objective analysis of the temporal phasing of pertinent circulation and land – atmosphere interactions. Are the evolutionary characteristics between the GPLLJ, precipitation, evaporation, and soil moisture during the events of 1988 and 1993 manifestations of recurrent spatio-temporal regional climate modes? To probe this question traditional EOF and Extended EOF analysis is performed on MJJ pentad (5-day) averaged 900 hPa meridional winds. Lead/lag regressions are computed to ascertain the phasing and magnitude of the key hydroclimate relationships. In this analysis The MJJ period is defined as 16 pentads, beginning with the first full pentad in May. The pentad averaging eliminates the diurnal and much of the synoptic variability while retaining lower frequency (submonthly) climatic fluctuations. For the regular EOF calculation, the sensitivity to seasonal evolution was inspected by performing the analysis on the first and second halves of the MJJ period separately. Similar patterns emerge regardless of subseasonal time period chosen.

6.1 GPLLJ Pentad Modes

6.1.1 PC Autocorrelation

The first six modes in the EEOF analysis were generated and each PC autocorrelated to determine which modes exhibited the most temporal stability and should be retained for further study. Figure 6.1 plots the autocorrelation of each of the first six PC's. The solid black line, denoting the pentad resolution GPLLJ index, shows that the jet autocorrelation is poor even at minus 1 pentad, as the index falls

well below the e^{-1} line at this time lag. The time correlation is far worse for PC's 2, 3, and 5 with 3 exhibiting a robust negative autocorrelation at one pentad lag. The PCs demonstrating the highest autocorrelations (1, 4, and 6) all remain above the e^{-1} demarcation at one pentad lag. These three modes exhibit the best potential for predictability based on their robust autocorrelations. Not surprisingly the loading vectors of these 3 modes resemble the first three monthly GPLLJ variability modes depicted in chapter 3 and are similarly retained here for further insight.

6.1.1 Spatial Patterns

The inclusion of the temporal constraint inherent in EEOF analysis does not guarantee that the order of the modes will be the same as that of standard EOF analysis. However one of the benefits of using EEOFs, as opposed to traditional EOF analysis, is the prospect for capturing coherent evolution of what are ultimately rapidly (submonthly) varying regional phenomena. Figures 6.2, 6.3, and 6.4 show the evolution of the three modes that exhibit the best spatial coherence among monthly and pentad EOF analysis (right panels) and pentad smoothed (1-2-1) and unsmoothed EEOF analysis (middle and left panels respectively).

In the case of mode 1 (figure 6.2) all EOF and EEOF analyses produce generally the same characteristic, meridionally stretched, jet suggesting the stability of this pattern in depicting GPLLJ variability. Comparison of the evolutionary features between the EEOF and EOF analysis demonstrates the power that the former provides. At a time lag of one pentad the GPLLJ in the EEOF analysis is strong and exhibits similar structure to the mature and nascent phases, while the EOF representation shows no such coherence. Furthermore, the evolution of the

magnitude of mode 1 is evident at t = 0 and shows the strongest jet. In the decay phase the jet is still robust, however the magnitude and the width are diminished.

Similar evolution characteristics are present in the second pattern. Here both the smoothed EEOF and EOF are the second leading modes in their respective analyses, however the pure EEOF is the fourth in its ranking; although due to spatial similarities is named Mode 2. Again the evolution of the pattern is more robust in the EEOF analysis and in the pure data (left panels) shows a three pentad strengthening of the meridionally displaced jet.

The third mode exhibits differing characteristics when comparing the pentad analysis regimes in figure 6.4. This mode is the only one that shows some connection to the antecedent phase in the regular EOF case (right panels). The pure EEOF analysis (left panels) shows coherence in the evolution of the positive meridional wind anomalies, but curiously, the negative northern Great Plains meridional winds are present at t –1 and t+1 but not at t 0.

6.2 Impact of GPLLJ Variability Modes

The identification and extraction of pentad resolution EEOF GPLLJ variability modes that demonstrate temporal stability may be exploited to assess the evolving hydrocliamate relationships. In this section the PCs of each mode will be used as indices for lead/lag regressions on precipitation, total moisture flux convergence (MFC), evaporation, surface air temperature (SAT), and soil moisture.

6.2.1 Mode 1

Figure 6.5 shows the evolution of the leading mode of GPLLJ variability (shaded), precipitation (contoured left panels), and total MFC (stationary + transient) (contoured right panels). Moisture flux convergence is defined as, MFC=$V \cdot \nabla q + q \nabla \cdot V$, where q is specific humidity and V is the horizontal wind vector. Note, that while the GPLLJ matures and is strongest at t = 0 (cf. Figure 6.2), the precipitation and MFC lags the maximum GPLLJ by one pentad. A similar relationship was noted in the pentad analysis of the drought of 1988 and flood of 1993; although this connection is not always present, nor a necessary condition for anomalous precipitation events. The delay in precipitation and moisture flux convergence suggests that the moisture transport term in the MFC equation may dominate in the generation of precipitation from this mode.

The evolution of evaporation (left), SAT (middle), and soil moisture (right) are shown in figure 6.6. The evaporation in connection with this mode is minor in both magnitude and spatial extent. This is not surprising given the strong presence of this mode during July 1993 (cf. figure 3.1, upper right panel) and the 2 week delay of evaporation when compared to the maximum in GPLLJ during July 1993 (cf. figures 5.5, 5.7).

Mild negative SAT anomalies are present at the exit region of the GPLLJ where the precipitation is slowly building up over the first two pentads. At the time of maximum precipitation (i.e., t + 1), the negative temperature anomaly has retrogressed and strengthened with a marked positive anomaly in the eastern half of the U.S. This eastward shifted anomaly (with respect to precipitation) may be a

manifestation of the combined effects of nocturnally eastward propagating MCCs, with thick clouds inhibiting longwave radiative emission at night, and clear summer days with enhanced receipt of shortwave radiation (lead/lag analysis on radiative fluxes is a subject of future work). The soil moisture anomalies are enhanced at the jet exit region, however, remain unchanged in other parts of the domain.

6.2.2 Mode 2

The key hydroclimate fields associated with the second mode are presented in figures 6.7 and 6.8. This is the second leading mode in the monthly and pentad EOF analysis and the fourth in the EEOF analysis. While the strongest northward shifted GPLLJ (positive meridional winds) exists at t + 1 (cf. figure 6.3) the difference between the positive and negative meridional winds between the northern plains and the Gulf of Mexico is approximately the same at t = 0 and t + 1 indicating a persistent low-level divergence anomaly in the central U.S. As in mode 1 the maximum precipitation and MFC anomalies temporally lag the build up of the meridional wind anomalies; suggesting that the advection term in the MFC may also be quite important here. This mode however is associated with negative precipitation and MFC anomalies stretching from the foothills of the Rocky Mountains to the east coast. Not surprisingly, this pattern existed during the 1988 drought.

The surface hydroclimate evolution of figure 6.8 shows that evaporation magnitude is small, however more expansive than in mode 1 at t + 1 and coincident over the area of the meridionally shifted GPLLJ. It appeared, at times, that during 1988 the GPLLJ and evaporation anomalies were not so delayed as in 1993 (cf. figures 5.6 and 5.8), which may suggest a stronger coupling of the jet and evaporation

anomalies in the drought scenario. A strong SAT anomaly develops in accordance with this mode and is, perhaps, reflective of the strong shortwave absorption during repeated clear days, as is common during anomalously dry events. The spatial extent of the positive soil moisture anomalies is decreasing throughout the evolution, while the negative soil moisture anomalies are expanding from the east coast of the U.S. westward toward the Mississippi river

6.2.3 Mode 3

The third mode of GPLLJ variability (sixth in EEOF) also shows interesting connections of the GPLLJ, precipitation, and MFC anomalies. However, the magnitude of the positive precipitation anomalies is diminished in comparison with modes 1 and 2, as evidenced by the monthly footprint (cf. figure 3.3 – bottom panel). Conversely, the development of the negative precipitation anomalies over the Gulf of Mexico and southeastern U.S. is strong and is a contributing factor to the negative portion of the precipitation dipole noted in the July regressions of the total GPLLJ index from chapter 2 (cf. figure 2.7b and 3.3). The largest positive northern Great Plains precipitation and MFC anomalies are found at t = 0, when the 900 hPa meridional wind convergence between the northern (negative) and southern (positive) plains is virtually absent. However, over the Gulf states, the nascent period shows the strongest precipitation anomalies. This suggests that the total MFC may also be dominated by the transport term as the negative MFC anomaly is strongest at t + 1 one pentad after the maximum in offshore (dry) negative meridional winds.

The evolution of the evaporation field is expanded when compared to modes 1 and 2, however, the magnitude is still weak. The strengthening SAT anomaly dipole,

which is mature at t +1, may be due to the radiative effect coupled with positive and negative meridional temperature advections. While stronger soil moisture anomalies exist in this mode, as compared with modes 1 and 2, the negative (east) to positive (west) opposes the optimal conditions of GPLLJ development proposed by Bosilovich and Sun (1999). Furthermore, positive evaporation which has been shown to be a negative feedback to the jet (Zhong 1996), while mild, is present over the area of the GPLLJ until t + 1 when it is shifted northward coincident with jet strengthening.

6.3 Large Scale Circulation Evolution

The evolution of Great Plains hydroclimate as diagnosed from EEOF PC lead/lag regressions demonstrates the importance of moisture transports in generating Great Plains hydroclimate anomalies. A majority of this thesis has been focused toward characterization of the large-scale circulation features accompanying GPLLJ variability. Here the evolution of the large-scale circulation associated with the northward shifted GPLLJ (mode 2) is analyzed. This mode is shown connected to a reduction in Great Plains precipitation and was strong in the summer of 1988.

The evolution of 200 hPa heights associated with mode 2 is shown in figure 6.11. It appears that this large-scale circulation anomaly is part of a propagated signal from East Asia as evidenced by the North Pacific wave train development and decay. The circulation anomaly exhibits explosive development between t=0 and t=1, especially with regard to the mid continental ridge over North America. This particular anomaly center continues to strengthen at t=2 and t=3, and with greater amplitude than its

pacific counterparts. One possibility for this notable characteristic may be anomalous flow interaction with Rocky orography.

To ascertain the potential effect of the topographic barrier, figure 6.12 depicts the evolution of the 850 hPa zonal wind (shaded) and divergence (contoured). The explosive development noted in figure 6.11 is evident here, at low-levels, as seen through the rapid evolution of a significant divergence anomaly couplet over the western and central U.S. from t=0 to t=1. The orographic interaction mechanism is implicated by noting that this divergence couplet is situated to the east of a low-level positive zonal wind anomaly that is evolving in concert with the 850 hPa divergence anomaly couplet and itself is impacted by the large mountain barrier. This explanation is further supported by the nondescript divergence anomalies upstream over the Pacific; essentially ruling out the potential that this anomaly is part of the original propagated signal.

6.4 Chapter 6 Figures

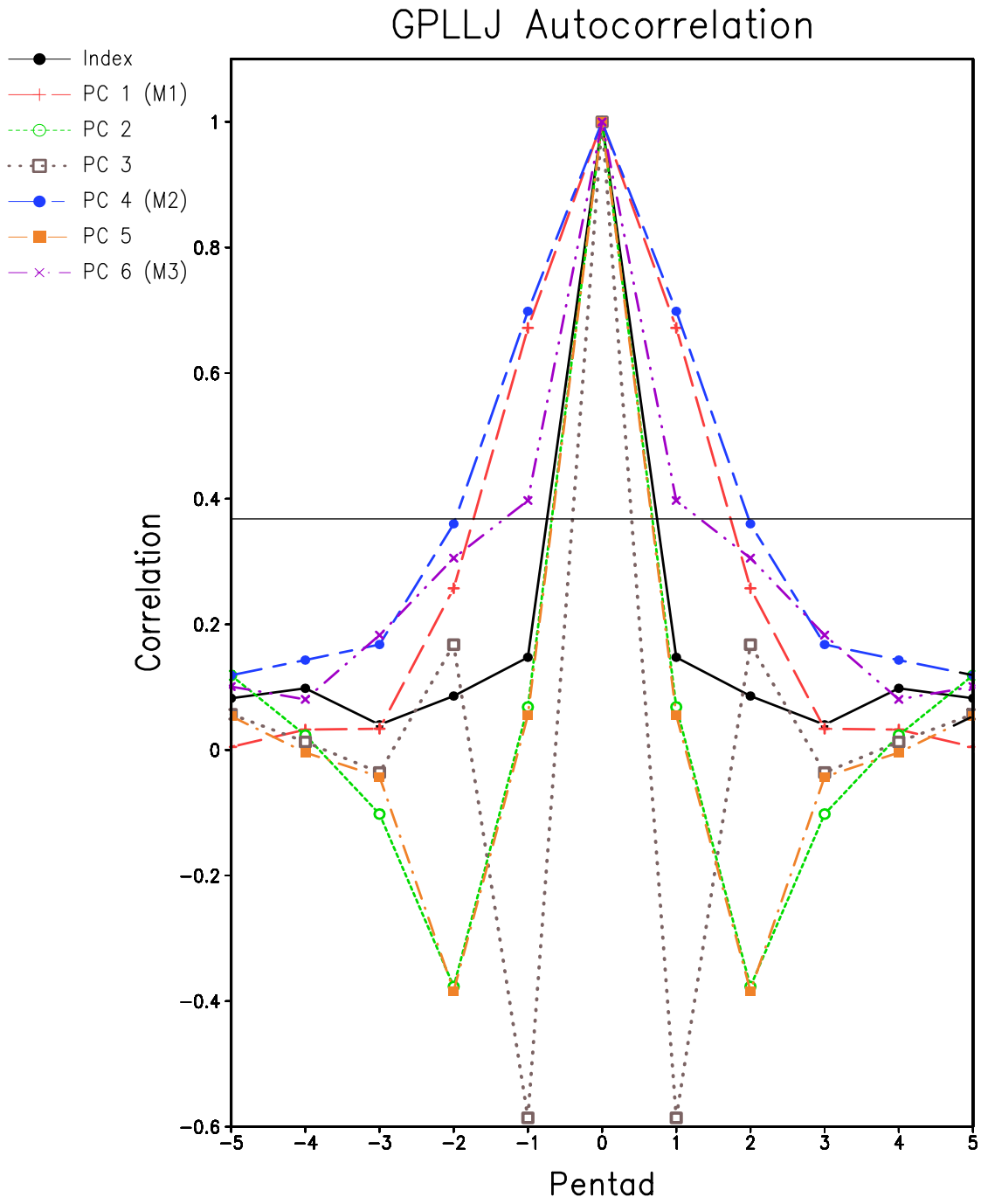

Figure 6.1. Autocorrelation of the pentad resolution GPLLJ index and the first six PCs generated from Extended EOF analysis. The horizontal line denotes the e^{-1} demarcation.

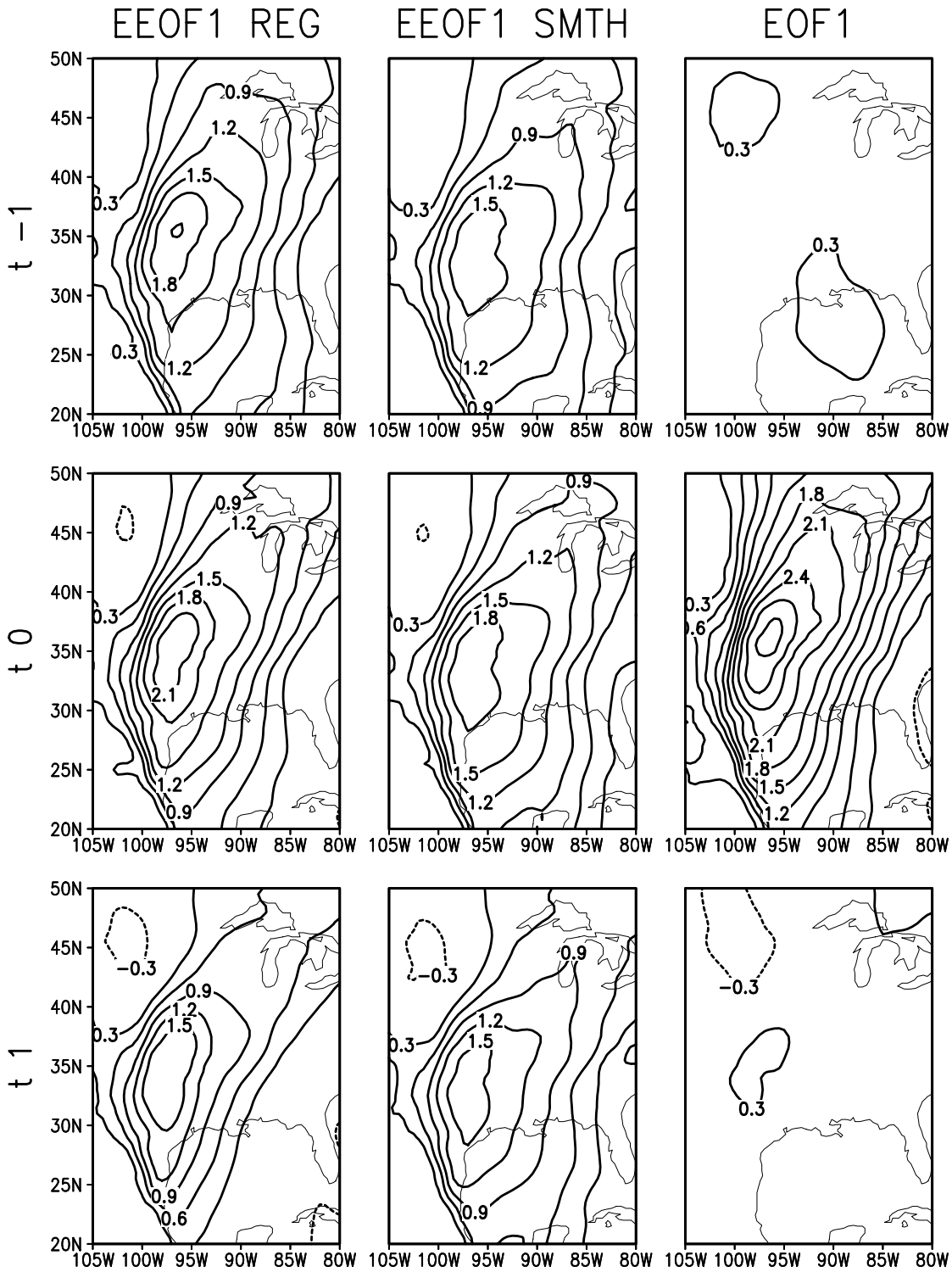

Figure 6.2. Evolution of the first mode of GPLLJ variability at pentad resolution. A 1-2-1 smoothing is applied to the data in the middle column prior to analysis. The left and middle columns are Extended EOF while the right is standard EOF analysis.

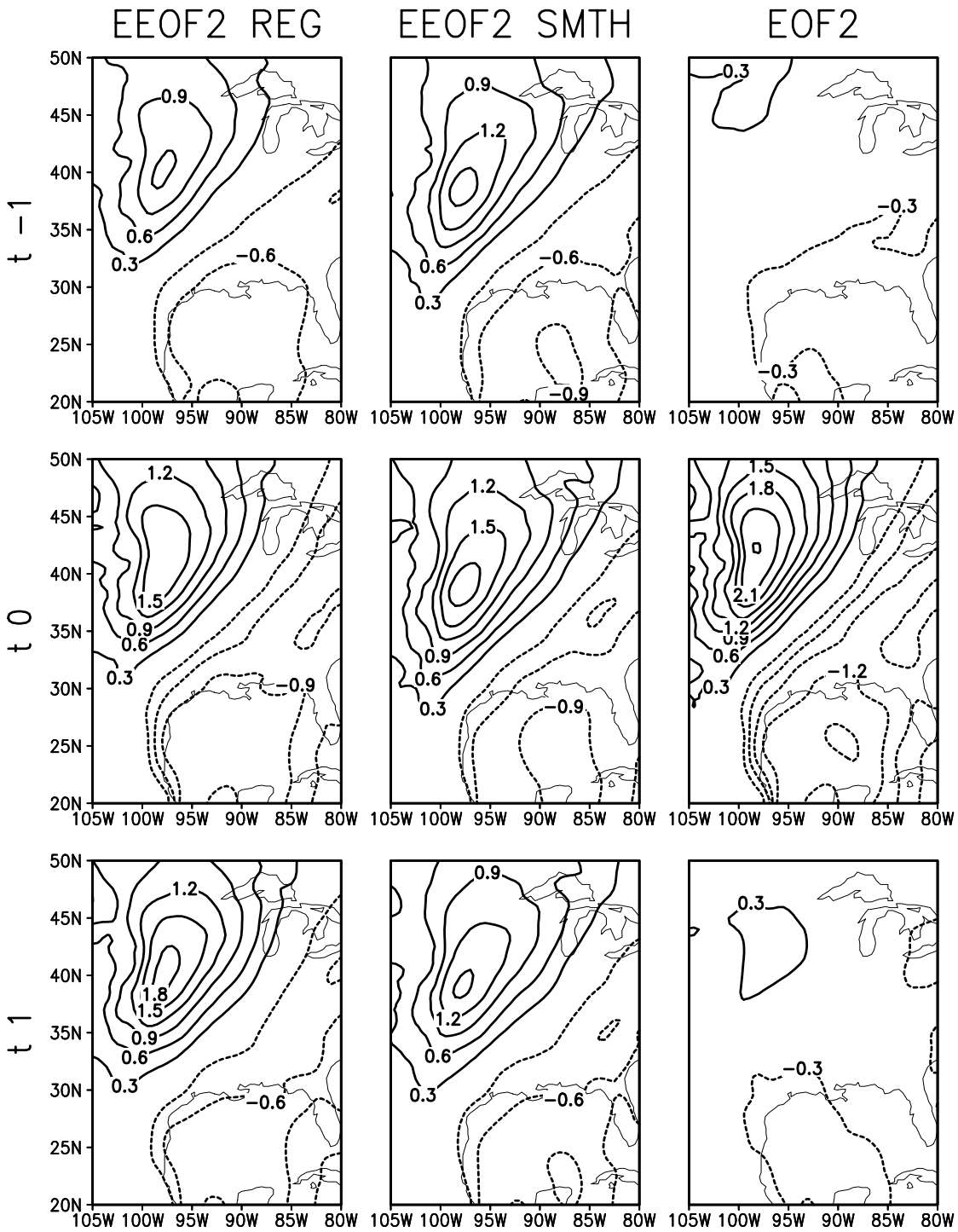

Figure 6.3. Evolution of the second mode of GPLLJ variability at pentad resolution. A 1-2-1 smoothing is applied to the data in the middle column prior to analysis. The left and middle columns are Extended EOF while the right is standard EOF analysis.

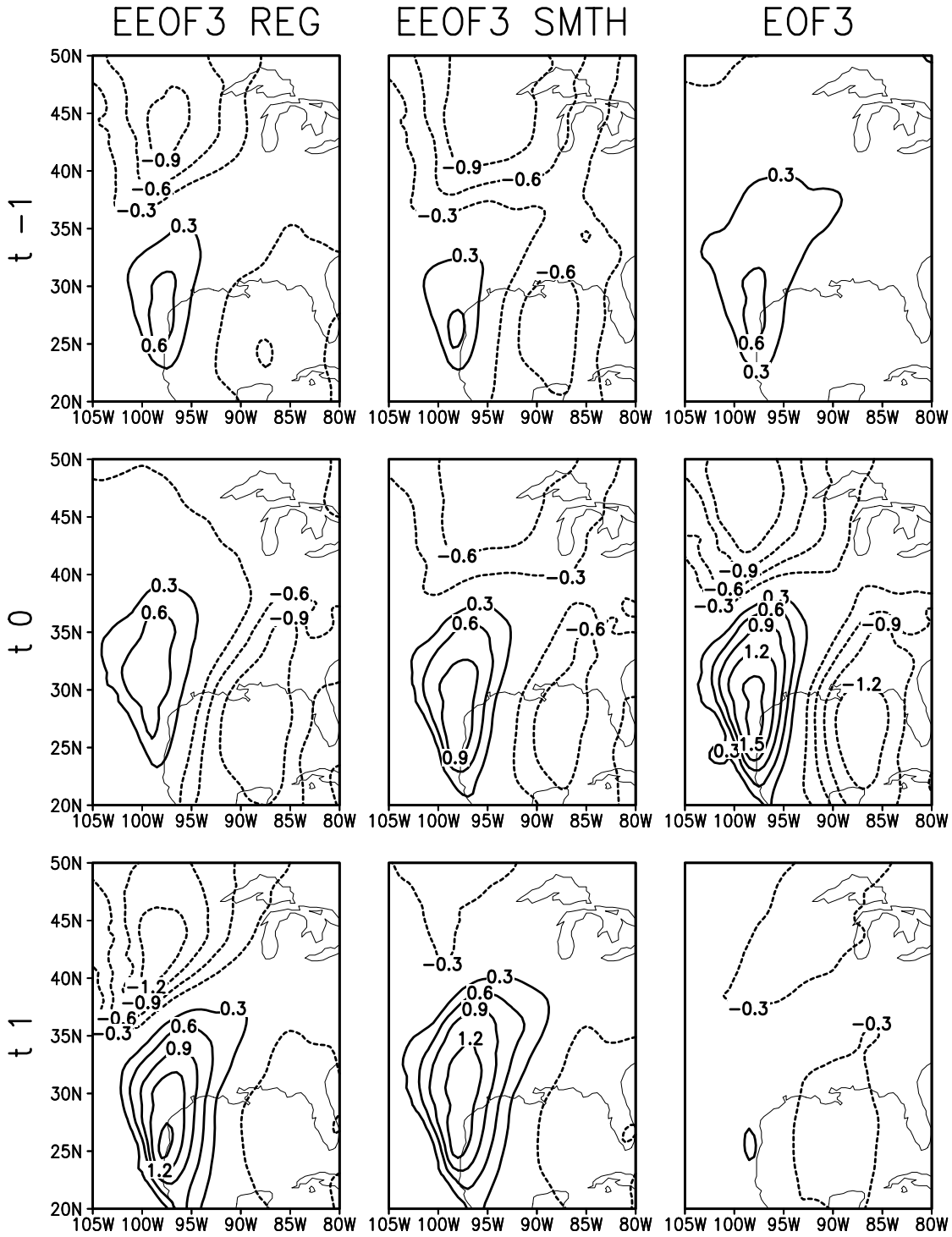

Figure 6.4. Evolution of the third mode of GPLLJ variability at pentad resolution. A 1-2-1 smoothing is applied to the data in the middle column prior to analysis. The left and middle columns are Extended EOF while the right is standard EOF analysis.

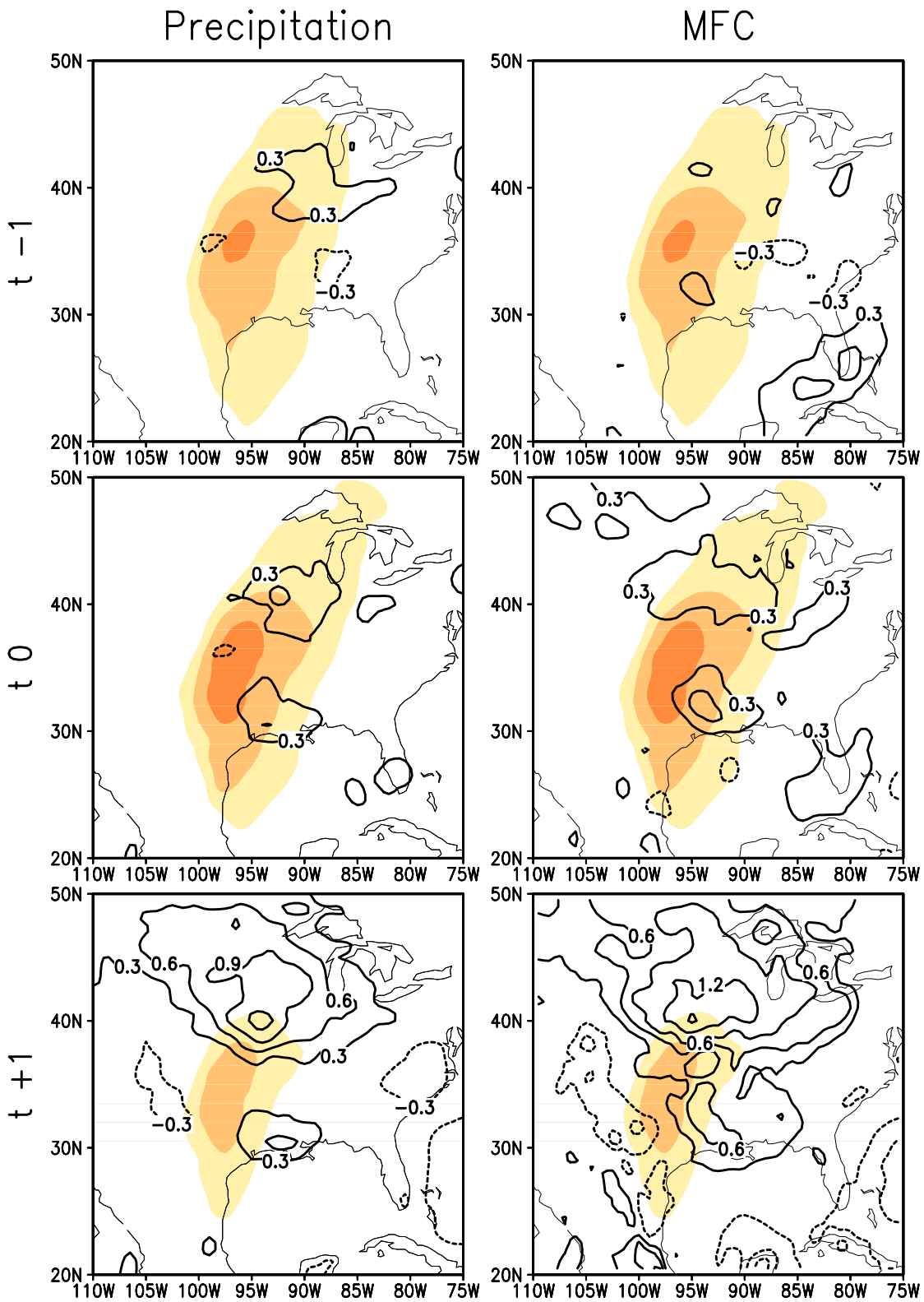

Figure 6.5. Evolution of the GPLLJ (shaded), precipitation (left column), and moisture flux convergence (right column) associated with EEOF mode 1. The contour interval is 0.3 mm day^{-1}.

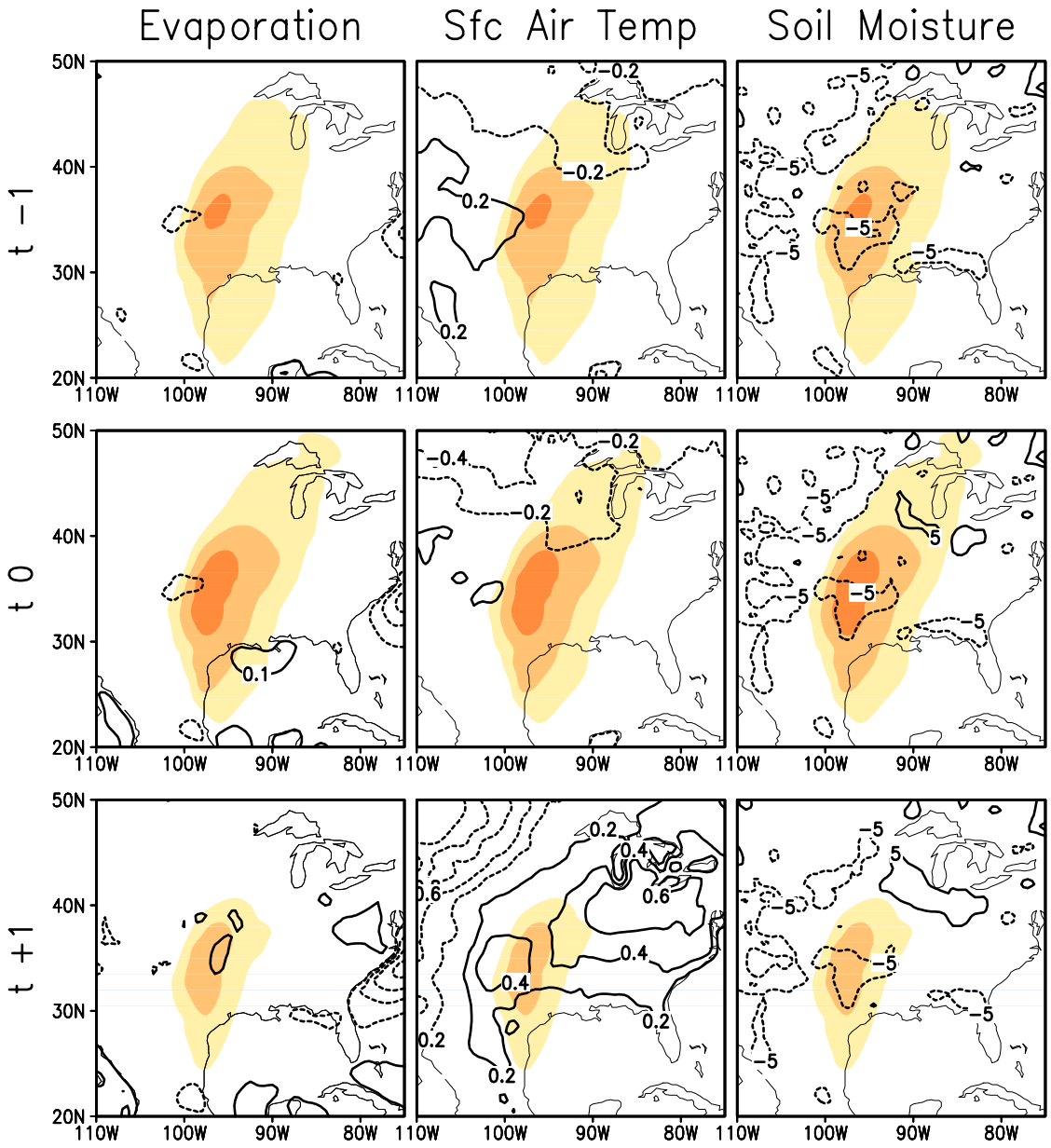

Figure 6.6. Evolution of the GPLLJ, evaporation (left column), surface air temperature (middle column), and soil moisture (right column) associated with EEOF mode 1. Evaporation, SAT, and soil moisture are contoured at 0.1 mm day^{-1}, 0.2 k day^{-1}, and 5 mm respectively.

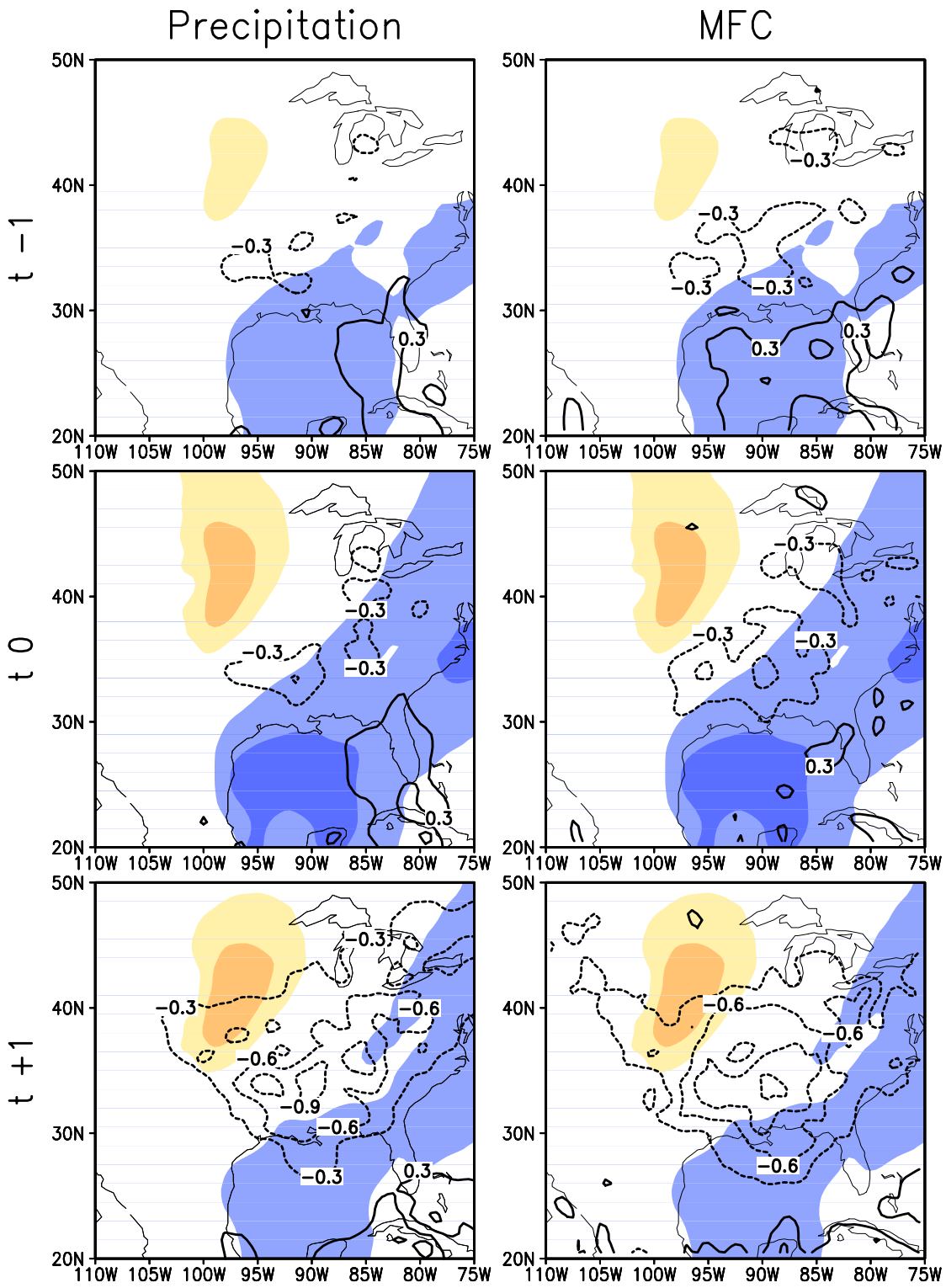

Figure 6.7. Evolution of the GPLLJ (shaded), precipitation (left column), and moisture flux convergence (right column) associated with EEOF mode 2. Positive (negative) values are shaded orange (blue) and the contour interval is 0.3 mm day^{-1}.

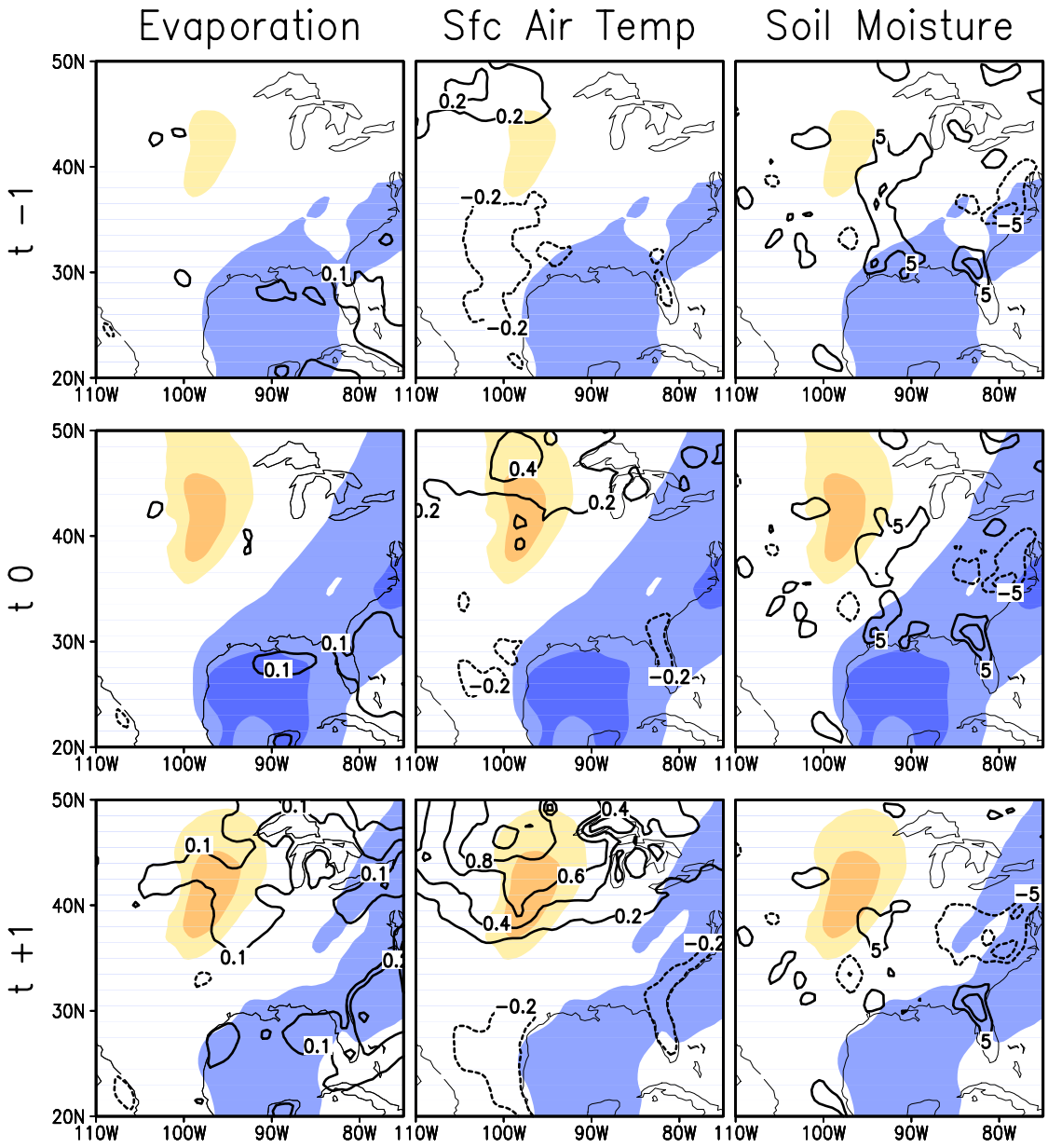

Figure 6.8. Evolution of the GPLLJ, evaporation (left column), surface air temperature (middle column), and soil moisture (right column) associated with EEOF mode 2. Positive (negative) values are shaded orange (blue). Evaporation, SAT, and soil moisture are contoured at 0.1 mm day^{-1}, 0.2 k day^{-1}, and 5 mm respectively.

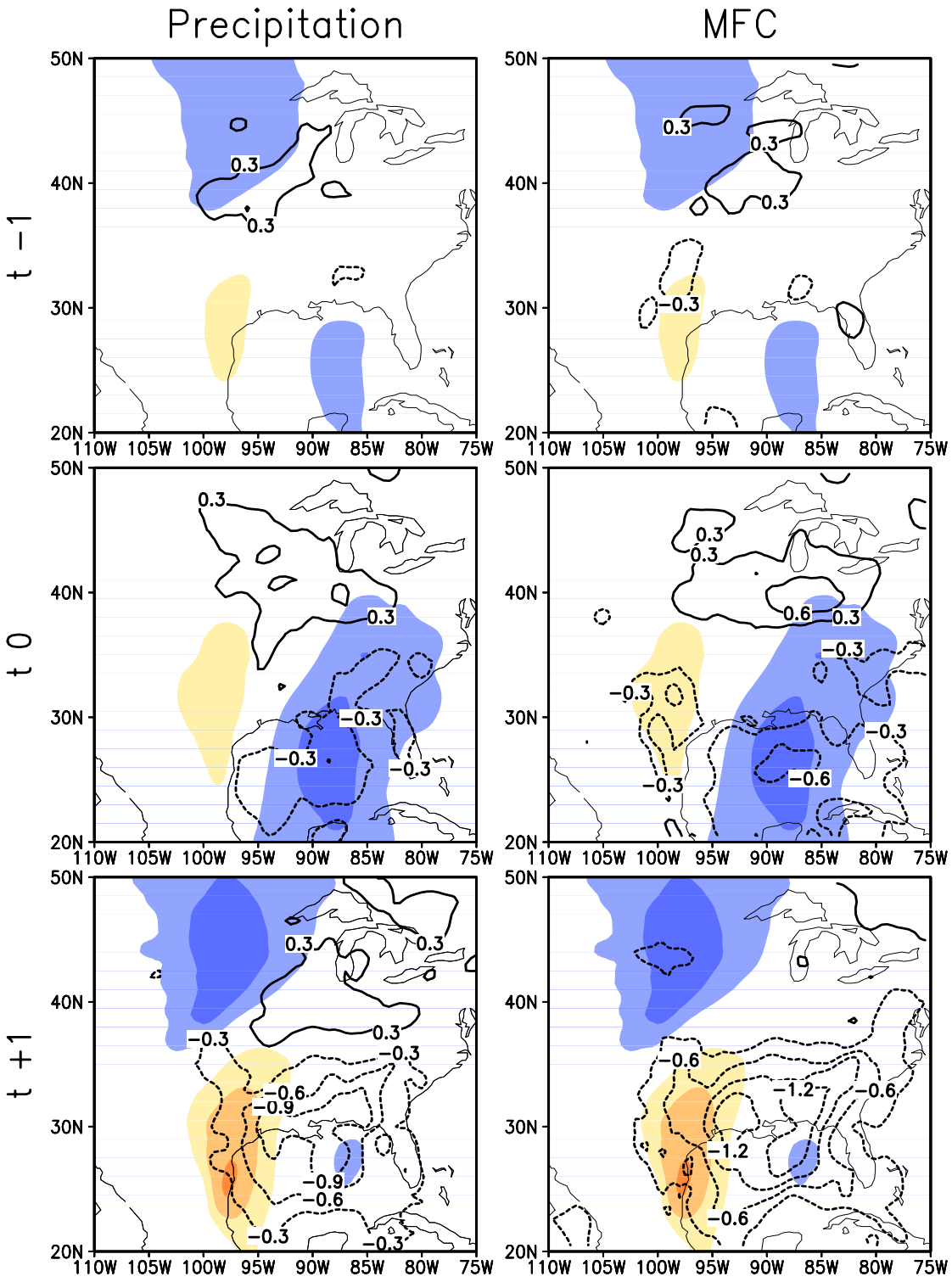

Figure 6.9. Evolution of the GPLLJ (shaded), precipitation (left column), and moisture flux convergence (right column) associated with EEOF mode 3 Positive (negative) values are shaded orange (blue) and the contour interval is 0.3 mm day^{-1}.

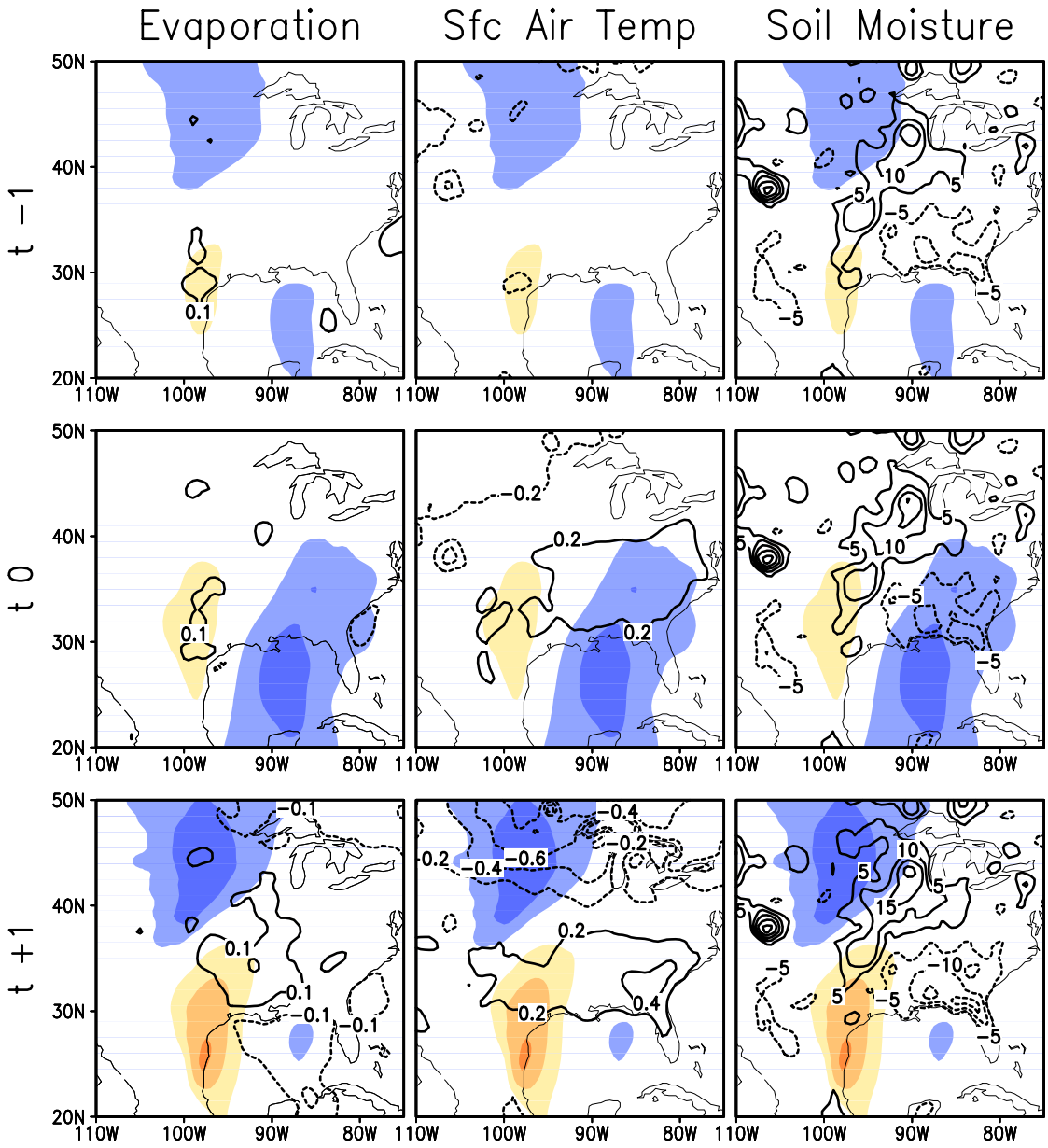

Figure 6.10. Evolution of the GPLLJ, evaporation (left column), surface air temperature (middle column), and soil moisture (right column) associated with EEOF mode 3 Positive (negative) values are shaded orange (blue). Evaporation, SAT, and soil moisture are contoured at 0.1 mm day^{-1}, 0.2 k day^{-1}, and 5 mm respectively.

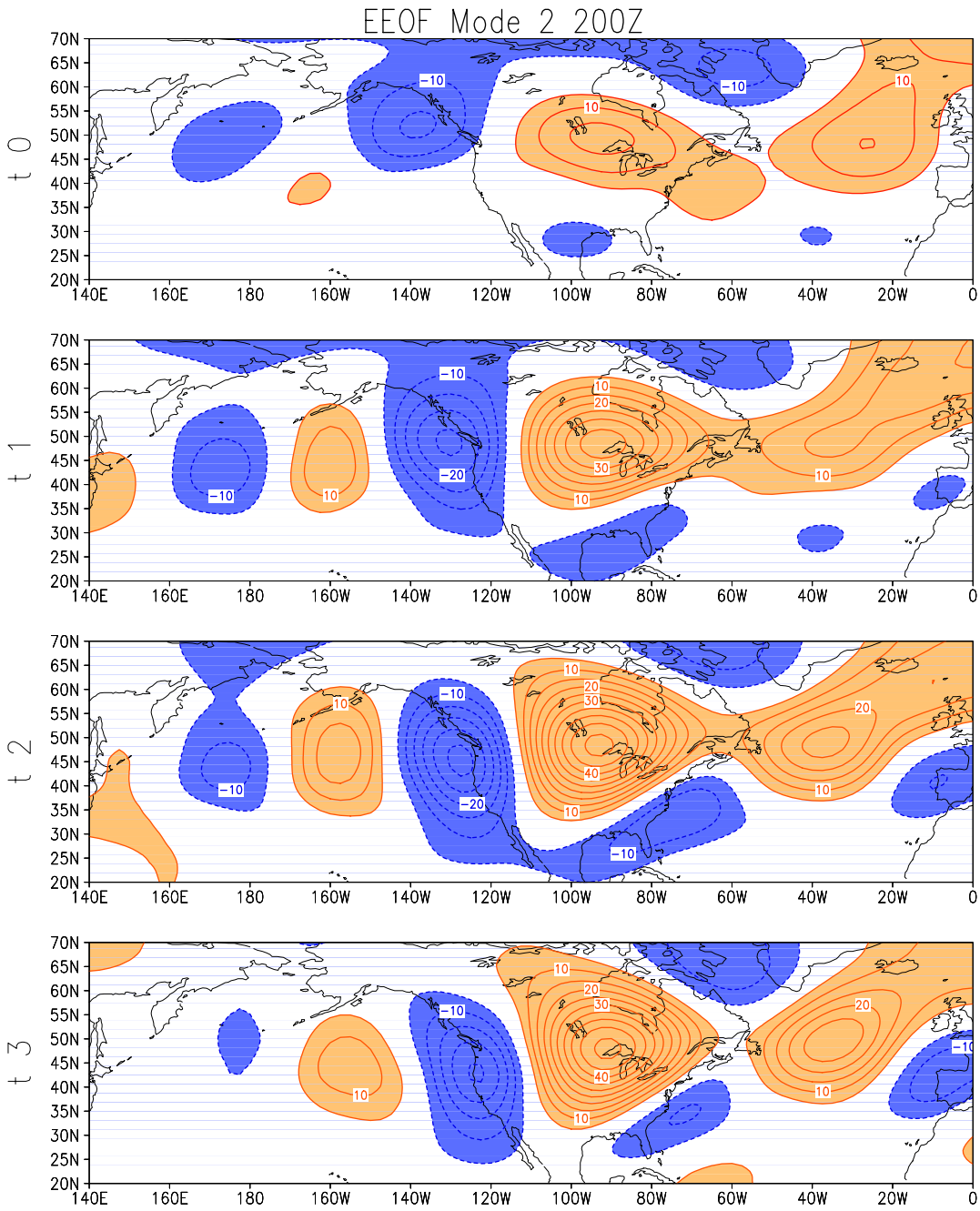

Figure 6.11. Pentad evolution of 200 hPa height anomalies (shaded) associated with GPLLJ EEOF mode 2. Negative (positive) heights are shaded in blue (orange) and contoured at 5 m intervals.

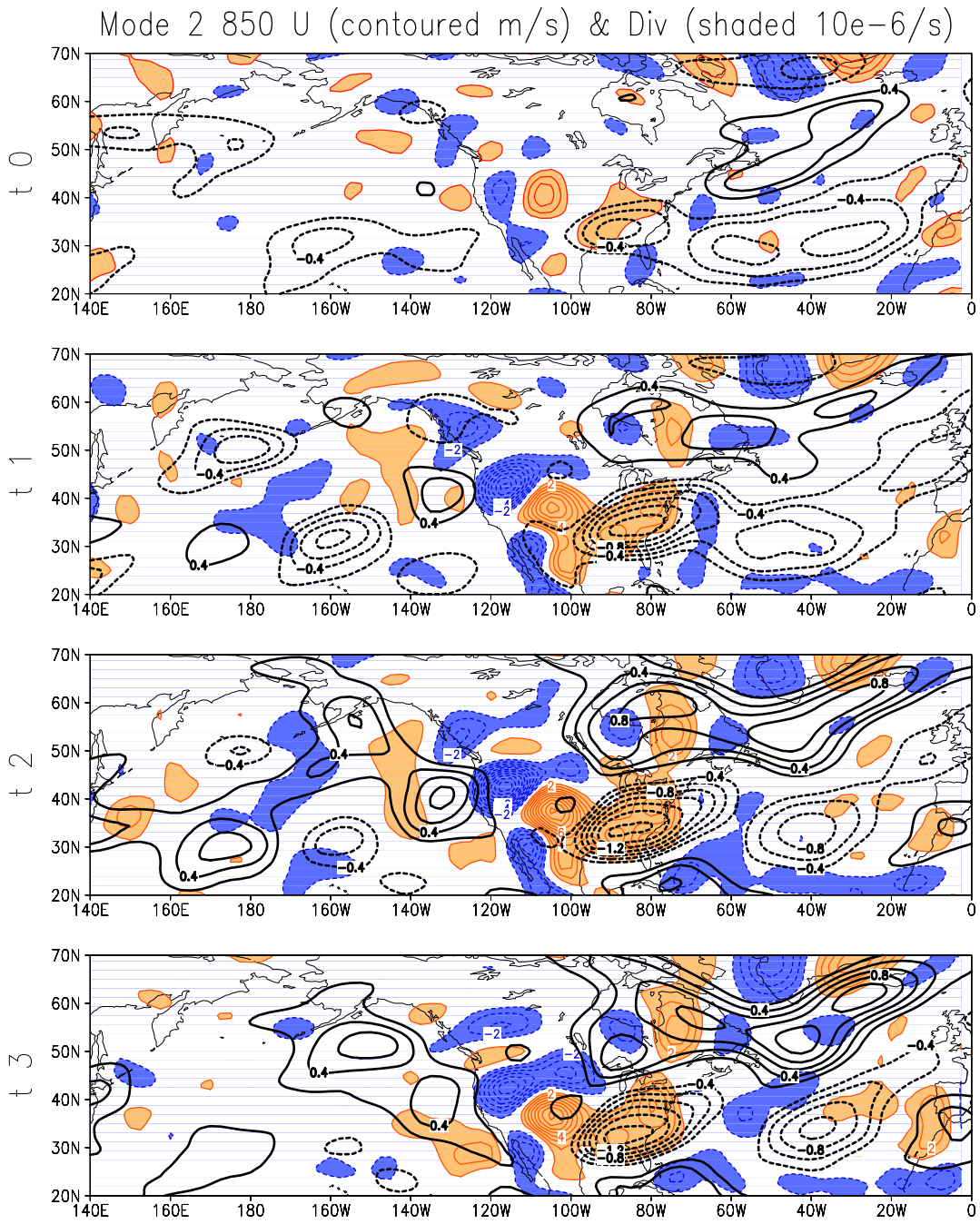

Figure 6.12. Pentad evolution of divergence (shaded) and zonal wind (contoured) associated with GPLLJ EEOF mode 2. Negative (positive) divergence is shaded in blue (orange) and contoured at 1e-6 s^{-1}. Zonal wind is contoured at 0.2 ms^{-1}.

Chapter 7: The GPLLJ in Climate Models

The introduction to this thesis discussed the need for regional characterization of climate variability in the face of emerging climate change scenarios. The notable GPLLJ – hydroclimate variability links presented in previous chapters motivates the need to assess the ability of general circulation models (GCMs) to depict this important regional scale relationship. Indeed it could be argued that a significant benefit of the results presented in this effort is to produce a comprehensive warm season Great Plains regional circulation – hydroclimate benchmark to be used in the assessment of various global and regional climate models. A basic inquiry into the fidelity of modern GCMs to depict the regional scale hydroclimate variability over the Great Plains is beneficial not only as an exercise in model validation, however can also be used to interpret hydroclimate variability depictions in future climate model projections with enhanced CO_2 concentrations. The results of this chapter may be seen as the first step towards this goal.

7.1 Model Description

To generate a basic picture of the current state of climate models in depicting the important warm season regional circulation – precipitation relationships over the Great Plains, the Community Atmospheric Model version 3 (CAM3) and the operational Climate Forecast System (CFS) are employed. These climate models are distinctly different in their respective formulation, integration, and intended purpose.

The CAM3 simulations are part of the AMIP model runs (1950-2000) used in the recently released fourth assessment report (AR4) of the IPCC. The CAM3 is forced

with known global evolution of monthly SSTs and sea ice concentrations. A 5-member ensemble is generated and for the results presented here the ensemble mean is used. The spatial resolution is 5.0° longitude x 2.5° latitude with 17 vertical isobaric levels. A detailed description of the CAM3 including physical parameterizations and SST formulations can be found in many papers presented in the special issue for the Community Climate System Model (CCSM) in the June 1 2006 edition of the Journal of Climate (Boville et al. 2006; Collins et al. 2006; Hack et al. 2006; Hurrell et al 2006).

While the ultimate goal of many GCMs (i.e., CAM3) is to provide some information about the long term future state of the climate given increasing greenhouse gas concentrations, the CFS has been designed to provide operational forecasts of the near term future climate (i.e., 9 month forecasts). Until the CFS became operational in 2004 the seasonal forecasts produced by the Climate Prediction Center (CPC) were based on statistical techniques such as canonical correlation analysis, constructed analog, and autoregressive methods. The CFS is the first coupled operational dynamical tier-1 seasonal prediction system. No anomaly flux corrections or tuning for climate applications is applied (Saha et al. 2006). The CFS includes a set of retrospective forecasts on a 2.5 x 2.5 horizontal grid with 64 vertical sigma levels that provide a history of the model over the period 1981-2004. CFS runs are initiated from 15 initial conditions that span each month. As the target months in much of the preceding analysis is MJJ, wind and precipitation data from the April retrospective forecast initializations is used for comparison statistics here.

7.2 Model Performance

In RBN (2005) the authors considered the depiction of Great Plains precipitation variability by analyzing the correlations between model (ensemble means and individual members) and observations of the JJA Great Plains precipitation index from the AMIP simulations. While the magnitude of the standard deviation over the data record was robust, the temporal correlations were nearly zero for monthly means and only slightly better in the smoothed seasonal index, suggesting poor ability of the models to produce realistic monthly precipitation variability over the Great Plains.

The evidence presented in the previous chapters shows a strong connection between the GPLLJ and precipitation variability, especially over the region studied by RBN (2005). The poor representation of Great Plains precipitation variability in the AMIP simulations and in particular the 0.11 correlation between observations and CAM3 begs the question: How is GPLLJ variability represented in CAM3 and the operational CFS? Will the jet be as poorly represented in these models, as is the precipitation due to the strong jet – precipitation connection? If the model depicts the jet – precipitation mechanisms with reasonable fidelity then a similar skill level should appear with respect to the GPLLJ. While poor hydroclimate skill is not desired, if the mechanisms between the jet and precipitation are correct (as evidenced by similar skill) then some success may be claimed.

7.2.1 Model Bias

The July 850 hPa meridional winds are depicted in figure 7.1 for the period 1981-2000 in ERA40 and NARR reanalysis and CAM3 and CFS model datasets. The years spanning 1981-2000 were chosen, as this is the overlapping period between all

datasets. The switch to 850 hPa in depicting the GPLLJ is due to the coarse resolution of the CAM3 and the absence of meaningful horizontal depiction at pressure levels > 850 hPa. Other GPLLJ studies have used 850 hPa as the level that defines the jet (Byerle and Paegle 2003; Ting and Wang 2006).

The top panels show the July mean 850 hPa meridional winds in the ERA40 and NARR. In general the characteristics are largely similar, not surprising given the strong correlation of the monthly GPLLJ indices between the two datasets (cf. figure 2.6) although some differences do exist. ERA40 has stronger winds over the GPLLJ region as evidenced by the large expanse of the 6 m/s contour in comparison to NARR. However, NARR shows more connection to the Gulf of Mexico and western Caribbean Sea. The higher resolution NARR is chosen as the simulation benchmark in this analysis.

The middle (CAM3) and bottom (CFS – Lead0 April) panels of figure 7.1 show the representation of the July mean (left) and the bias of each model as compared to NARR (right) respectively. The CAM3 GPLLJ shows greater magnitude of the meridional winds and a different spatial orientation of the wind contours. The CAM3 bias (CAM3-NARR) is large in both magnitude and spatial extent and encompasses much of the Great Plains region. The meridional wind difference is also notable over the northeastern Pacific Ocean although there is not much bias over the northwestern Atlantic.

The situation for the CFS is much different in that it produces a spatially improved depiction of the GPLLJ, especially when compared with the CAM3. The 850 hPa meridional winds over the Great Plains are underestimated and the

magnitude and spatial extent of the bias is diminished in comparison to that of the CAM3. Perhaps more important is the lack of a strong connection to the Gulf of Mexico when compared to NARR. This could have implications for moisture transports into the Great Plains as represented in the CFS. Furthermore one could argue that the negative bias in both the entrance and exit regions of the GPLLJ in the CFS may have implications for moisture transports, and their convergence. Verification of the large bias over western Mexico and the southwestern U.S. is tenuous as NARR has recently been shown to have accuracy issues in the low-level wind fields over this region (Mo et. al 2005).

7.2.2 Interannual Variability

Models are not expected to be exact representations of nature. The fact that these models exhibit bias is not necessarily indicative of poor skill, especially given the resolution differences between the reanalysis benchmark (NARR) and the climate models (CAM3.0, CFS). A more interesting measure of model skill is analyzing their depiction of interannual variability. Figure 7.2 presents the July regressions of the GPLLJ index on 850 hPa meridional wind (left panels) and precipitation (right panels) in NARR, CAM 3.0, and the CFS. The GPLLJ index is calculated as in chapter 2 except that the lat-lon box restriction is relaxed to 25-40° N and 105-95° W. The relaxed domain is to allow for the degradation in GCM resolution and for latitude in the expressed variability.

The top panels (NARR) are the same as in figure 2.7 and are repeated here for ease of comparison. The CAM3 (middle panels) is severely challenged in depicting the variability structure of both the GPLLJ and regional precipitation. The jet

footprint is barely visible although there is some skill in capturing the western and eastern negative meridional wind feature. This may suggest that the model has difficulty representing the coincident large scale – GPLLJ strengthening discussed in chapter 2. The large positive meridional winds in the Pacific are unique to CAM3. The depiction of the interannual variability of precipitation fares no better in the CAM3. The large positive precipitation anomaly over the northern Great Plains is entirely absent and there are spurious features off the east and west coasts of North America and in the Gulf of Mexico. Due to the weak footprints of the jet and precipitation it is not clear if the GPLLJ precipitation relationship is robust in the CAM3.

The CFS seems to capture the general features of the July GPLLJ anomalies as indicated by the negative meridional winds in the northeast Pacific and northwest Atlantic, with positive jet anomalies in the central U.S. The width and strength of the anomalous July GPLLJ is overestimated by the CFS. While the July climatology in NARR showed some connection to the subtropical meridional winds, this feature is absent in the depiction of interannual variability. However, the CFS shows a strong connection to the subtropical meridional winds in this case. As in CAM3 the precipitation field is not well depicted, however some features show similarities with NARR. There does appear to be some fidelity in capturing the jet-precipitation connection as evidenced by the positive anomalies centered north of Lake Huron and along the 45th parallel although the small spatial extent diminishes the excitement. There are large negative anomalies over the western U.S. This may be due to some issues with resolution or topographical representation. The northward push of the

ITCZ precipitation is represented although it has stronger magnitude and spatial extent.

7.2.3 Model Skill

While calculation of bias and regression statistics provide some insight into the ability of the CAM3 and CFS to depict Great Plains circulation and precipitation features they do not provide specific information regarding the skill of the models to represent the magnitude and placement of the GPLLJ throughout the 20-year record. Two common measures of forecast skill in use are the root mean square error (RMSE) and anomaly correlation (AC). The RMSE and AC are defined in Wilks (1995).

Figure 7.3 shows the RMSE (top panel) and AC (bottom panel) of the GPLLJ in both CAM3 and the CFS for MJJ during the period 1981-2000 using NARR as the benchmark. The area over which the averaging was applied is 25-40N and 105-95W to include the possible effects of the GPLLJ being meridionally or zonally stretched, while the 2 m/s benchmark is arbitrary. Furthermore, the anomalies in the computation of the AC are centered, meaning that the area mean anomalies were subtracted from the anomaly at each grid point.

The CFS (blue) has much better skill than CAM3 (red) in depicting the magnitude of the GPLLJ. The inclusion of more data during initialization of the CFS as opposed to CAM3, which only has monthly updates of SSTs, is likely the reason for the difference in RMSE. The AC is low in both the CFS and CAM3 and a vast majority of months exhibit a correlation below 0.5. This 0.5 threshold for the AC has been shown to be indicative of useful forecasting skill (Wilks 1995). The CFS does show

better skill in representing the GPLLJ anomalies, at least in terms of the sign of correlation coefficients as 44 out of the 60 months show a positive correlation, while CAM3 only has 22.

How do these models perform with respect to the representation of precipitation anomalies when compared with NARR? Figure 7.4 shows the RMSE and AC for precipitation over the area exhibiting the maximum in warm season interannual variation in precipitation (35-45°N, 100-90°W). Again the CFS performs better in precipitation magnitude as many of the months exhibit RMSE < 0.5 mm day^{-1}. While CAM3 has some months in this range much of the record is dominated by large errors. The skill of each model in tracking the anomaly patterns is not conclusive at least in terms of representing positive correlations with the CAM3 having positive coefficients in 38 out of 60 months and the CFS exhibiting 37. Interestingly, when comparing the number of months above the 0.5 AC threshold in figures 7.3 (GPLLJ) and 7.4 (precipitation) the CFS represents the GPLLJ with more fidelity while the CAM 3.0 seems to better represent the precipitation anomaly pattern. However, in general neither model necessarily captures either GPLLJ or precipitation variability with much skill. Furthermore the correlation of the precipitation and GPLLJ AC is –0.08 in the CFS and 0.04 in CAM3 suggesting that neither model is robustly depicting the jet-precipitation mechanism operative in nature over the Great Plains during the warm season months.

Possible reasons for the lack of a connection between the GPLLJ and precipitation may lie in horizontal resolution and topographical representation in GCM's. Inadequate depiction of the ageostrophic wind component may result from coarse

topographical representation. It is probable that the failure of GCM's to adequately represent the nocturnal precipitation over the Great Plains (i.e., LLJ-precipitation mechanism) may be caused by the inability of the model to sustain the ageosotrophic (i.e., divergent) component of the wind in the lee of the Rockies decreasing the likelihood that the convective parameterization would be invoked (Anderson and Arritt 2001).

7.3 Chapter 7 Figures

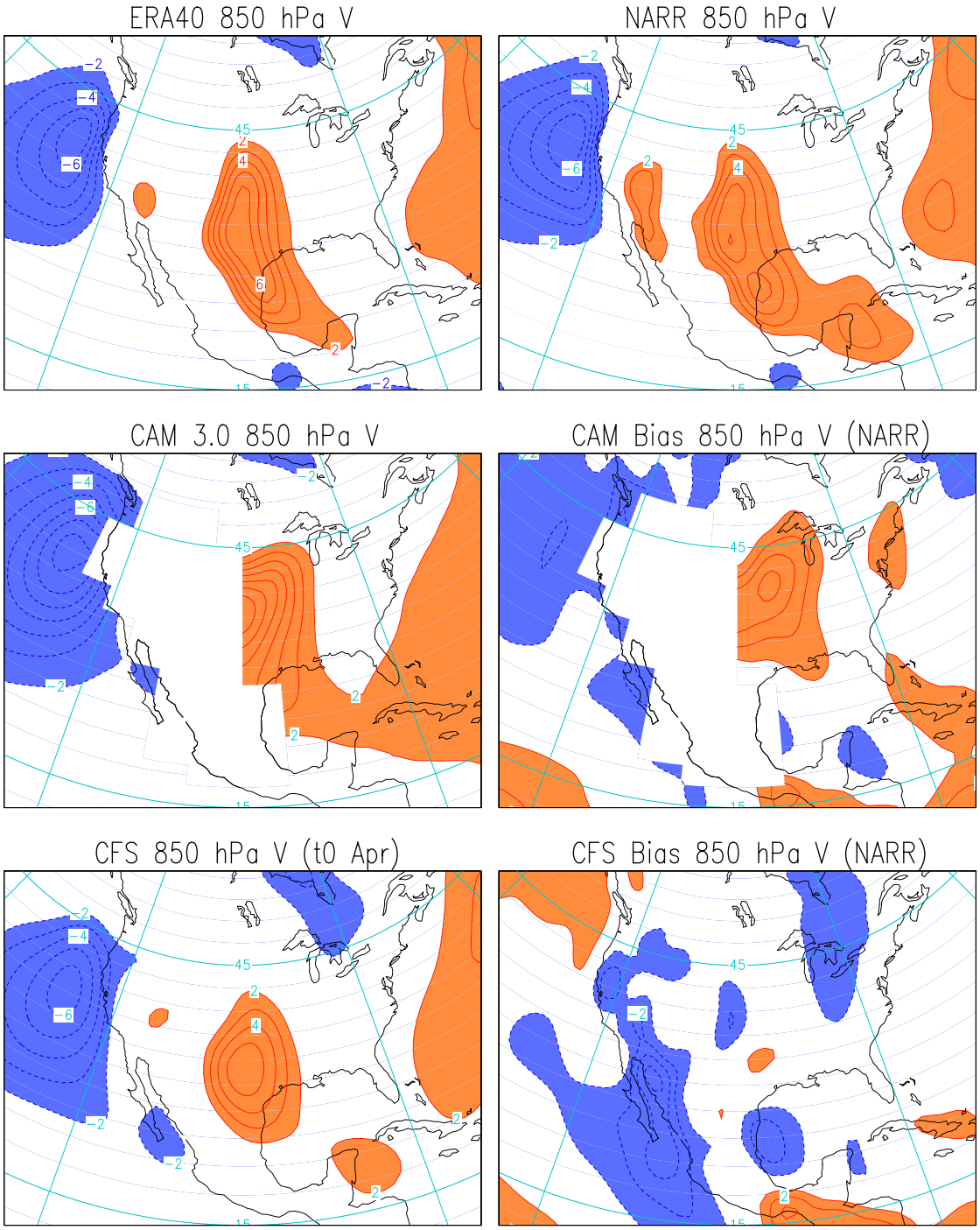

Figure 7.1. July climatology of the 850 hPa meridional winds in ERA40 (top left), NARR (top right), CAM3 (mid left), CFS (lower left). July bias with respect to NARR in CAM3 (mid left), and the CFS (lower right). Values > 2 m s^{-1} are contoured at 1 m s^{-1} intervals and shaded orange while those < -2 m s^{-1} are contoured at 1 m s^{-1} intervals and shaded blue.

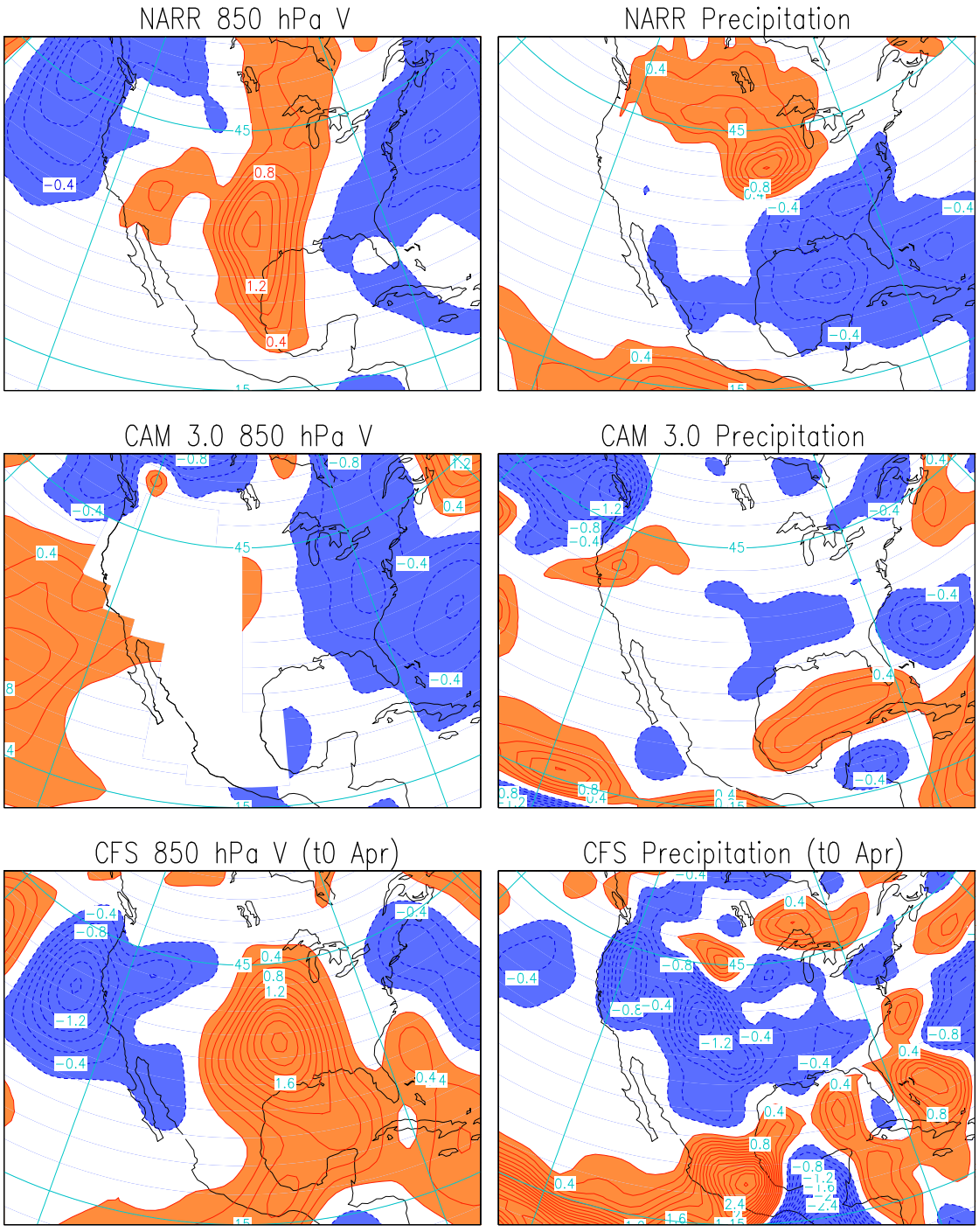

Figure 7.2. July regressions of the GPLLJ index on 850 hPa (left column) and precipitation (right column) in NARR (top), CAM3 (mid), and CFS (lower). The contour intervals are 0.2 m s^{-1} and 0.2 mm day^{-1} for winds and precipitation resectively. Positive (negative) values are shaded in orange (blue).

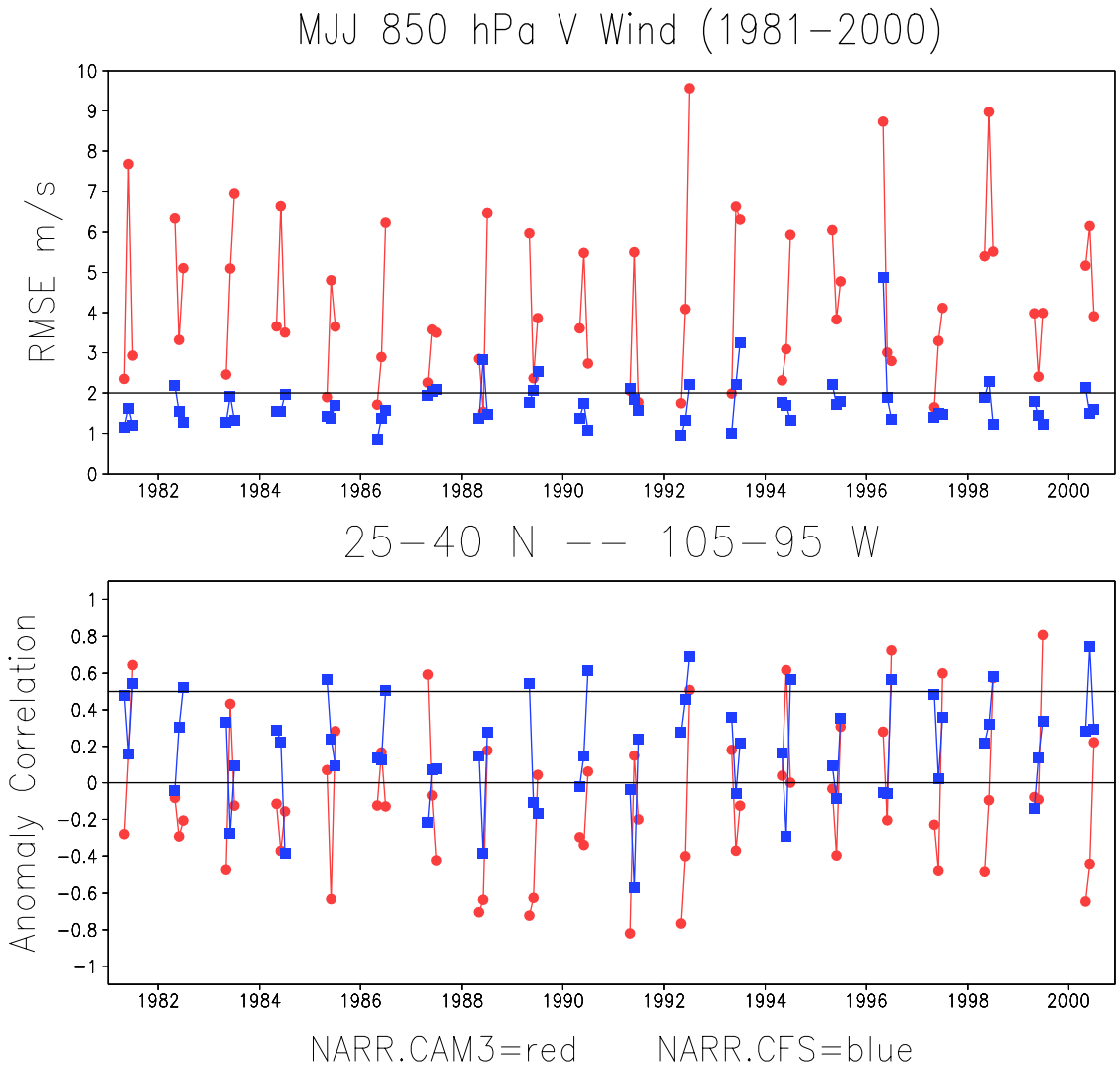

Figure 7.3. Root mean square error (top) and anomaly correlation (bottom) of CAM3 (red) and the CFS (blue) as compared to NARR for 1981-2000. Root mean square error is in m s^{-1} while the anomaly correlation is unitless.

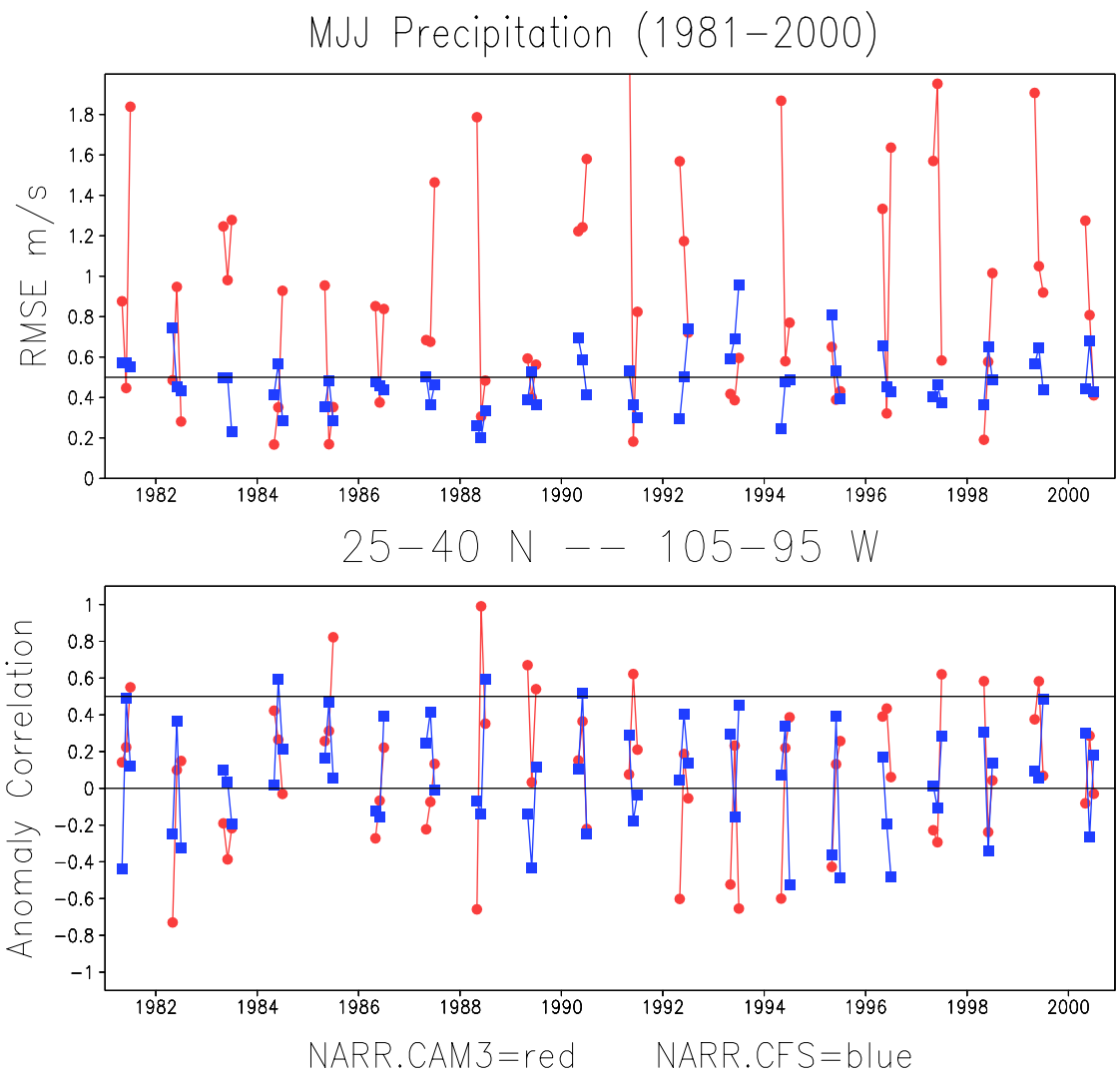

Figure 7.4. Same as in figure 7.3 except for precipitation. Root mean square error is in mm day^{-1}.

Chapter 8: Conclusions and Directions for Future Work

The research presented here has sought to answer specific questions related to the role of the GPLLJ in Great Plains hydroclimate variability. The conclusions may best be summarized by offering responses to the questions of section 1.4.

- The GPLLJ is influenced by hemispheric wide circulation anomalies emanating from the Pacific and Atlantic basins. The large scale circulation patterns of a circumglobal nature are linked to western and eastern tropical Pacific diabatic heating anomalies. While intriguing, verification and attribution of the forcing mechanism is prohibited by the analysis strategy here and may depend on future diagnostic modeling studies.
- Meridional expansions and shifts of the GPLLJ are linked to larger scale circulation variations that are characteristic of wet and dry Great Plains hydroclimate episodes. The meridionally expanded jet (Mode 1) is related to a west to east dipole of tropospheric circulation anomalies over North America while the northward shifted (moisture starved) jet (Mode 2) is related to a continental scale upper tropospheric anticyclone. Mode 3 is embedded in a continental scale meridional circulation dipole with negative height anomalies over the northern U.S. and positive in the south. Modes 1 and 2 show linkages to Pacific SSTs, while mode 3 exhibits a connection to North Atlantic SSTs.
- The largest monthly positive precipitation anomalies are associated with mode 1 (meridionally stretched GPLLJ). Not surprisingly this mode was active during the flood of 1993. Conversely GPLLJ mode 2 shows reduced

precipitation anomalies over the continental U.S. The lack of a moisture source coupled with the northward shifted jet lead to the reduced precipitation footprint. This mode was a contributor to the early summer drought of 1988. The third mode representing an in place strengthening is related to modest precipitation anomalies in the northern plains.

- The GPLLJ during the 1988 drought and 1993 flood is primarily connected to the large scale circulation variations. Analysis of land surface features (i.e, evaporation and soil moisture anomalies) in connection with these events reveals that their influence was minor as evidenced by the temporally lagged evaporation field in comparison to the GPLLJ, suggesting that evaporation was not instrumental in forcing the GPLLJ on this timescale. Connections to antecedent ENSO and contemporaneous NAO variability show links to the GPLLJ and warm season Great Plains precipitation variability.
- EEOF analysis on 900 hPa meridional winds show that the rapidly evolving modes of GPLLJ variability are similar to the monthly patterns. The spatio-temporal evolution of the pentad scale hydroclimate (a notable attribute of EEOF analysis) reveals that the GPLLJ is primarily linked to circulation variations and that moisture transports dominate the land surface features in the generation of Great Plains hydroclimate variability.
- The CAM 3.0 and CFS are extremely challenged in depicting GPLLJ and associated rainfall variations over the Great Plains. This is not totally surprising given the target – representation of the structure of highly variable mesoscale circulation and precipitation fields. Some features of the

midsummer climatology were captured, however the apparent lack of a GPLLJ precipitation linkage in the models is discouraging. Some success could have been claimed if the poor model skill in representing the jet and precipitation features were temporally consistent. The nearly zero correlations of the respective GPLLJ and Precipitation AC can attest to this deficiency.

The ultimate goal of this research was to enhance the knowledge base with regard to GPLLJ variability, related anomalous large-scale circulation, and ultimately its hydroclimate impacts. While some success towards this goal can be claimed here and much new information has been learned, several issues remain to be probed further.

The most obvious extension to the work presented here would be to further clarify the role of the western and eastern tropical Pacific diabatic heating anomalies in generating the stationary wave patterns that are of consequence to monthly GPLLJ variability. Given that Atlantic and Pacific based circulation variability structures have been shown to play a role in warm season Great Plains hydroclimate variability, elucidating the contribution by each of these potential tropical forcings to either the Atlantic or Pacific based atmospheric and oceanic midlatitude variability structure may provide interesting information.

Is it possible that the eastern Pacific diabatic heating anomaly influences the Atlantic atmospheric circulation variability in a similar manner as that in the western Pacific? Especially given the curious similarities in the relative positions of each diabatic heating anomaly and midlatitude circulation footprint (i.e. the high – low – high emanating from just northeast of both the western and eastern diabatic heating

anomalies). Alternatively, perhaps the eastern Pacific heating and divergent wind impact is negligible and the westerly flow impinging on the topography is the major contributor to the perpetuation of the circulation anomalies into the Atlantic as Ting (1994) argues.

The limitations imposed by employing observational data in this study would necessitate the use of a linear diagnostic model in conducting experiments geared toward answering questions regarding the role of variable forcing mechanisms. Prescribing the separate diabatic heating anomalies diagnosed from GPLLJ index and principal component regressions to the linearized model may provide some clues as to their relative importance in GPLLJ fluctuations on the monthly timescale. Furthermore, the flow anomalies produced from simple model simulations can be tested for sensitivity to the topography of the North American Cordillera to ascertain the effect that this large barrier has on the model generated anomalous flow.

Another unresolved issue is the questionable GPLLJ and warm season precipitation representations in state of the art GCM's. The inquiry into the fidelity of GPLLJ variability depiction of two climate models in chapter 7 is merely a start in assessing the important why and how questions that are inevitable upon reviewing model performance. Further study along this avenue is especially pertinent given that one of these models (CAM 3.0) was used in the recent IPCC assessment. Until GCMs capture regional climate variability their utility in assessing future regional climate change is suspect. While some may argue that the success of GCMs in representing the large scale climate variability is encouraging for assessing future

climate change scenarios, regional implications, especially in the agriculturally (economically) sensitive Great Plains, must be the ultimate test of model success.

Some recent studies point toward model resolution or convective parameterization deficiencies as reasons why GCMs may have trouble depicting the connection between the GPLLJ and precipitation (Anderson and Arritt 2001; Mo et al. 2005). Testing the ability of the GCM to sustain the nocturnal ageostrophic component of the wind long enough to invoke the convective parameterization has been suggested (Anderson and Arritt 2001). Furthermore the ability of the convective parameterization to represent the proper type of convection for a given GPLLJ induced ageostrophic forcing need to be assessed. The 3-hourly high resolution NARR may prove worthy as the benchmark in this scenario.

Future studies need not be constrained to model evaluation and sensitivity testing. Further work on the rapidly evolving pentad hydroclimate anomalies may be necessary, particularly in diagnosing the relative contributions to the total moisture flux convergence. The different moisture flux convergence patterns in EEOFs 1 (positive) and 3 (negative) along the Gulf coast are similar to the NARR stationary and transient moisture flux convergences respectively shown in figures 6 and 9 in Nigam and Ruiz-Bararadas (2006). Decomposition of the stationary and transient components may provide additional insight into the nature and forcing of the spatio-temporal evolution of these two GPLLJ modes. Additionally, analysis of the separate terms in the moisture flux equation is warranted, as it appears that the transport term may be the most important for the MFC in the retained GPLLJ modes as evidenced by the notable lag in maximum precipitation. This cannot be robustly determined

here by analyzing the total integrated moisture flux components provided by NARR. Acquiring the necessary data at pentad resolution is currently underway and will enable the calculation of the transport and divergence terms as well as the stationary and transient flux components.

As science, society, and politics have been recently engaged in meaningful discussions of climate change issues, a necessary component of future study related to the work herein lies in quantifying the characteristics of Great Plains hydroclimate under global warming scenarios. The GPLLJ figures prominently in this scheme given that it is the major component of the warm season moisture bearing circulation. One may argue that the poor skill of the CAM 3.0 and CFS demonstrated in this work would prohibit employing GCMs in this regard. However, the GPLLJ is, in fact, simulated in both models, although placement and amplitude are problematic. Nevertheless, a similar examination of other widely used GCMs may show improved results. Even if the skill in other GCMs is comparable, it still may be worth looking at the change in GPLLJ variability, as the potential for the shifting of the agricultural belts exists in a warmer world.

It is clear that climate predictability is a formidable challenge. Diagnostic analyses such as that presented here can significantly enhance our ability to predict regional climate. Gaining insight into the observed behavior of variability in a system and the linkages to possible forcing mechanisms may enable future adjustment of statistical prediction algorithms and climate model assessment. While much more needs to be done it is hoped that this work is a small step towards the goal of improved hydroclimate predictions.

References

Anderson, C. J.and R. Arritt, 2001: Representation of summertime low-level jets in the Central United States by the NCEP-NCAR Reanalysis. *J. Climate*, **14**, 234-247.

Arritt, R. W., and coauthors, 1997: The Great Plains low-level jet during the warm season of 1993. *Mon. Wea. Rev.,* **125,** 2176-2192.

Atlas, R., N. Wolfson, and J. Terry, 1993: The effect of SST and soil moisture anomalies on GLA model simulations of the 1988 U.S. summer drought. *J. Climate,* **6,** 2034-2048.

Bates, G. T., and M. P. Hoerling, 2001: Central U.S. springtime precipitation extremes: Teleconnections and relationships with sea surface temperature. *J. Climate,* **14,** 3751-3766.

Bell G. D. and J. E. Janowiak, 1995: Atmospheric circulation associated with the Midwest floods of 1993. *Bull. Amer. Met Soc.*, **76**, 681-695.

Benton, G. S., and M. A. Estoque, 1954: Water-vapor transfer over the North American continent. *Journal of Meteorology.* **11,** 462-477.

Blackadar, A. K., 1957: Boundary layer wind maxima and their significance for the growth of nocturnal inversions. *Bull. Amer. Meteor. Soc.*, **38**, 283-290.

Bonner, W. D., 1968: Climatology of the low- level jet. *Mon. Wea. Rev.*, **96**, 833-850.

Bosilivich, M. G., and W. Y. Sun, 1999: Numerical simulations of the 1993 midwestern flood: Land-atmosphere interactions. *J. Climate*, **12,** 1490-1505.

Boville, A. B., and coauthors, 2006: Representation of clouds and precipitation processes in the community atmosphere model version 3 (CAM3). *J. Climate,* **19,** 2184-2198.

Byerle, L. A. and J. Paegle, 2003: Modulation of the Great Plains low-level jet and moisture transports by orography and large-scale circulations. *JGR*, **108**, 6.1 – 6.16.

Chen, T. C., and A. Kpaeyeh, 1993: The synoptic-scale environment associated with the low-level jet of the Great Plains. *Mon. Wea. Rev.,* **121,** 416-420.

Chen, P., and M. Newman, 1998: Rossby wave propagation and the rapid development of upper-level anomalous anticyclones during the 1988 U.S. drought. *J. Climate,* **11,** 2491-2504.

Collins, W. D., and coauthors, 2006: The community climate system model version 3 (CCSM3). *J. Climate,* **19,** 2122-2143.

Compo, G. P., P. D. Sardeshmukh, and C. Penland, 2001: Changes of subseasonal variability associated with El Niño. *J. Climate,* **14,** 3356-3374.

Ding, Q. and Bin Wang,. 2005: Circumglobal teleconnection in the northern hemisphere summer. *J. Climate*, **18,** 3483–3505.

Ek, M.B., and coauthors, 2003: Implementation of NOAH land surface model advances in the National Centers for Environmental Prediction operational mesoscale Eta model. *J. Geophys. Res.,* **108,** 8852, doi:10.1029/2002JD003296.

Ghan, S. J., X. Bian, and L. Corsetti, 1996. Simulation of the Great Plains low-level jet and associated clouds by general circulation models. *Mon. Wea. Rev.*, **124,** 1388-1408.

Giorgi, F., and coauthors, 1996: A regional model study of the importance of local versus remote controls of the 1988 drought and 1993 flood over the central United States. *J. Climate,* **9,** 1150-1162.

Graham, N. E., and T. P. Barnett, 1987: Observations of sea surface temperatures, convection and surface wind divergence over tropical oceans. *Science*, **238,** 657-659.

Guan B., and S. Nigam, 2007: Pacific SSTs in the Twentieth Century: An evolution-centric variability analysis. *To be submitted to Journal of Climate. Draft available.*

Hack, J. J., and coauthors, 2006: Simulation of the global hydrological cycle in the CCSM community atmosphere model version 3 (CAM3): Mean features. *J. Climate,* **19,** 2199-2221.

Held, I. M., and D. G. Andrews, 1983: On the direction of eddy momentum flux in baroclinic instability. *J. Atmos. Sci.,* **40,** 2220-2231.

Helfand, M. H., and S. D. Schubert, 1995: Climatology of the simulated Great Plains low-level jet and its contribution to the continental moisture budget of the United States. *J. Climate*, **8**, 784-806.

Higgins, R. W., Y. Yao, E. S. Yarosh, J. E. Janowiak, and K. C. Mo, 1997: Influence of the Great Plains low-level jet on summertime precipitation and moisture transport over the central United States. *J. Climate*, **10**, 481–507.

Hoxit, L. R., 1975: Diurnal variations in planetary boundary-layer winds over land. *Bound.-Layer Meteor.,* **8**, 21-38.

Hurrell, J. W., 1995: Transient eddy forcing of the rotational flow during northern winter. *J. Atmos. Sci.,* **52,** 2286-2301.

Hurrell, J. W., and coauthors, 2006: The dynamical simulation of the community atmospheric model version 3 (CAM3). *J. Climate,* **19,** 2162-2183.

Joseph, R., and S. Nigam, 2006: ENSO evolution and teleconnections in IPCC's twentieth century climate simulations: Realistic representation? *J. Climate,* **19,** 4360-4377.

Kalnay E. et al, 1996: The NCEP/NCAR 40-Year Reanalysis Project. *Bull. Amer. Meteor. Soc.,* **77**, 437-471.

Kutzbach, J. E., 1967: Empirical eigenvectors of sea-level pressure, surface temperature and precipitation complexes over North America. *J. Appl. Meteor.,* **6,** 791-802.

Lau, K.-M., and H. Weng, 2002: Recurrent teleconnection patterns linking summertime precipitation variability over East Asia and North America. *J. Meteor. Soc. Japan,* **80,** 1309-1324.

Liu A. Z., M Ting, and H. Wang, 1998: Maintenance of circulation anomalies during the 1988 drought and 1993 floods over the United States. *J. Atmos. Sci.,* **55,** 2810-2832.

Means, L. L., 1954: A study of the mean southerly wind maximum in low levels associated with a period of summer precipitation in the Middle West. *Bull. Amer. Meteor. Soc.,* **35,** 166-170.

Mesinger F. et al, 2006: North American Regional Reanalysis. *BAMS, **87,*** 343-360.

Mo, K. C., J. Nogues-Paegle, and J. Paegle, 1995: Physical mechanisms of the 1993 summer floods. *J. Atmos. Sci.,* **52,** 879–895.

Mo, K. C., .J. Nogues-Paegle, and W. Higgins, 1997: Atmospheric processes associated with summer floods and droughts in the central United States. *J. Climate*, **10**, 3028-3046.

Mo, K. C., and coauthors, 2005: Atmospheric moisture transport over the United States and Mexico as evaluated in the NCEP regional reanalysis. *J. Hydrometeorology,* **6,** 710-728.

Mo, K. C., and coauthors, 2005: Imapct of model resolution on the prediction of summer precipitation over the United States and Mexico. *J. Climate,* **18,** 3910-3927.

Namias, J., 1991: Spring and summer 1988 drought over the contiguous United States – causes and prediction. *J. Climate,* **4,** 54-65.

Nigam, S., I. M. Held, and S. W. Lyons, 1986: Linear simulation of the stationary eddies in a general circulation model. Part I: The No-Mountain model. *J. Atmos. Sci.,* **43,** 2944–2961.

Nigam, S., I. M. Held, and S. W. Lyons, 1988: Linear simulation of the stationary eddies in a general circulation model. Part I: The "Mountain" model. *J. Atmos. Sci.,* **45,** 1433–1452.

Nigam, S., and H. S. Shen, 1993: Structure of oceanic and atmospheric low-frequency variability over the tropical Pacific and Indian oceans. Part I: COADS observations. *J Climate,* **6,** 657-676.

Nigam, S., 1994: On the dynamical basis for the Asian summer monsoon Rainfall-El Niño relationship. *J. Climate,* **7,** 1750-1771.

Nigam, S., C. Chung, and Eric DeWeaver, 2000: ENSO diabatic heating in ECMWF and NCEP–NCAR reanalyses, and NCAR CCM3 simulation. *J. Climate*, **13,** 3152–3171.

Nigam, S., 2003: Teleconnections. *Encyclopedia of Atmospheric Sciences.*

Nigam, S. and A. Ruiz-Barradas, 2006: Seasonal Hydroclimate Variability over North America in Global and Regional Reanalyses and AMIP Simulations: Varied Representation. *J. Climate,* **19,** 815-837.

Nigam S., B. Guan, and A. Ruiz-Barradas, 2007: Pacific low-frequency sea-surface temperature variability 1900-2002: Structure and evolution. *To be submitted to the Journal of Climate.*

Opsteegh, J.D., and H. M. Van den Dool, 1980: Seasonal differences in the stationary response of a linearized primitive equation model: Prospects for long-range weather forecasting? *J. Atmos. Sci.*, **37**, 2169-2185.

Paegle, J., K. C. Mo, and J. Nogues-Paegle, 1996: Dependence of simulated precipitation on surface evaporation during the 1993 United States summer floods. *Mon. Wea. Rev.*, **124**, 345-361.

Qin, J., and W. A. Robinson, 1993: On the Rossby wave source and the steady linear response to tropical heating. *J. Atmos. Sci.*, **50**, 1819-1823.

Rasmusson, E. M., 1967: Atmospheric water vapor transport and the water balance of North America: Part 1. Characteristics of the water vapor field. *Mon. Wea. Rev.,* **95,** 403-426.

Rodwell, M. J., and B. J. Hoskins, 2001: Subtropical anticyclones and summer monsoons. *J. Climate,* **14,** 3192-3211.

Ruiz-Barradas, A., and S. Nigam, 2005: Warm season rainfall variability over the U.S. Great Plains in observations, NCEP and ERA-40 reanalyses, and NCAR and NASA atmospheric model simulations. *J. Climate,* **18,** 1808-1830.

Ruiz-Barradas, A., and S. Nigam, 2006: IPCC's twentieth-century climate simulations: Varied representation of North American hydroclimate variability. *J. Climate,* **19,** 4041-4058.

Saha, S., and coauthors, 2006: The NCEP climate forecast system. *J. Climate,* **19,** 3483-3517.

Sardeshmukh, P. D., and B.J Hoskins, 1988: The generation of global rotational flow by steady idealized tropical divergence. *J Atmos. Sci.,* **45,** 1228-1251.

Stensrud, D. J. 1996: Importance of low-level jets to climate. A review. *J. Climate*, **9**, 1698-1711.

Sud, Y. C., and coauthors, 2003: Simulating the Midwestern U.S. drought of 1988 with a GCM. *J. Climate,* **16,** 3946-3965.

Ting M., 1994: Maintenance of Northern Summer Stationary Waves in a GCM. *J. Atmos. Sci.,* **51,** 3286–3308.

Ting M., and H. Wang, 1997: Summertime U.S. precipitation variability and its relation to Pacific sea surface temperature. *J Climate,* **10,** 1853-1873.

Ting M., and H. Wang, 2006: The Role of the North American Topography on the Maintenance of the Great Plains Summer Low-Level Jet. *J. Atmos. Sci.*, **63**, 1056–1068.

Trenberth, K. E., G. W. Branstator, and P. A. Arkin, 1988: Origins of the 1988 North American Drought. *Science,* **242,** 1640-1644.

Trenberth, K. E. and G. W. Branstator, 1992: Issues in establishing causes of the 1988 drought over North America. *J. Climate,* **5,** 159-172.

Trenberth K.E., and C.J. Guillemot, 1996: Physical processes involved in the 1988 drought and floods in North America. *J. Climate*, **9**, 1288-1298.

Uccellini, L. W. and D. R. Johnson, 1979: The coupling of upper and lower tropospheric jet streaks and implications for the development of severe convective storms. *Mon. Wea Rev.,* **107,** 682-703.

Weare, B. C., and J. S. Nasstrom, 1982: Examples of extended empirical orthogonal function analyses. *Mon. Wea. Rev.,* **110,** 481-485.

Weaver, S. J., and S. Nigam, 2007: Variability of the Great Plains low-level jet: Large scale circulation context and hydroclimate impacts. *J. Climate,* revised March 2007.

Wexler, H., 1961: A boundary layer interpretation of the low level jet. *Tellus*, **13**, 368-378.

Wilks, D. S, 1995: Statistical methods in the atmospheric sciences. *Academic press,* 467 pp.

Zhang, D.-L., S. Zhang, S. J. Weaver, 2006: Low-level jets over the Mid-Atlantic region: Warm season climatology and a case study. *J. Appl Meteor,* **45,** 194-209.

Zhong, S., J. D. Fast, and X. Bian, 1996: A case study of the Great Plains low-level jet using wind profiler network data and a high-resolution mesoscale model. *Mon. Wea. Rev.*, **124,** 785–806.